METHODOLOGY FOR EFFICIENTLY ESTABLISHING PROCESSING-STRUCTURE-PROPERTY RELATIONSHIPS FOR ADDITIVE-MANUFACTURED AGE-HARDENED ALLOYS

A Thesis
Presented to
The Academic Faculty

by

Benjamin Seitz

In Partial Fulfillment
of the Requirements for the Degree
Master of Science in the
George W. Woodruff School of Mechanical Engineering

Georgia Institute of Technology
December 2016

METHODOLOGY FOR EFFICIENTLY ESTABLISHING PROCESSING-STRUCTURE-PROPERTY RELATIONSHIPS FOR ADDITIVE-MANUFACTURED AGE-HARDENED ALLOYS

Approved by:

Dr. Richard W. Neu, Advisor, Advisor
George W. Woodruff School of Mechanical Engineering
School of Materials Science and Engineering
Georgia Institute of Technology

Univ.-Prof. Dr. rer. nat. Siegfried Schmauder
Institute for Materials Testing, Materials Science and Strength of Materials (IMWF)
University of Stuttgart

Dr. David L. McDowell
George W. Woodruff School of Mechanical Engineering
School of Materials Science and Engineering
Georgia Institute of Technology

Univ.-Prof. Dr.-Ing. habil. Dr. h.c. Oliver Sawodny
Institute for System Dynamics
Joint Degree Program Georgia Tech and University of Stuttgart
University of Stuttgart

Date Approved: 08/09/2016

ACKNOWLEDGEMENTS

The work presented in this thesis would not have been possible without the contribution of a number of different people. Their support and advice influenced my progress as a student and individual significantly. I would like to express my gratitude to these people.

First of all, I would like to thank my advisor, Dr. Richard W. Neu for his continuous support of my study and research. His guidance, patience and enthusiasm helped me in all the time of research and writing this thesis. Working with him was both highly valuable for my personal as well as my academic development.

I would also like to thank my committee members, Dr. David L. McDowell, Dr. Siegfried Schmauder and Dr. Oliver Sawodny, for their assistance and insight in reviewing this thesis.

My special thanks goes to the Oakridge National Laboratory Manufacturing Demonstration Facility for their financial and technical support, specifically Dr. Michael M. Kirka. Without his expertise this work would not have been possible.

My sincere thanks also goes to James D. Huggins, Ali Khosravani, Ashley Goulding, Kyle Brindley, Sanam Gorgan Nejad, Ernesto A. Estrada Rodas, Jonathan Fok Wai Leung, Chuchu Zhang, Andrew Radzicki, Anirudh Srinivas Bhat and Patxi Fernandez-Zelaia, for their valuable help and advice.

Finally, I would like to thank my family for their continued encouragement and support throughout my academic career. I would particularly like to thank my friends who made this stressful and trying period of my life so much easier to get through.

TABLE OF CONTENTS

LIST OF TABLES

LIST OF FIGURES

LIST OF ABBREVIATIONS

AM	Additive Manufacturing
EBM	Electron Beam Melting
DoE	Design of Experiments
PSPP	Processing Structure Property Performance
SLM	Selective Laser Melting
HIP	Hot Isostatic Pressing
RT	Room Temperature
EDM	Electrical Discharge Machining
YS	Yield Strength
UTS	Ultimate Tensile Strength
TCP	Topologically Closed Packed Phases

SUMMARY

In Additive Manufacturing (AM) of Inconel 718 the main focus lies on the primary solidification occurring in the build. The next critical processing step for age-hardened alloys is the post-built heat treatment. Since diffusivity depends on the spatial distribution of the elements, the solution treatment and age parameter established for conventionally manufactured Inconel 718 components will likely not be optimal for Additive Manufactured components.

This study specifically focuses on developing methods to rapidly establish the post-built heat treatment for age-hardened alloys. It will be showcased on Inconel 718 fabricated by Electron Beam Melting (EBM). The method incorporates as well as reveals challenges and considerations that go along with the unique processing route of AM.

Based on a thorough literature review on Inconel 718, Processing-Structure-Property-Performance (PSPP) relations and Electron Beam Melting, a PSPP chart is outlined and used to detect further research goals. It is recognized that the work on systematically evaluating and improving the influence on mechanical properties is most efficiently conducted by utilizing post-processing parameter. After identifying promising post-processing parameter in solution treatment and aging, a material library is defined based on a selection of strain-rate jump tests which are found to be advantageous based on the demand of AM and efficiency considerations. An efficient test geometry enables evaluating strucutral and property features in the direct vicinity of each other. Design of Experiments has shown to be useful for establishing efficient test matrixes on post-built heat treatment parameter. Analyzing the data revealed major porosity concerns in the AM feedstock material which are found to detrimentally affect the material's ductility.

CHAPTER I

INTRODUCTION

The following chapter covers the motivation, objective and summary of the research conducted in anticipation of a Master's Degree in Mechanical Engineering at the Georgia Institute of Technology.

Motivation

The success of fabricating structural components with a sufficient reliability and repeatability requires comprehensive understanding of the Processing-Structure-Property-Performance (PSPP) relations given by the respective material. Gaining this knowledge is a huge and challenging task which cannot be fulfilled by one researching entity alone.

Facing the goal to accelerate this process, the White House launched the *Materials Genome Initiative* (MGI) in 2011. In this context making the development of advanced material "twice as fast, at a fraction of the cost" [1] is defined as a leading mandate for material scientists and engineers and is acknowledged as "essential to economic security and human well-being" [1] in the 21st century.

Efficiently combining individual results to unveil the big picture of material behavior discloses the need not only for sound but also standardized methods to agree on. This is especially necessary in Additive Manufacturing, where the plurality in processing systems and parameters is large and the knowledge in how to reliably build parts is still at its beginning. In order to achieve a fast and cost efficient development of process understanding and also to take account of the structural heredity that goes along with this complex processing method, uniform ways to capture both the structural features as well as the mechanical properties at the same location are required. Additionally, there is a need for smart ways to pattern possible processing parameter spaces.

Research Objective

Based upon the motivation described above, proposing aspects of a high-throughput methodology to establish PSPP relationships for Additive Manufacturing of metal is a main goal of the presented research. Contributing to a more standardized procedure of performing experiments related to Additive Manufacturing process development is anticipated.

Therefore a material library needs to be designed in order to provide a generally applicable basis for conducting important investigations regarding metallographic configuration and mechanical performance. Further requirements to give consideration to the current challenges in generating AM builds are identified and incorporated in the design. Additionally, the state-of-the-art in process development is reviewed and a systematic method for its display is proposed in the context of high-throughput PSPP investigation in Additive Manufacturing. Furthermore, methods to explore the parameter space systematically are identified and applied to current research challenges which were found based on the state-of-the-art in AM processing the nickel-base superalloy UNS N07718, commonly known as Inconel® 718. Using the AM technology of Electron Beam Melting an example library is built and afterwards analyzed. Therefore quantitative methods are focused which meet the needs of high-throughput experiments.

Thesis Layout

Chapter 2 provides a background of Additive Manufacturing processing based on Electron Beam Melting technology. Furthermore, a material specification of Inconel 718 is discussed as well as previous work on this superalloy with respect to EBM processing. Chapter 3 gives a thorough explanation on the considerations and methods utilized for establishing an efficient methodology for the tasks of objective. Chapter 4 discusses the experimental set up used for the implementation of the methodology on Additive Manufactured EBM Inconel 718. This contains an overview of the sample design,

furnace set up, mechanical testing, metallography and data analysis. Chapter 5 shows the results of the conducted microstructure and mechanical property characterization. These include the evaluation of the strain-rate jump test, porosity and grain structure. Finally, chapter 6 and 7 summarize and conclude on the methodology and observed material behavior, and provide further recommendations for future work.

CHAPTER II

BACKGROUND

The following chapter outlines the literature review on relevant aspects for this thesis. At the beginning the basic principle of generating parts in Powder Bed Fusion Additive Manufacturing is described based on the Electron Beam Melting process.

A Processing-Structure-Property-Performance chart provides an overview of the relations between Additive Manufacturing processing, structural features of the nickel-base superalloy 718 used for this study and its mechanical response. These relations are thereafter discussed in the material specification which reviews the most important structural features and their influence on mechanical properties. A background in heat treating processes on Inconel 718 is discussed with respect to the influences on microstructure and mechanical behavior. This is followed by a review of the state-of-the-art in Additive Manufacturing Inconel 718 using the Electron Beam Melting process which is as well discussing the influences of processing parameter on the Additive Manufactured microstructure of Inconel 718. Furthermore, this chapter gives an introduction to mechanical properties of the alloy, including a review of viscoplastic behavior.

Additive Manufacturing with Powder Bed Fusion

Additive Manufacturing offers a variety of processes to generate structural parts. Regarding metallic parts the Powder Bed Fusion Additive Manufacturing processes of Electron Beam Melting (EBM) and Selective Laser Melting (SLM) are of outstanding relevance. General requirements for producing metallic structural components are for

example suitable welding properties and sufficient corrosion resistance that allows the handling of the basic powder without severe change in composition due to reaction with the environment. This thesis focuses on EBM processed parts and the anticipated results are also expected to be useful for the implementation in other Additive Manufacturing processes. In the following, the main processing steps of EBM are outlined.

Operating Principle of Electron Beam Melting

In order to prepare the AM build a CAD model of the respective part needs to be converted to an STL data file. This file provides a surface model of the part which is then debugged in a pre-processing software like Materialize Magics. Main geometrical restriction of Powder Bed Fusion AM parts is that hollow parts are not possible without guaranteeing an outlet for the included powder. Also, parts need to be cut from the baseplate, which in some cases requires geometrical adaptions. The baseplate tends to warp within the first layers of the build because the plate's center is heated supplementary or cooled slower than the outskirts and therefore shows a different thermal expansion. First, a metallic baseplate is needed to build the Additive Manufactured parts upon. For this plate, it is often necessary to use the same material of which the part is made. However, it is also possible to use base plates of a different material as long as the transition zone is large enough to keep diffusion effects within the two materials outside the final AM part. This baseplate is mounted upon multiple layers of metallic foil and net to generate thermal isolation. Above that, a basic powder bed of about 40 mm serves as the fundament for the baseplate. This powder bed allows to evenly mount the baseplate in order to guarantee a uniform first layer of powder.

After initial heating to build temperature and outgassing [2] the build of an AM part geometry starts with an initial layer. This layer, such as all the following layers, is applied on the baseplate by three swipes of a rake. Layer thicknesses are between 50 μm and 200 μm [3]. Once this layer is established, an electron beam is used to sinter the

whole layer. This step is needed because the electron beam would otherwise charge the powder particles negative. That would lead to powder evaporation which has an undesirable impact on the build. The part geometry within that layer is afterwards scanned with a higher energy density which makes the powder melt to a solid layer on those sites. Depending on the material used, a variety of different melt themes exists. These melt themes assure appropriate melting conditions and therefore influence the microstructure of the resulting build. To apply the next layer, the build platform is lowered by the layer thickness. The previous described process is then repeated, adding multiple layers until the final part geometry is reached. This allows an extraordinary freedom in designing complex parts.

The thermal history within structural parts is considerable and a natural result of the build process. Therefore – especially for age hardened materials – post-built heat treatments are required to make up for microstructure heterogeneity that results from spatial variation in thermal history. Additionally a Hot Isostatic Pressing (HIP) cycle is often applied to powder bed AM parts in order to eliminate porosity which results from the build process.

Technical Specification of Electron Beam Melting

In the following some technical specifications of the EBM system used for producing the samples of this study are summarized.

Minimum wall thicknesses of EBM parts are reported to be in the range of about 0.5 mm [4]. Maximal build heights of up to 100 mm are possible using the given Arcam manufacturing system. The general build speed is at about 30 to 80 cm^3/h [3] at scanning speeds of up to 8000 m/s [5]. Nevertheless, no time consuming process is needed e.g. to generate a casting mold. Dimensional accuracy is reported to be within 0.2 mm and 1.5 mm, where a surface roughness of Rz = 30 µm is considered optimal [3]. This implies that at least at critical surfaces a post-processing step is necessary. According to

Reference [6] high built temperatures between 700°C and 1000°C are possible. The build temperature is measured by a thermocouple applied underneath the baseplate. Feasible melting temperatures exceed the build temperatures and go up to 3400°C [5], [7] provided by an electron beam gun which is emitting electrons from a heated tungsten filament which are then accelerated by high voltage and focused by electromagnetic lenses [5]. The builds take place in vacuum (~10^{-4} torr according to Reference [5]). Two rates of cooling are feasible – slower cooling in vacuum or faster cooling through flooding the chamber with helium [2]. Afterwards the parts are powder blasted with the same powder that is used for the build in order to remove the sintered surrounding powder which then can be recycled.

PSPP Chart

The following chapters sum up the knowledge on Processing-Structure-Property-Performance (PSPP) relations as published in recent literature. In order to derive further research goals Olson [8] introduces a helpful method to summarize and illustrate the PSPP landscape. It is "a standard method of communication regarding the physical and chemical mechanisms that drive a materials system" [9]. Figure 1 shows a map which represents the PSPP relations of Inconel 718 in the context of EBM processing. It is structured by the three columns of processing parameters, structural features and relevant property measures which sum up to a performance profile if applicable. Additionally the entries of these columns are linked if the respective structural feature is influenced by the respective processing parameter or if the property measure is affected by the constitution of an individual structural feature.

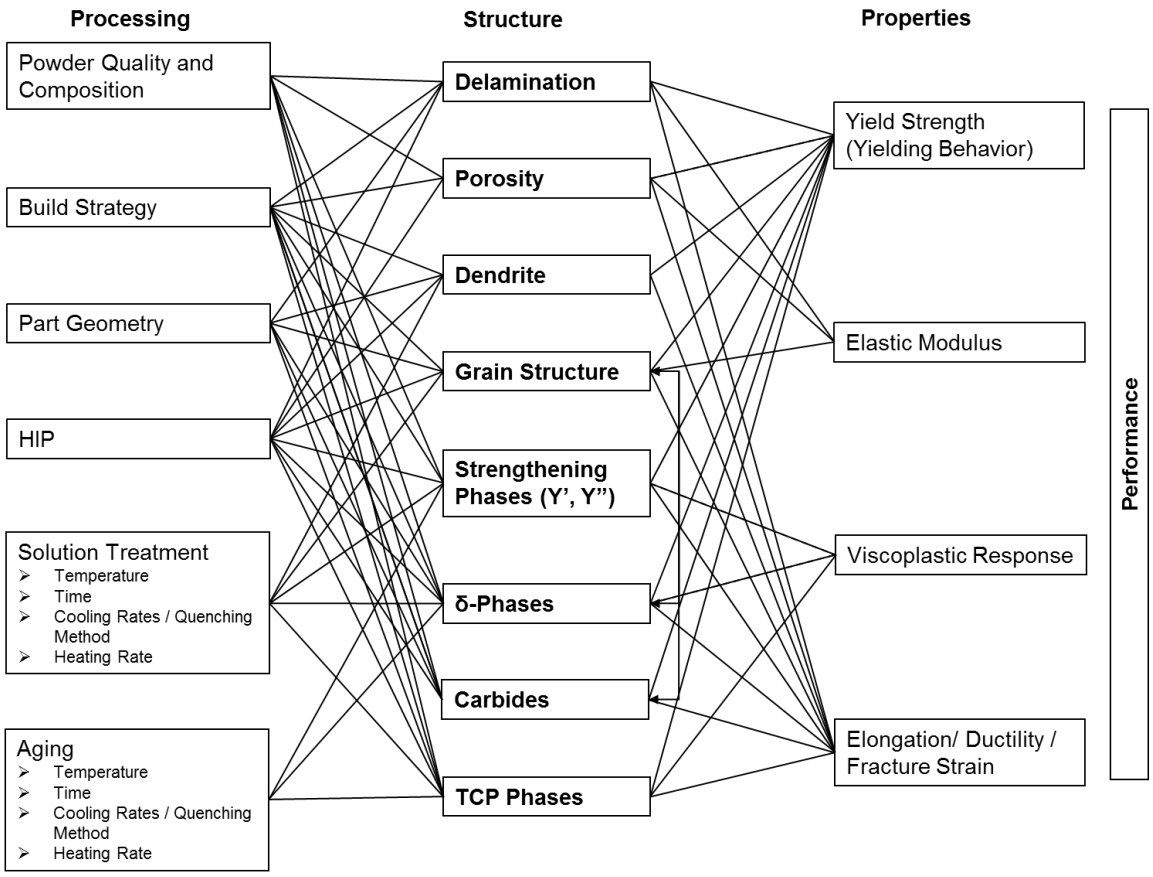

Figure 1: PSPP Chart for EBM Additive Manufactured Inconel 718

Material Specifications

As mentioned above, the age-hardening nickel-base superalloy Inconel 718 is the subject of consideration for the presented study and used to illustrate the set-up of the presented strategy. It is one of the few alloys for which melt themes and primary research publications are available concerning their EBM processing. The following paragraph gives an introduction to this alloy's material specification.

Nickel-Base Superalloys

Shortly after World War II the term "superalloy" was first used to describe alloys which were specially developed for good performance at high temperatures [10]. These temperatures could often exceed 0.7 of the respective material's absolute melting temperature [11]. The primary applications have been in turbosuperchargers and aircraft turbine engines. Later, further applications, for example in land-based gas turbines and rocket engines as well as chemical and petroleum plants, extended the range of the superalloy's use [10], [12].

Next to cobalt-base superalloys an important sub-group of the superalloys are the so-called nickel-base superalloys. As the name implies, the basic material of these alloys is the element nickel. However, a variety of alloying elements is added to enhance the material's high temperature performance. The main focus is on material strengthening, either through solid solution or precipitation [10]. Alloying elements, according to Bowman [10] can be categorized – by the difference in atomic diameter with respect to the basic nickel atoms – in γ formers which partition in the nickel matrix, also called the γ matrix. The γ' formers are elements that cause the precipitation of γ' phases such as aluminum, titanium, niobium – elements that differ in size by 6-18% with respect to the γ matrix [10]. Elements such as chromium, molybdenum, niobium and titanium can be categorized as carbide formers. Grain boundary elements such as carbon differ from the nickel atomic diameter by more than 20% and segregate to the grain boundaries [10].

Inconel 718

The considered material is Inconel 718, also often referred to by Special Metals Corporation's tradename INCONEL® Alloy 718 (IN718) or by UNS N07718 or W.Nr. 2.4668, a polycrystalline precipitate strengthened and corrosion-resistant nickel-chromium alloy [13], [12]. According to Special Metals [12] it provides good welding characteristics especially in terms of post-weld cracking. This circumstance makes it an interesting candidate for AM processing. Traditionally manufactured it is commonly used for example in liquid fueled rockets, rings, casings and sheet metal parts for aircraft purposes, land-based gas turbine engines, and cryogenic tankage, as well as for fasteners and instrumentation parts [12].

Table 1 gives a general overview over Inconel 718 material properties. These values are considered typical for traditionally manufactured Inconel 718 and can vary slightly with composition and processing condition of the material [12].

Table 1: Typical Inconel 718 Material Properties [12]

Density annealed [kg/m^3 (lb/in^3)]	8193 (0.296)
Density annealed and aged [kg/m^3 (lb/in^3)]	8221 (0.297)
Melting Range [°C]	1260 – 1336
Modulus (70°F,21°C) [MPa (ksi)]#	$199.9*10^3$ ($29.0*10^3$)
Modulus (1200°F, 649°C) [MPa (ksi)]#	$163.4*10^3$ ($3.7*10^3$)
#: Hot-rolled flat, heat treated 1800°F/1h, air cooled +1325°F/8h, furnace cooled to 1150°F, held for total time of 18h	

The feedstock material utilized in this study was Arcam Inco 718 powder with a nominal size distribution of 25 µm to 105 µm [14]. The composition is shown in Table 2.

Table 2: Nominal Chemical Composition of Inconel 718 Powder [30]

Cr	Fe	Nb	Mo	Ti	Cu	Al	C	Ni
18.5	18.5	5	3	1	0.15	0.5	0.05	Bal

General Material Structure

If the material is Additive Manufactured, it has in most cases a columnar grain structure [15], [16], oriented in the build orientation [21], even though some newer scan strategies also achieve equiaxed grains [17], [18] & [19] which is further discussed in sections below. Grain sizes are expected to be within the range of 20 µm up to 2 mm [20]. Figure 2 shows typical reference grain structure published in recent papers, compared to forged Inconel 718 microstructure. The structure in Figure 2 B is reported to be several millimeters in length and up to 1 millimeter in diameter [21]. Further, the columnar grains are reported to have a strong 1 0 0 texture [21], [18].

With regard to the PSPP relations, yield strength is reported to be optimized by a fine grain structure [22], [23] as more grain boundaries are causing higher resistance to dislocation movement (Hall-Petch effect [24]). On the other side, larger grains can be beneficial in terms of creep rupture life as discussed in the viscoplasticity section below. The texture of the AM microstructure is reported by [19] to be influencing the elastic modulus.

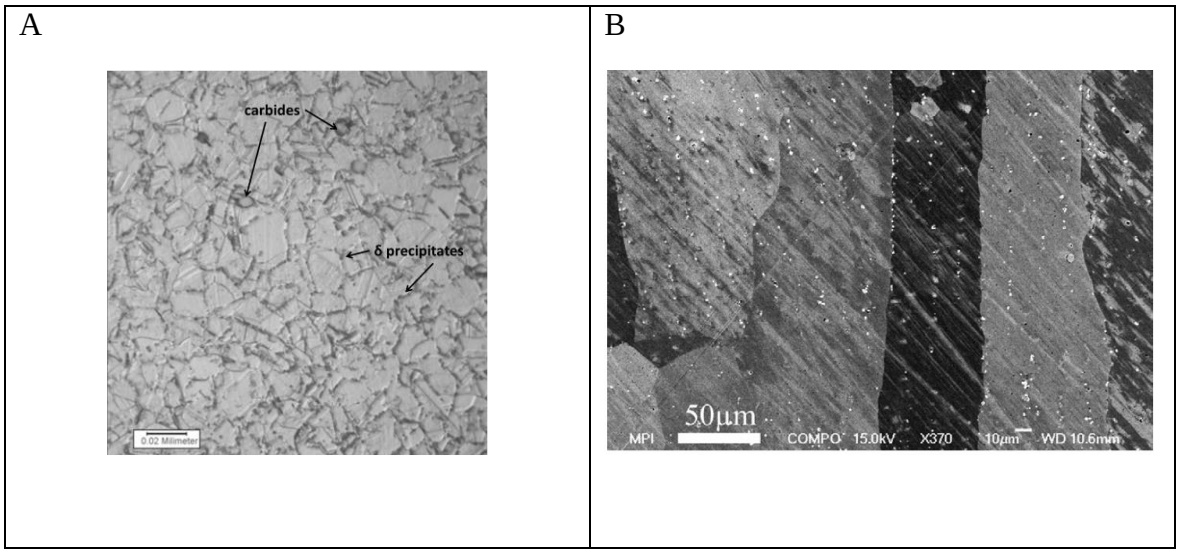

Figure 2: Grain Structure: A: Fine Grained Forged Inconel 718 Micrograph (Approximately ASTM 10 Grain Size) [25], [26], B: Columnar Grained EBM Inconel 718 Micrograph [15].

Control over porosity has been reported to be good enough to meet the ASM5383 industrial standards of casting [16]. In successfully built AM parts though, higher expectations were set by ASTM F-3055 [27]. In some cases agglomerated porosity or higher extends of porosity were reported to cause detrimental ductility [21]. Less than 1% or 0.5% porosity is considered a goal in melt theme strategies, discussed in Reference [28] and [29].

As could be seen in the PSPP chart, porosity most likely has the most important effect on reducing ductility in AM parts: Strondl et al. [21] reported considerably reduced elongation tested perpendicular to the EBM build orientation due to stringer porosity. The measured Yield Strength is affected by flaws like those caused by delamination and porosity as they cause notch effects which lead to local stress concentration. The measured modulus can also be affected by the amount of flaws from delamination and porosity sites.

Kirka et al. [30] reported that EBM Inconel 718 builds show a pronounced core dendritic structure at the top of the build. With further time at build temperature and

therefore further distance from the top of the build this structure vanishes. According to Strondl et al. [21] the dendrite structure leads to a gradient in alloying elements throughout the material, which affects the precipitation behavior and therefore also the strength. Cracking is occurring along the Nb, Ti, and Mo-enriched interdendritic region and therefore also the dendrite structure has an effect on ductility [2], [31]. Finer dendrites were reported to lead to superior mechanical properties [32]. Additionally Nb, Mo, Ti segregation to the interdendritic regions has been reported to lead to laves phase formation and therefore embrittlement [33]. Strondl et al. [21] reports inhomogeneous precipitation and porosity and carbide concentration in the interdendritic regimes.

In the following section the most important phases formed by Inconel 718 are discussed: One micrograph of Inconel 718 is shown in Figure 4 which is showing three phases in the γ matrix.

Gamma Matrix γ: The matrix of Inconel 718 is the so-called γ phase, an austenitic phase of face-centered-cubic (fcc) structure which is typical for nickel-base superalloys [10]: For Inconel 718 this phase consists of Ni, Fe and Cr [34], [35].

Gamma prime γ': The γ' phase Ni3 (Al, Ti) [10] is the typical strengthening phase in nickel-base superalloys and as well formed by Inconel 718. It is coherently precipitating within the γ matrix with an ordered L12 (fcc) crystal structure [10], shown in Figure 3. As the lattice parameter of γ and γ' match very closely and the phases provide the required chemical compatibility the γ' phase precipitates homogeneously throughout the matrix material and provides good stability against dissolution. Reference [10] attributes an increase of flow stress with temperatures up to 650°C to γ' and also the

favorable ductility of γ' is mentioned to be the reason for causing the phases strengthening effect without significantly decreasing the ductility.

Gamma doubleprime γ": Next to the γ' phase commonly formed in superalloys Inconel 718 forms γ" precipitates. This provides superior strength in applications of the lower range of which superalloys are used for [11]: In Inconel 718 niobium is responsible for forming this phase such as illustrated in Figure 3. Its chemical composition is then Ni3Nb [11]. γ" forms a D022 body centered tetragonal (bct) lattice [36].

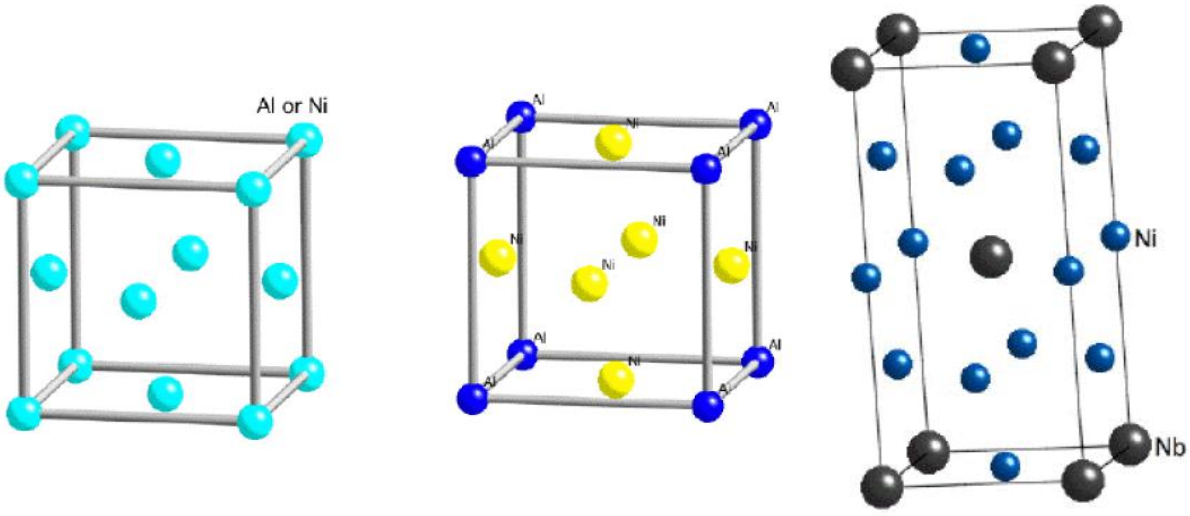

Crystal Structure of γ Crystal Structure of γ' Crystal Structure of γ"

Figure 3: Crystal Structure of the Matrix γ and the Strengthening Phases γ' and γ" [11]

The PSPP chart indicates significant influence of the strengthening precipitates on the mechanical properties. The size of the strengthening phases, according to Reference [22], affects the interaction of dislocations with the precipitates where for large precipitates dislocation bowing is dominant whereas small precipitates are more likely to cause dislocation cutting. Therefore the yield strength of nickel-base superalloys is reported to be dependent on precipitate size [22]. Yield strength is also reported to be

dependent on volume fraction of the strengthening phases [22], [51]. Kirka et al. [16], [37] also reports the γ" volume fraction to yield stress relationship and reports a peak concentration of γ" to be 15%. In general, in precipitation hardening, the more and the finer the precipitates are the better for increasing strength [24]. Strengthening phases while enhancing the materials strength also reduce the ductility. For example Rao et al. [38] partially attributes lower ductility to the strengthening phases in the matrix.

Delta Phase δ: Next to γ' and γ" Inconel 718 also commonly forms a third intermetallic precipitation phase: the δ-phase which is having the same Ni_3Nb composition as γ" but shows an orthorhombic (D0a) crystal structure. These circumstances make the two phases concurrent in precipitation. δ mostly precipitates at grain boundaries and grows in thin plates but is reported to also form intragranular [36], [39]. δ is sluggish in its formation and therefore always preceded by γ" formation. Although δ is known to be thermodynamically more stable [36].

As delta phases consume the same elements as γ" precipitates, they grow at the expense of those strengthening phases and therefore are known to reduce the yield strength [36]. Also Hong et al. [40] reported decreasing tensile strength in Inconel 718 with increased amount of δ phase. Additionally, as denoted earlier with increasing time at temperature the γ" phase can transform to δ phase which can reduce the strengthening effect [36]. Moderate amounts of δ phase are known to cause grain boundary pinning and therefore to limit grain growth in solution treatments [36], [41] and due to that to some extent, can be beneficial for the yielding properties as denoted above. Additionally it is reported to provide resistance to grain boundary creep fracture in some circumstances [36], [42], [43]. The δ phases are reported to be brittle which is detrimental for ductility [5].

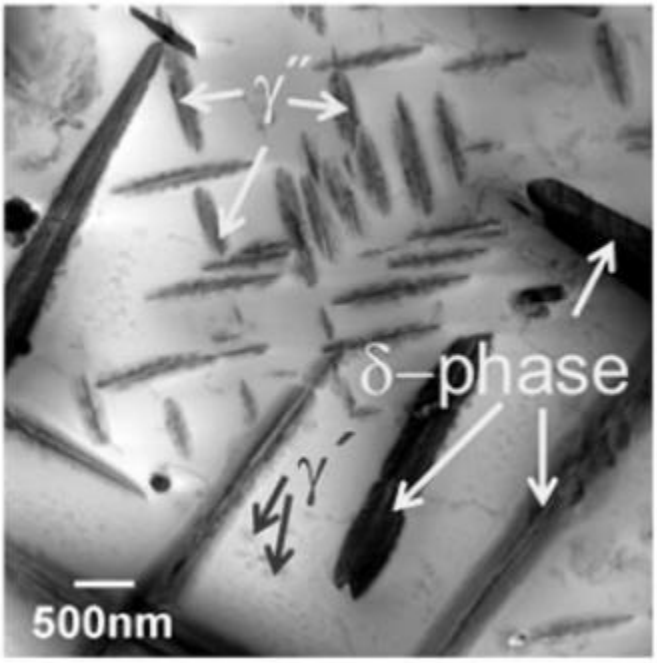

Figure 4: SEM Image of the γ', γ" and δ Phase Precipitates in the γ Matrix of EBM Inconel 718 [2]

Carbides: Inconel 718 of the composition as used in this project contains about 0.05% carbon (Table 2). In reaction with certain elements e.g. titanium it is reported to form carbides like TiC [10]. Due to thermal exposure either during heat treatment or in elevated temperature service, these carbides can decompose to lower carbides such as $M_{23}C_6$ or M_6C [10]. Carbides in general show an fcc structure [10].

Carbides are, like grain boundary δ, reported to be able to contribute to grain boundary pinning [5], [21].

TCP phases such as Laves Phases (Figure 5) consist of close-packed atom layers separated by larger atoms [10]. They use up atoms otherwise potentially could form strengthening phases and are therefore detrimental [10]. For example [44] states that Laves consume the Nb elements that were needed for γ" precipitates and found laves particles to be primary responsible for low tensile ductility by providing sites for micro-void initiation. Also Reference [44] reports Laves phases to be crack initiation sites and therefore embrittle the material.

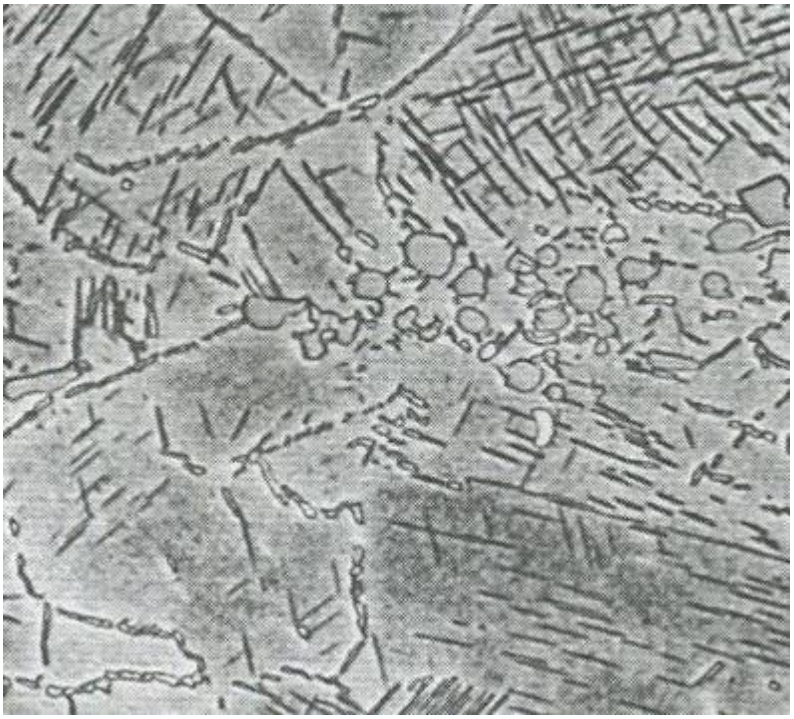

Figure 5: Carbides and Laves Phases [45] of Solution Treated and Aged Inconel 718, Laves Phases (Light Gray Particles); MC Carbides (dark) and Needle-Like δ in γ Matrix. 1000x Magnification

Solution Treatment and Aging

The often stated maximum use temperature of Inconel 718 is often referred to be limited to 650°C or 1200°F e.g. Swindeman et al. [46], though some literature also reports ranges from -423° to 1300°F (-253°C to 704°C) [12]. Swindeman et al. [46] claims that the database for Inconel 718 exceeds up to 760°C. The main reason for the limitations is the comparable instability of the γ" precipitates at temperatures above that point which also can be seen at the TTT diagrams discussed in Figure 6. At higher temperatures they coarsen faster and experience a transition to γ' or δ phases which reduces the precipitation hardening effect and therefore the strength [2].

Furthermore the complex and spatially varying as-built phase formation resulting from EBM processing which leads to microstructural gradients is discussed in detail in [2] and [30].

The basis for heat treatment optimization are the precipitation temperatures of the most relevant precipitates as well as the reported standard heat treatments temperature ranges and preliminary reported work on heat treatment optimization.
So far there are no generally optimized heat treatment procedures for EBM Inconel 718. There are certain solution treatment and aging processes reported, which, based on their widespread use and their origin can be considered as standard for forging applications. These are also commonly used to heat treat EBM Inconel 718.

Solution treatment can cause grain growth, dendrite dissolution (which already takes place at lower temperatures [30]) and is intended for phase dissolution. Nevertheless it is most likely not able to dissolve the carbides which takes place at too high temperatures (TTT chart in Reference [47]).

Aging time and temperature are selected with the intent to generate a good configuration of the precipitation of strengthening phases, δ phases and without forming laves phases. Usually a first aging step at higher temperatures is performed to achieve precipitation initiation. Afterwards, a lower temperature step for precipitation growth is added.

The following table gives an overview over the standard HTs performed for Inconel 718.

Table 3: Reported Solution Treatment and Aging [12]

Solution Treating ST			Precipitation Initiation PI			Aging A		
Temperature	Time	Cooling Process	Temperature	Time	Cooling Process	Temperature	Time (PI + A)	Cooling Process
°C	h		°C	h		°C	h	
926-1010	1	Water Quenching	720	8	Furnace Cooling	620	18	Air Cooling
1038-1066	1	Water Quenching	760	10	Furnace Cooling	650	20	Air Cooling

The lower temperature heat treatment in Table 3 is referred to be optimum heat treatment for traditionally processed Inconel 718 in terms of “rupture life, notch rupture life and rupture ductility” and if ductility is in the main focus. It is denoted to achieve the

highest room temperature tensile and yield strengths and to provide favorable grain structure for fatigue strength [12].

The higher temperature heat treatment in Table 3 is referred to be "preferred in tensile-limited applications because it produces the best transverse ductility in heavy sections, impact strength, and low-temperature notch tensile strength." However, higher notch brittleness in stress rupture is more likely than for the lower temperature heat treatment [12].

Next to the information mentioned above, the Time Temperature Transformation (TTT) diagram of Inconel 718 provides valuable insight into the precipitation behaviors and temperatures. Figure 6 shows TTT Diagrams for material similar in composition to the one used for this work. Those diagrams are acquired using the software JMat Pro and are provided by ORNL [48].

For solution treatment temperatures below and close to 1000°C such as those of the lower temperature standard heat treatments in Table 3, the TTT diagram shows δ-phase precipitation and a complete solution of the δ-phase cannot be expected.

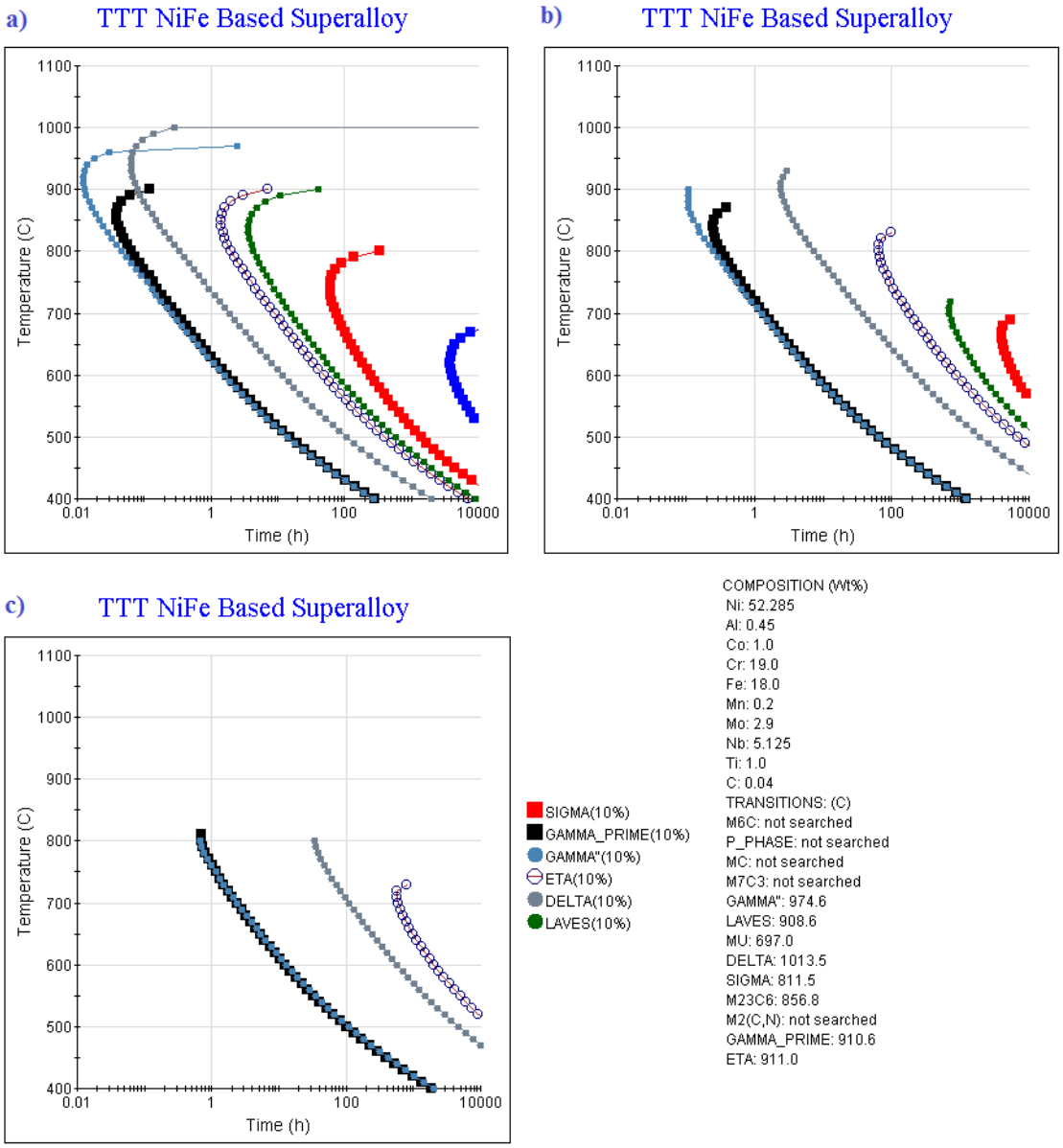

Figure 6: TTT Diagram Inconel 718: a) for 0.1% Precipitation; b) for 5% Precipitation and c) for 10% Precipitation of the Respective Phase Generated Using JMat Pro. [48]

Additional to these references, preliminary reported results can be used to set-up a test matrix.

A study on δ-phase precipitation in Inconel 718 by Azadian et. al. [49] reports insight in heat treatments on temperature levels that provide relevant information for the solution treatment step. Figure 7 shows the solution treatment effect on δ-phase volume fraction at relevant temperatures for four different Inconel 718 feedstock. It shows a

significant decrease in δ-phase remainder for temperatures above 1000°C. A peak in δ precipitation can be seen in all four curves between 920°C and 1000°C. After a five hour heat treatment (Figure 7) the displayed peak moved to lower values around 950°C. The decrease in δ-phase from that peak to higher values remains and shows no more δ-phase after 5 hours at 1020°C whereas for one hour δ-phase is no more visible at 1050°C. Azadian et. al. [49] concludes "that for 1-h treatments, the apparent solution temperature for the Spray formed (SF) alloy was approximately 1030 °C while those of the ring rolled(W1, W3) and wrought (W2) alloys lay between 1035 and 1050 °C." This indicates the dependence of the solution treatment on the microstructure of the as-manufactured material.

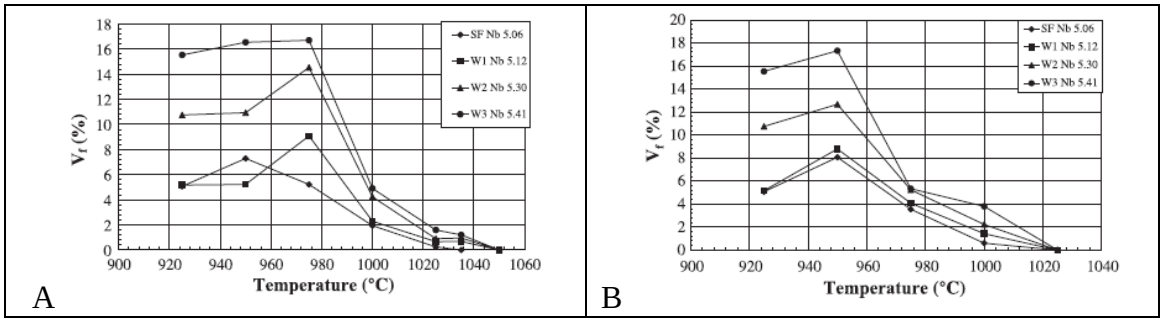

Figure 7: Effect of 1-Hour (A) and 5-Hour (B) Heat Treatment on δ Phase for Four Processing Routes [49]

Next to the δ-phase solution, grain growth is another interesting effect of solution treatment, expected to reduce strength (Hall-Petch-effect). As the δ-phase is known to pin the grain boundaries, it cannot be assumed that total dissolution of δ-phase leads to the only desired heat treatments. In fact, Azadian et. al. [49] illustrated results demonstrating this effect as shown in Figure 8: For the feedstock material (not Additive Manufactured) presented in this study significant grain growth is observed at temperatures higher than 1040°C. Azadian et. al. [49] concludes, the grain growth "is almost certainly associated with the dissolution of δ –phase".

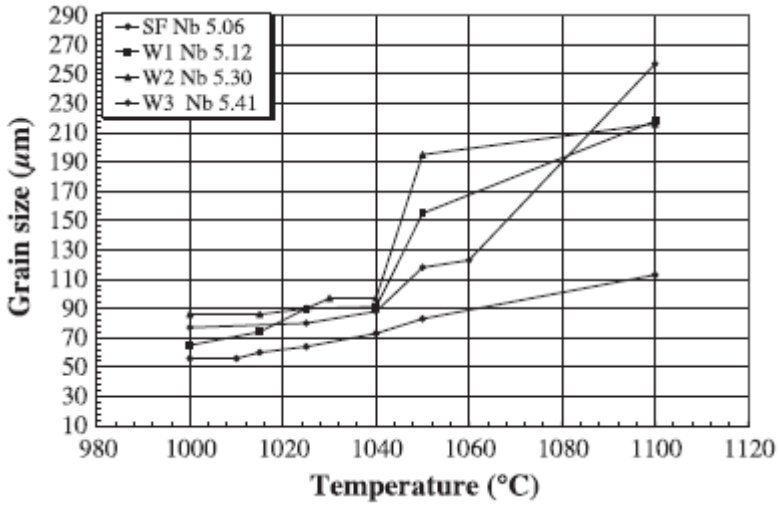

Figure 8: Effect of 1-Hour Solution Treatment Temperature [49]

Special Metals [12] provides information on grain growth as well, shown in Figure 9 (for 0% deformation): The effect of annealing in the ranges of the reported standard heat treatments (Table 3) for 30 minutes display a peak in grain size number after annealing at ca. 980°C (1800°F). This results are in line with Azadians [49] findings (Figure 8) as the grain size number is inverse related to the grain size which in both cases increases for rising temperatures above 1000°C. The minimum grain sizes for annealing at 980°C could be related to the maximum in grain boundary pinning δ-precipitation between 900°C and 1000°C as illustrated in the TTT-diagram (Figure 6).

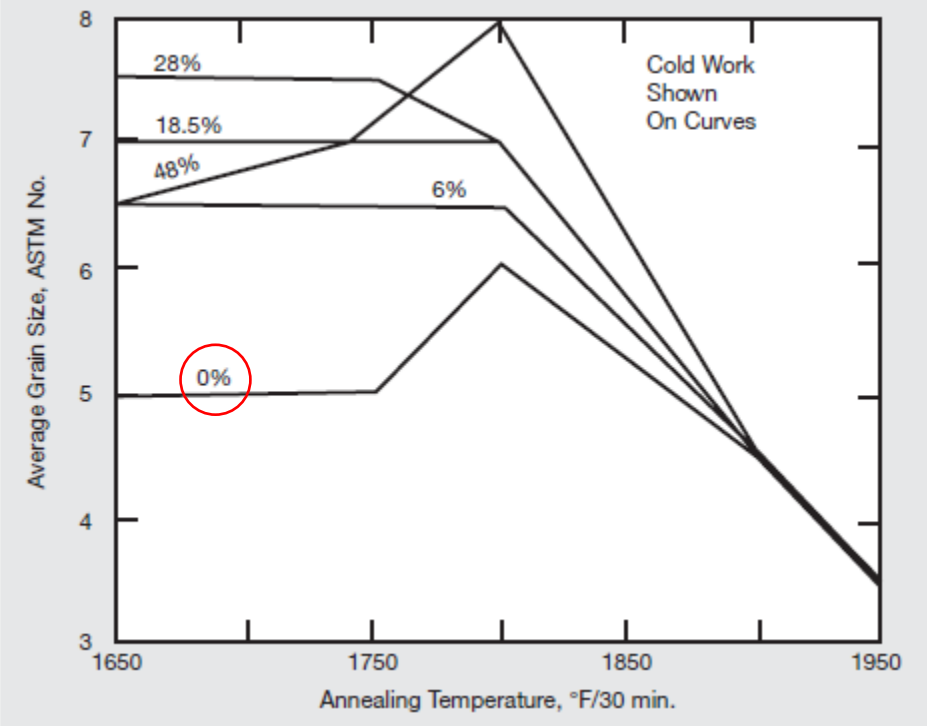

Figure 9: The Effect of Solution Treatment Temperature on Grain Size Number in Sheet Inconel 718 [12]

The TTT diagrams (Figure 6) show that the temperature at which the illustrated amount of precipitation phase is attained subsides continuously. Also it shows that with higher temperature the amount of precipitated γ" and γ' strengthening-phases increases. Furthermore, along with increasing temperatures the amount of the δ-phase increases. The ranges of precipitation and aging temperatures addressed in the standard heat treatments (620°C – 760 °C, Table 3) show no peak in precipitation of the relevant phases within 100 hours of observation but predict a monotonically increasing amount of precipitation with increasing temperature.

No considerable amount of brittle Laves-Phase precipitation is expected. According to Figure 6 b) the precipitation of 5% Laves-Phase is expected to be reached after more than 100 hours throughout the whole displayed temperature range.

The study on aging treatment illustrated in Figure 10 shows the effect of aging at constant temperatures between 650°C and 750°C for an aging time of 20 hours on

Inconel 718 (triangle symbols). The graph shows a parabolic shaped dependence of yield strength on the temperatures used for precipitation and aging according to the standard heat treatments. The difference in yield strength is significant, 300 MPa, within temperatures as low as 650°C and the peak in yield strength at approximately 725°C.

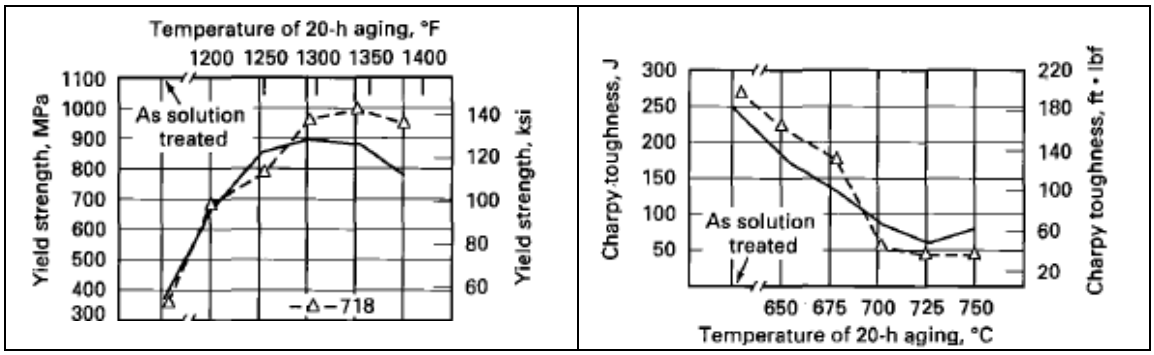

Figure 10: Effect of Aging Temperature on Yield Strength and Toughness [47]

Figure 11 displays the variation of hardness values over aging temperature and time for sheet-type Inconel 718. It shows a significant variance in hardening throughout the window of 620°C (1150°F) and 760°C (1400°F) for 20 hours. Also it shows that the variance of hardening over aging time is less significant for aging times longer than one hour (logarithmic scales). Especially for temperatures other than ca. 700°C (1300°F).

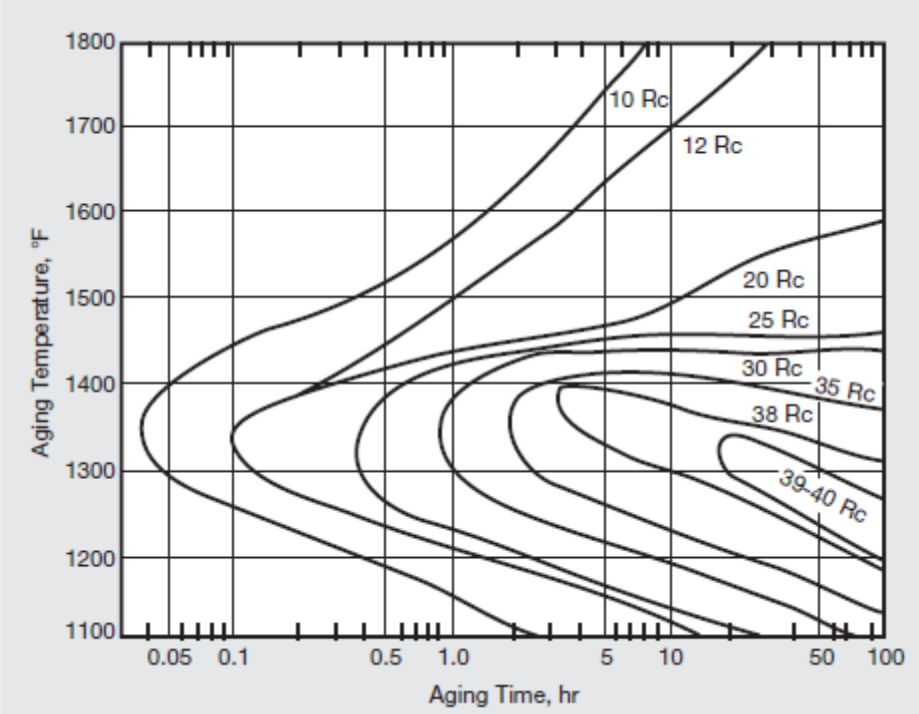

Figure 11: Effect of Aging Conditions on Hardness of Annealed Sheet Inconel 718. Initial Hardness, As-Annealed: Rc 4. [12]

Previous Work on EBM Inconel 718

The previous chapter gives insight in the material specification of Inconel 718 including the Structure-Property relations as displayed in the PSPP Chart (Figure 1) and the underlying correlations between post-processing parameters and microstructure of Inconel 718 in general. The following chapter displays the previous work published for Inconel 718 which gives insight in the EBM specific correlations between processing parameters and microstructure.

After outlining the operating principle of Electron Beam Melting in the first passage of this chapter, the review that follows intends to give a summary on what is the state-of-the-art in published research specifically focusing on EBM Inconel 718. Beginning with powder assessment this will lead from the basic features of EBM Inconel 718 builds and feasibility studies over methods to come up with scan strategies other than

the standard Arcam melt theme for Inconel 718 to a review of post-built heat treatment assessment in EBM.

Powder

EBM Inconel 718 is a powder based process and therefore powder quality and composition are of interest concerning the PSPP relations illustrated in Figure 1. In 2015 Nandwana et al. [50] came up with a Recyclability Study on Inconel 718 powders for use in Electron Beam Melting for which they researched the impact of reusing the powders for multiple builds in order to reduce the costs of the AM technology. Powder quality has been defined e. g. in terms of flow ability, chemistry, size distribution or porosity. These features have been found to be influencing the surface finish, the chemistry and consistency as well as the mechanical properties of the parts. As powder features are influencing the surface finish of the material they naturally also affect the linking to the next layer and therefore the risk of delamination. Inconel 718 powders have been found to be reusable multiple times until physical characteristics such as flow ability and oxygen pick up limit its use.

Just recently this study has been followed by a comprehensive methodology for developing processing parameters for nickel-base superalloys for the Electron Beam Melting published by Medina et al. [5]. This method was demonstrated on Inconel 718. Amongst other measures, multiple tests were proposed to characterize the powder quality. This way a standardized method for identifying suitable candidate feedstock powder for EBM is available.

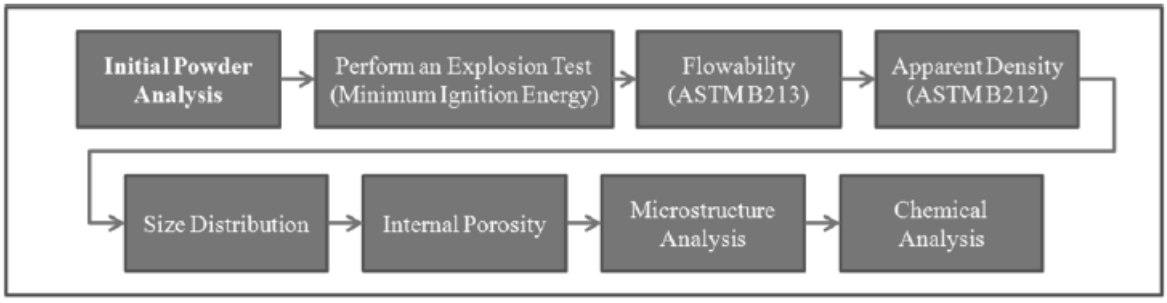

Figure 12: Process Flow Diagram for Powder Assessment by Medina et al. [5]

Amongst others the powder's susceptibility to explosion was identified as a quality feature which has been proposed to be tested by a standardized test (ASTM E2019). The minimum flowability required for the Arcam EBM Process used for this study is there defined to be 25 s/50 g. The apparent density of the powder has been defined as a vital necessity for avoiding porosity. Next to requirements in size distribution, the amount of internal porosity is recommended to assess as entrapped gas in hollow powder particles are found not to escape during solidification which also leads to pores [32]. In addition, the composition of the powder can influence the precipitation phase structure [10].

Main Built Properties

Various studies have been presented on general feasibility of highly dense and delamination free builds. For example Strondl et al. [15] published a study showing columnar grain structure (see Figure 2). They found similar metallography features like precipitates when comparing their as-built material to conventionally processed and heat treated Inconel 718. Additionally they found inhomogeneous precipitation of carbides, coming from concentration of alloy elements in the liquid phase during dendritic solidification. Grains have found to be crystallographic textured with the 1 0 0 orientation in build direction.

Sames et al. [2] noted in their study on microstructural heterogeneity in EBM Inconel 718 that precipitation behavior varies along the build direction. Also they

achieved different mechanical properties in identical geometries by varying the cool-down rate from build to room temperature.

The microstructure gradients from top to bottom of EBM builds have also been reported by Kirka et al. [30] which they reported to form three distinct zones depending on the time the respective material has remained on build temperature. Region 1, at the top layers of the build shows a cored dendritic structure whereas in Region 2 shows a more diffuse dendritic structure. These two zones only span about the top 4 mm of the build. The bulk of the researched build (96%) showed no dendritic character but columnar grains, as also reported by Strondl et. al [15] (see Figure 2).

Next to the circumstance that the melt theme is influencing the dendrite structure by applied hold time [30] and by the applied scan pattern [19]. Ram et al. [23] states that the "scale of dendritic structure is inversely proportional to the solidification cooling rates".

The as-built configuration of the strengthening phases (γ', γ"), the δ-Phase, and Laves Phase formation were influenced by factors such as hold temperature and hold time (build speed achieved by the melt theme) and cool-down rate [2]. The cool down rate from build to room temperature can be varied by either selecting vacuum or inertial gas cooling [2]. Carbides form at high temperatures between melting and EBM hold temperature depending on scan strategy [47].

Kirka et al. [30] also evaluated the tensile performance of as-built samples along the build height (Figure 13) and showed that mechanical properties (yield strength, ultimate tensile strength, ductility) continuously increase with the distance from the baseplate (decrease with time at temperature).

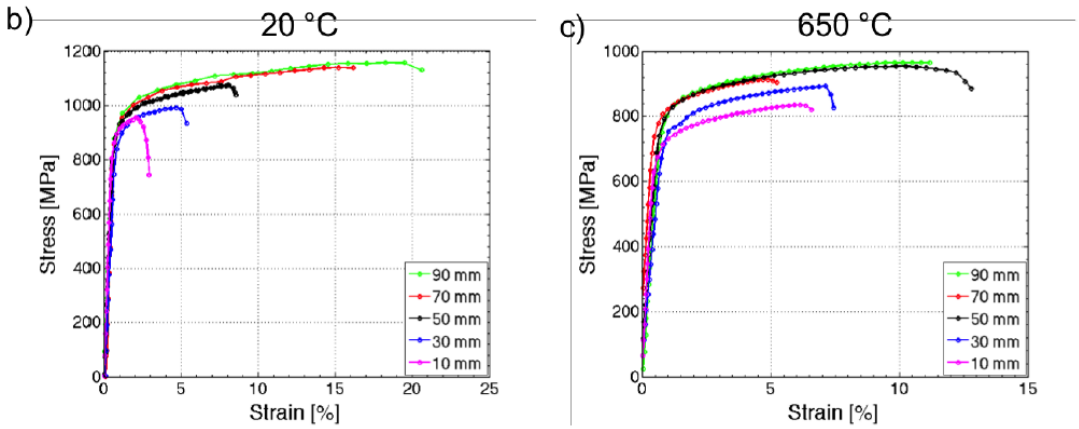

Figure 13: As-built Height Dependent Tensile Behavior of Inconel 718 in Horizontal Orientation [30]

Helmer et al. [29] reported the microstructure gradient in build direction in terms of grain size (Figure 14). Attributed to growth competition between differently oriented grains they report coarser grains closer to the top of the build [29].

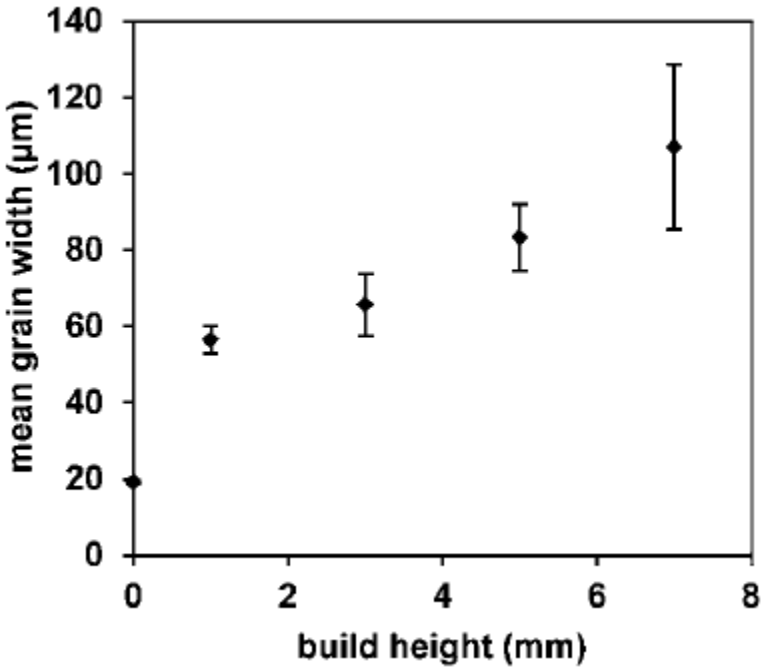

Figure 14: Grain Growth in Build Direction [29]

From Standard Strategies to Texture Engineering

The studies mentioned above all report the common columnar grain growth. As the grain structure is dependent on processing parameters [17], [18],[19], [29] and

columnar grains were not always optimal e.g. if the loading of the parts is not oriented along with the texture, further investigations designed to come up with alternatives to the melt theme that produces the columnar structure e.g. the standard Arcam melt theme. First approaches to develop new build themes focus on development of delamination and porosity free builds as goals for sufficient scan strategies without looking at microstructural and mechanical performance [28], [29], [5].

One strategy to achieve such melt themes in powder bed AM is reported by Kamath [28]. They combine simple simulations with special line scan experiments in order to efficiently narrow down the design space for non-porous AM samples. Tilted baseplates were used to investigate the effect of different layer heights. Thereon line scans were performed with various parameter settings. Only if the parameter combinations result in solid lines it is assumed that a promising combination is found which can then be used to be evaluated in larger builds. This method allows a highly efficient way to depict correlations between speed, power and density. The method by Kamath [28] comes up with promising general approaches for high-throughput process development by increasing the experiments complexity step by step while narrowing down the design-parameter-space.

Coming back to Inconel 718, the strategy of Medina et al. [5], already mentioned above, not only proposes methods to evaluate powders but also covers recommended steps for melt theme development for Inconel 718. It is at first necessary to conduct smoke tests to identify the maximum current to prevent smoking of the powder which occurs in exceed of the critical limit of the charge distribution density of the powder. Furthermore, as the powder needs to be pre-sintered, the optimal sintering conditions need to be assessed. Also, appropriate start plates have to be tested. The top surface finish is influenced by the focus offset of the beam which is resulting in the variation of the beam spot size and the energy per unit area. Therefore cube shaped samples for assessing the influence of different focus-offsets were proposed. Presumably the surface quality is

also influencing the delamination of the layers. Medina et al. [5] refers to the speed function as the most important process variable next to focus-offset. This function is explained to be taking care of the correlation of beam current, velocity and line scan length. Higher values result in a higher deflection speed and therefore less melting-energy. If this energy is too low, potentially not the whole layer thickness – a variable itself – is melted which leads to delamination. The method by Medina et al. [5] concludes with evaluating thermal shrinkage at cool-down and a standardized confirmation build. The results of applying this method are high dense and delamination free builds. No attempt is taken of addressing further microstructural and mechanical performance features.

Helmer et al. [29], while researching processing windows for non-porous and delamination free builds, proposes theory on how to restrict columnar grain growth. In another publication Körner et al. [17] introduces methods to either produce textured columnar or texture-free fine grain structures.

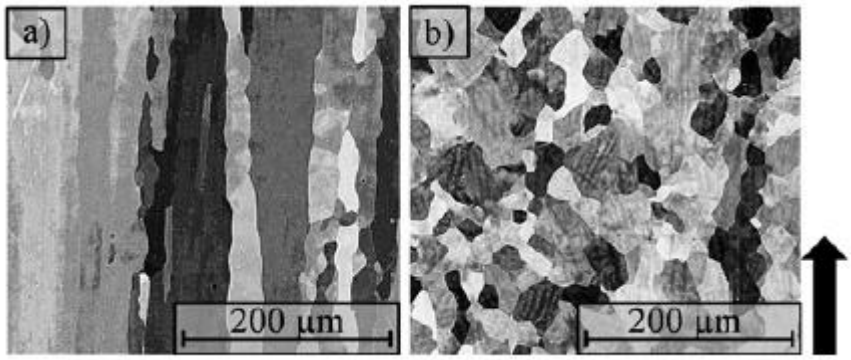

Figure 15: Different Grain Structures in EBM Builds [17]. The Black Arrow Indicates the Build Direction

Dehoff et al. [18] reports that varying the scan pattern from a line to a spot melt mode helps to alter the grain size as well as the degree of texture. In another publication, Dehoff et al. [19] comes up with site specific control opportunities for grain structure in EBM builds (Figure 16).

If line scans are used, further parameters are the width of scan, layer height. Porosity can form by applying an inappropriate scan spacing or scan pattern. Furthermore a special outgassing step is applied according to [2].

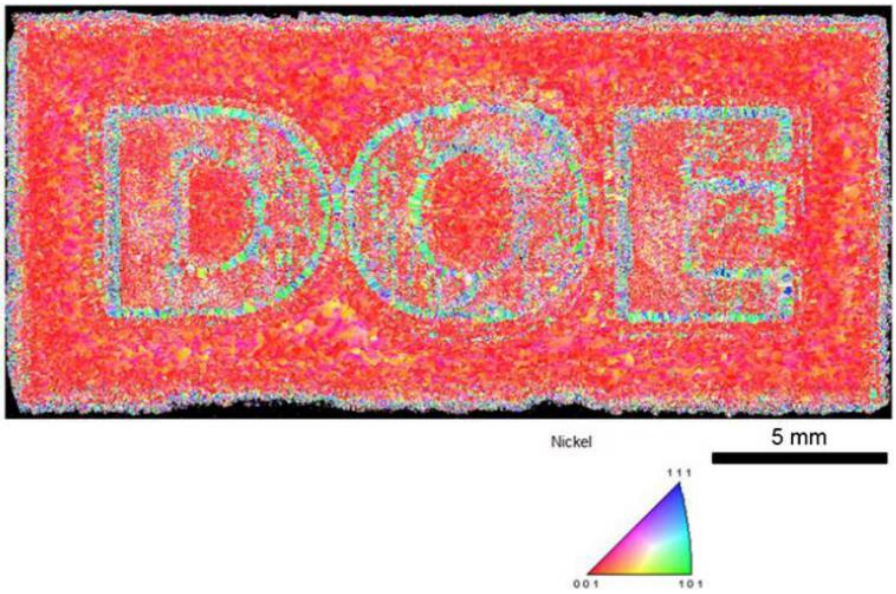

Figure 16: Site Specific Control of Grain Structure [19]

Part Geometry

The part geometry is also influencing the resulting microstructure locally as it is affecting the time per layer which depends on the area that has to be scanned to generate the respective part geometry and also influences the temperature history of each location. The hold time is dependent on the total height of the build. Also, the cooling time from beam to build temperature relates to the melted area around the respective spot. As experienced in previous builds by ORNL [20], altering the part geometry has a huge influence on the degree of warping of the base plate.

Part geometry affects the grain structure [29] and the dendrite structure [30] as the temperature history (time per layer, hold time) depends on size and geometry of the build. It also affects the delta phase, laves phase and secondary carbide structure as these phases precipitate in the temperature regime between melting and hold temperature and also depend on the time on that temperature which depends on the size of the build. Sames et

al. [2] noted in their study on microstructural heterogeneity in EBM Inconel 718 that precipitation behavior varies along the build direction. Strengthening phases precipitate below hold temperature and therefore are only dependent on cool-down rate (scan strategy) and not on part geometry (time at temperature).

Heat Treatment Assessment:

Post build parameters proved to be vital to make up for as-built irregularities in EBM microstructure [30], [16]. HIP is therefore often used to make up for porosity and is mainly influencing through temperature, time and pressure. Additionally EBM Inconel 718 is usually solution treated and aged by a one-step solution treatment and a two-step precipitation initiation and aging treatment as discussed above.

The purpose of HIP treatments is to eliminate internal porosity and delamination effects which are therefore the focused related structural features addresses by HIP. HIPing is done at temperatures sufficiently high to dissolve the precipitates but strengthening phases were reported to form in the succeeding cooling step.

Next to studies on powder requirements, general build features and development of specific build parameter for various tasks, post build studies have been performed recently. One of them, published by Unocic et al. [13] evaluated EBM Inconel 718 in three conditions: Next to the as-built state, samples have been tested after hot isostatic pressing and following a combined HIP and heat treatment cycle. The HIP step was performed for two hours at 1200°C. Aging treatment was done directly after the HIP step without applying the usual solution treatment step. The precipitation initiation step was performed at 720°C for eight hours, followed by a furnace cooling and another eight hours and 620°C aging step. Afterwards the material was cooled in air. Tensile testing was performed at a strain rate of 10^{-3} 1/s in room temperature (RT) and at 650°C. HIP treatment was reported to cause considerable grain growth on the build conditions [13] and dissolved the precipitates. But strengthening phases were reported to form in the

succeeding cooling step. The heat treatment was reported to trigger γ" precipitation and growth of both γ" and γ'. Also δ phases were reported to form along the grain boundaries. Tensile Prosperities are shown in Figure 17 and Table 4 for comparison purposes. They show no improvement in ultimate tensile strength but rather a decrease in mechanical properties due to reduced ductility. Tests have been performed in vertical orientation.

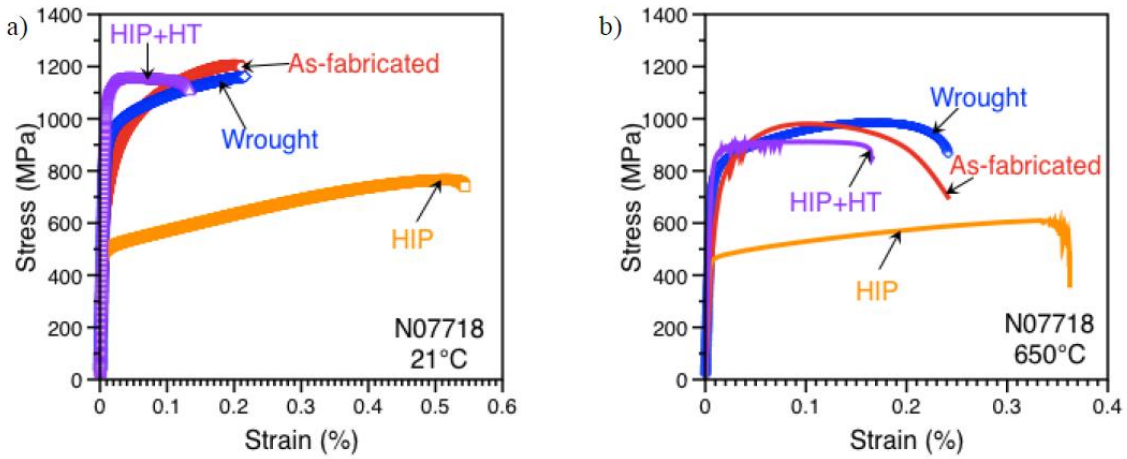

Figure 17: Stress Strain Curves of EBM Inconel 718 with different processing conditions in Comparison to Wrought Inconel 718 [13]

Table 4: Tensile Results of EBM Inconel 718 with different processing conditions in Comparison to Wrought Inconel 718 [13]

Specimen	T (°C)	Strength (ksi)		Strength (MPa)		Elongation %	
		YS	UT	YS	UT	Uniform	Total
Wrought	21	127	169	876	1165	24.4	26.3
As-built	21	97	175	669	1207	19.8	21
HIP	21	69	111	476	765	50.9	54.1
HIP+HT	21	150	167	1034	1151	3.5	12.5
Wrought	650	103	144	710	993	15.8	28.2
As built	650	90	142	620	979	8.6	25.3
HIP	650	60	83	414	572	28.9	32
HIP+HT	650	118	132	814	910	8.7	16.1

Another study on post-built treatment was published by Strondl et al. [21]. The material has therefore not been HIPed but solution heat treated at 1000°C followed water quenching and a subsequent two step heat treatment at 718°C for eight hours and furnace cooling to 621°C which was hold for another ten hours and finally cooling in air. The solution treatment temperature in that study was too low to dissolve all δ phases precipitated by the applied scan strategy.

Strondl et al. [21] reported an interesting microstructural feature, the stringer porosity (see Figure 18).

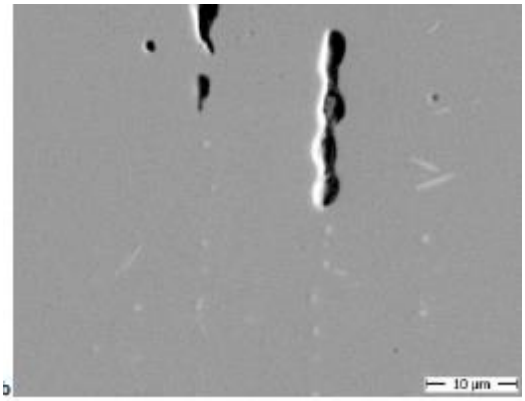

Figure 18: Stringer Porosity Reported by Strondl et al. [21]

This pores were elongated in build direction and reported to be detrimental for the elongation when tested perpendicular. The horizontal shape of these stringer pores is reported to be round and they were attributed to former dendrite structure. Next to the vertical tests [13], this study contains tensile tests on horizontally oriented samples. Test results for comparison can be found in Table 5.

Table 5: Tensile Test Results by Strondl et al. [21]

Table 3 Results of tensile tests perpendicular and parallel to layers in as processed condition and after heat treatment

	Without heat treatment		With heat treatment	
	Parallel	Perpendicular	Parallel	Perpendicular
UTS, MPa	1060±26	929±20	1238±22	1232±16
YTS (0·2), MPa	822±25	744±44	1154±46	1187±27
Elongation, %	22	5·5	7	1·1
Area reduction, %	25	12	14	5

The latest study on post processing EBM Inconel 718 has been published by Kirka et al. [16]. As the material used for this thesis study has been built by the exact same processing parameters (except for build geometry) and in the same facility as the one used for Kirka et al. [16], it has the highest relevance in terms of comparability to this study. Tensile tests have been performed in both vertical and horizontal orientation

and at room temperature as well as at elevated temperatures of 650°C. Other than in the study by Strondl et al. [21], the builds did undergo a HIP treatment for four hours at 1200°C – two hours longer than by Unocic et al. [13], but other than this, the study of Kirka et al. [16] contains a solution treatment of 1066°C for 80 minutes. Precipitation initiation has been performed at 760°C for ten hours followed by another ten hours of aging at 650°C. Kirka et al. [16] showed, that the inhomogeneous microstructure and mechanical properties reported in an earlier study [30] (see Figure 13) have been successfully homogenized and the mechanical properties of the lower levels have increased to those already found at higher levels in as-built condition (see Figure 19).

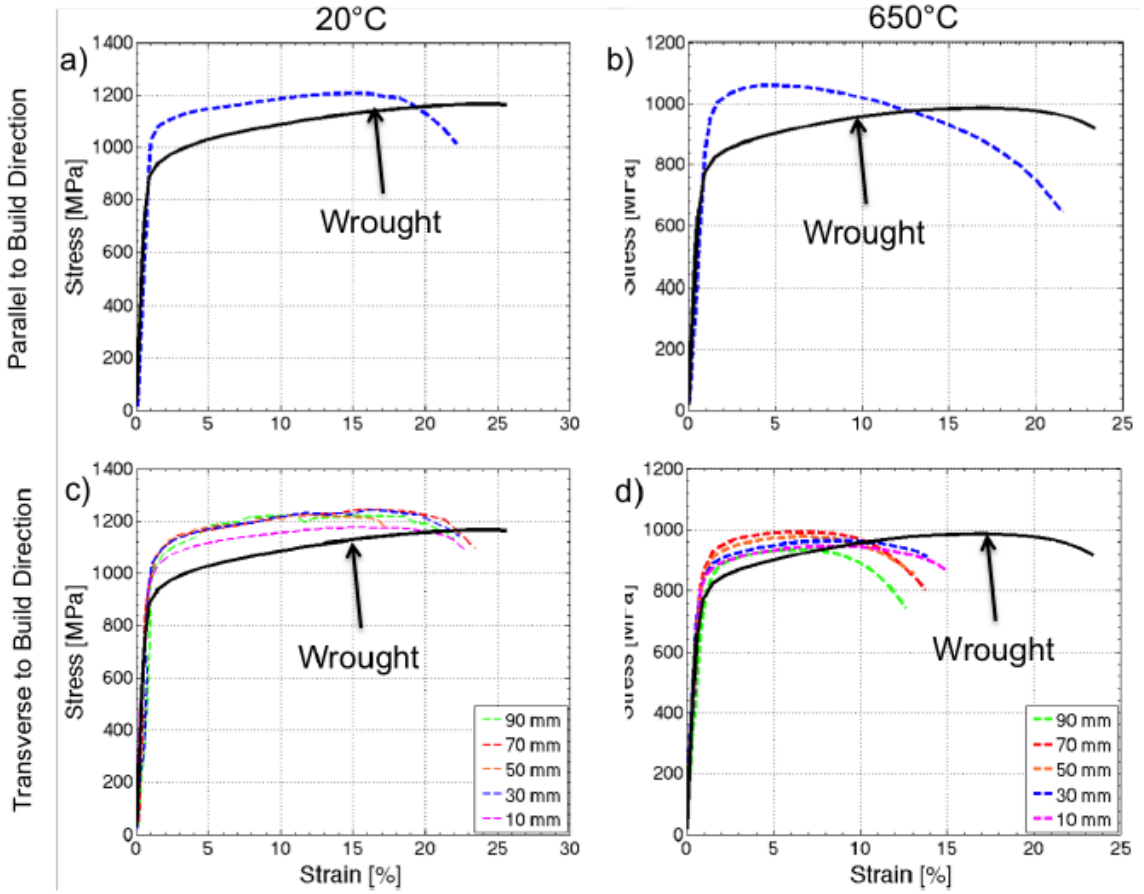

Figure 19: Post-Processed Reference Conditions [16]

Elongation exceeding the AMS 5383 industrial standard of 5% for cast Inconel 718 [16] have been reported on all tests performed at 650°C. This findings are in line

with what Unocic et al. (Table 4) and Strondl et al. (Table 5) showed for the elevated temperature tests. Only Strondl et al. [21] experiences low ductility in heat treated state, attributed to stringer porosity. The as-built columnar grain structure has been retained through applying the heat treatment of Kirka et al. [16] and – other than in the results presented by Unocic et al. [13] no considerable grain growth was detected for the microstructure produced by the considered scan strategy. Furthermore no extensive porosity in the as-built condition have been reported. As one of the conclusions [16] recommends further investigations on post processing parameters in order to optimize the heat treating of AM Inconel 718.

Strain Rate Dependent Behavior

Since Inconel 718 is often targeted for high temperature applications, mechanical properties need to be measured at elevated temperatures. Most materials plastic deformation behavior is rate dependent at these temperatures. Therefore this dependence needs to be measured so it can be understood, optimized and taken into account for application in structural parts.

In many of those high temperature applications like turbine blades tight tolerances mainly in the spacing between turbine blades and the engine housing [51] are needed and therefore a high resistance against slow deformations at lower stresses is one of the main design goals that high temperature parts have to meet.

Constitutive Viscoplasticity Model

A constitutive model that is often applied [51], [52], [21] to describe secondary creep is the Norton power law creep equation in the form [53]:

$$\varepsilon'_{ss} = A * \sigma^n \exp\left(-\frac{Q}{R * T}\right)$$

where ε'_{ss} is the creep strain rate, A is a creep constant, σ is the applied stress, n is the stress exponent, and Q is an activation energy for creep [52], R (=0.008314 kJ/mole-K) is the universal gas constant and T is the absolute temperature.

In the following deformation processes will be considered at only one temperature (650°C). Therefore the influence of the temperature dependent term $\exp\left\{-\frac{Q}{RT}\right\}$ will not be considered separately and included in a variable K together with the creep-constant A. The simplified constitutive model then has the form:

$$\varepsilon'_{ss} = \mathrm{K} * \sigma^n$$

with

$$K = A * \exp\left\{-\frac{Q}{RT}\right\}$$

Creep Strengthening

Precipitation of the strengthening phases γ' and γ'' has a significant influence on the creep strengthening in nickel-base superalloys. Flow stress increase for the same strain rate with the increasing volume fraction of the γ' precipitate in nickel-base superalloys [51] and Reed [51], [54] shows a dependence of the precipitation strengthening in nickel-superalloys on grain size in a way that larger grains promote precipitation strengthening against creep [51], [54]. The strengthening phase γ'' is known to coarsen and to transform to δ phase at elevated temperature and time. This could lead to a decrease of the creep hardening and therefore to a decrease in Norton power law exponent n.

As mentioned above creep damage through cavitation at the grain boundaries could lead to creep rupture. Therefore the reduction of grain boundary area with increasing grain size is relevant [51]. This is in line with Pieraggi et al. [55] reporting that rupture time in stress rupture tests is proportional to grain size of Inconel 718. Also, they report that δ phases have a significant influence on rupture time which have a deleterious effect if they are acicular. Carbides and nitrides have been reported not to have a

significant effect [55]. The above discussion on the influence of grain size with the result that larger grains are beneficial in terms on creep performance stands in contrast to the goal to remove grain size for better strength and fatigue life [55].

Published Test Results

Relative few studies have been published on creep behavior of EBM Inconel 718. Next to tensile tests discussed above, Strondl et al. [21] provides compression creep data on the post processed EBM Inconel 718. The tests have been performed above the typical use temperatures of Inconel 718 at 800°C. Norton power law exponents have been reported to change from 4 at lower stresses to 10 at higher stresses (Figure 20). Tensile creep tests have been performed but failed without giving good results attributed to the porosity.

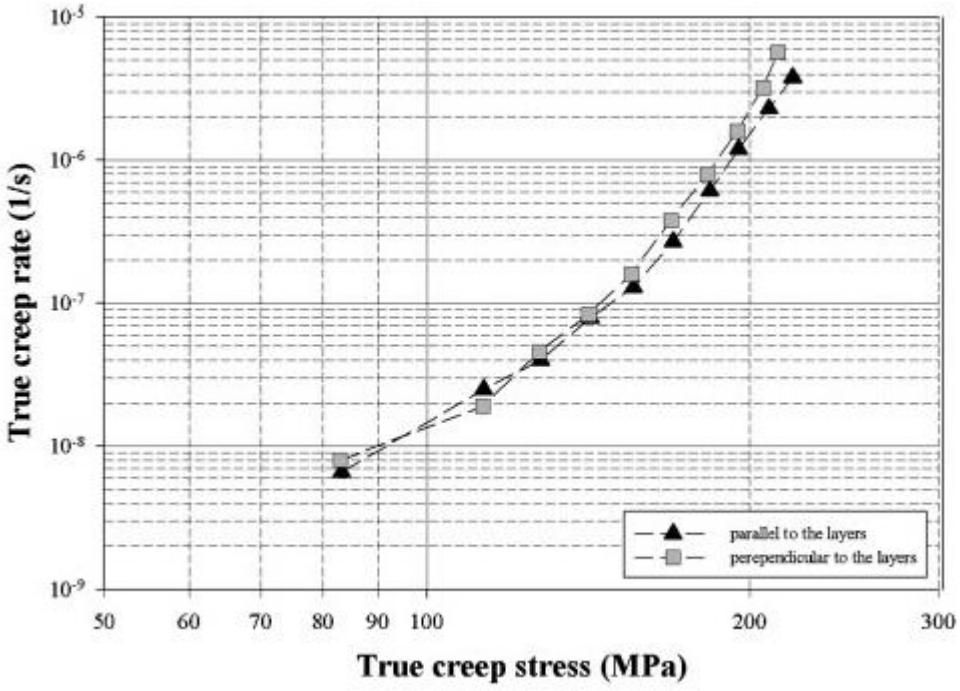

Figure 20: Compression Creep Results on Solution Treated and Aged EBM Inconel 718 at 800°C [21]

The rate dependent flow curves of annealed Inconel 718 at high temperatures between 900°C and 1050°C on strain rates between 0.1 1/s and 0.0005 1/s are shown in Figure 21 [56]. Next to the significant increase in flow stress contingent on the increase of strain rate by the order of magnitude and the decrease of flow stresses with temperature.

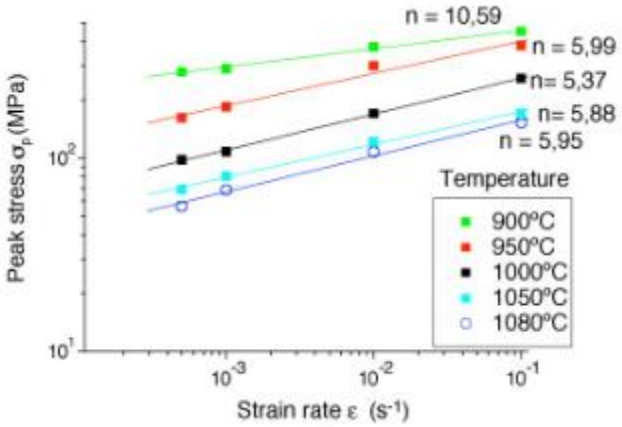

Figure 21: Double Logarithmic Plot of Strain Rate and Temperature-Dependent Behavior of annealed (1010°C / 1h) Inconel 718 [56]

The creep exponents for these temperatures illustrated by Figure 21 does not vary significant for temperatures above 950°C. Lower temperatures reveal a bigger strain exponent. At 900°C the strain exponent is about double the value observed between 950°C and 1080°C. This indicates that the rate dependency decreases at lower temperatures. The conclusion that has been made by Thomas et al. [56] is that the increase in creep exponent n is related to the presence of hardening precipitates below their precipitation temperature.

In another publication on hot rolled Inconel 718 creep at 650°C a creep exponent at 650°C of n = 36.5 is reported [57]. This is significantly higher than what has been reported by Thomas et al. [56] at higher temperatures and points to significant creep hardening by precipitation.

Table 6: Creep Data for Hot Rolled Inconel 718 [57]

T (°C)	σ (MPa)	t_p (h)	$\dot{\varepsilon}_s$ (1/h)	t_r (h)	ε_r (mm/mm)
650	700	9.0	0.000024	225	0.0562
	750	6.00	0.0000406	92.70	0.0604
	814	0.25	0.00616	4.00	0.0612

CHAPTER III

OBJECTIVE AND METHODOLOGY

The following chapter gives an introduction to the primary objective for the presented research and the methodology that was found to best represent these research goals.

Objective

The target of this thesis – as indicated in the title – is the set-up of an efficient methodology for the investigation of Processing-Structure-Property Relationships for Additive Manufacturing of metal components. Ideally, a high-throughput methodology is desired to systematically adjust processing parameters and therefore generate a wide range of processing histories. It is aimed to establish a microstructure gradient library which makes it possible to integrate this range in processing histories in a single AM build. This library needs to be spatially characterized using relevant microscopy and mechanical property tests. The linkages between processing, structure and properties can be established enabling the design of the processing parameter for AM.

Methodology

In order to systematically integrate this objective in the state-of-the-art in the AM process for the targeted material, a specific workflow is necessary. A possible workflow is shown in Figure 25. First of all, the state-of-the-art in AM-fabricating the respective material needs to be analyzed thoroughly. This allows the identification of critical research which contributes to the development of the AM processing route for the respective material. Furthermore, this gives the opportunity to identify the processing parameters which shall be analyzed with respect to their influence on structure and mechanical performance. Experimental methods to apply this analysis are supposed to

meet the requirements demanded by the AM process, the targeted material and efficiency considerations. Moreover a systematic and efficient approach in order to set up an experimental design which patterns the selected parameter space is needed. The extend of the sampling has to be defined, based on the desired output and the affordable number of samples, both in terms of time and cost considerations. The test library then needs to be manufactured and post treated according to the experimental design. Afterwards the designed experiments have to be set up and the library has to be spatially evaluated. The resulting structural features and mechanical properties have then to be linked in an efficient way. Finally the outcome of this process should allow to draw conclusions about further research goals in terms of enhancing the state-of-the-art in AM. The following flow chart depicts the necessary steps discussed above.

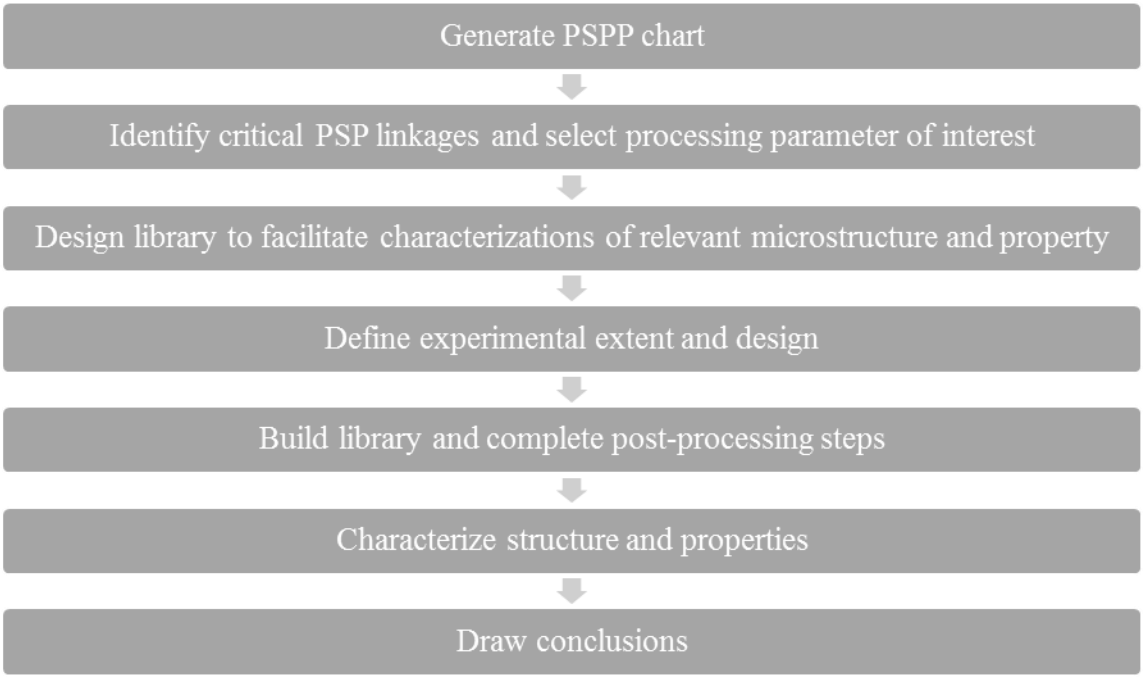

Figure 22: Flow Chart of Proposed Strategy

The following chapter discusses methods and tools to implement the required steps on an AM process and illustrates their use on Inconel 718.

Analysis of the State-of-the-Art

The PSPP chart illustrates and summarizes the researching entity's understanding on the current state-of-the-art based on preliminary projects and relevant published literature. This chart provides an important basis for identifying what is already known about the PSPP relations within a given material system with respect to a specific processing route. It is a valuable tool to divide this processing chain into parts for which the state-of-the-art already provides promising results and steps which need further consideration.

Applying it to EBM Inconel 718 this chart can be used to illustrate which parts of the processing column have already been investigated in previous work. These columns were highlighted by the bolt yellow frames and links in Figure 23. Basic strategies have been published addressing the powder quality. Furthermore various scan strategies have been developed recently which did provide promising grain structures, and did not show delamination and only minor porosity.

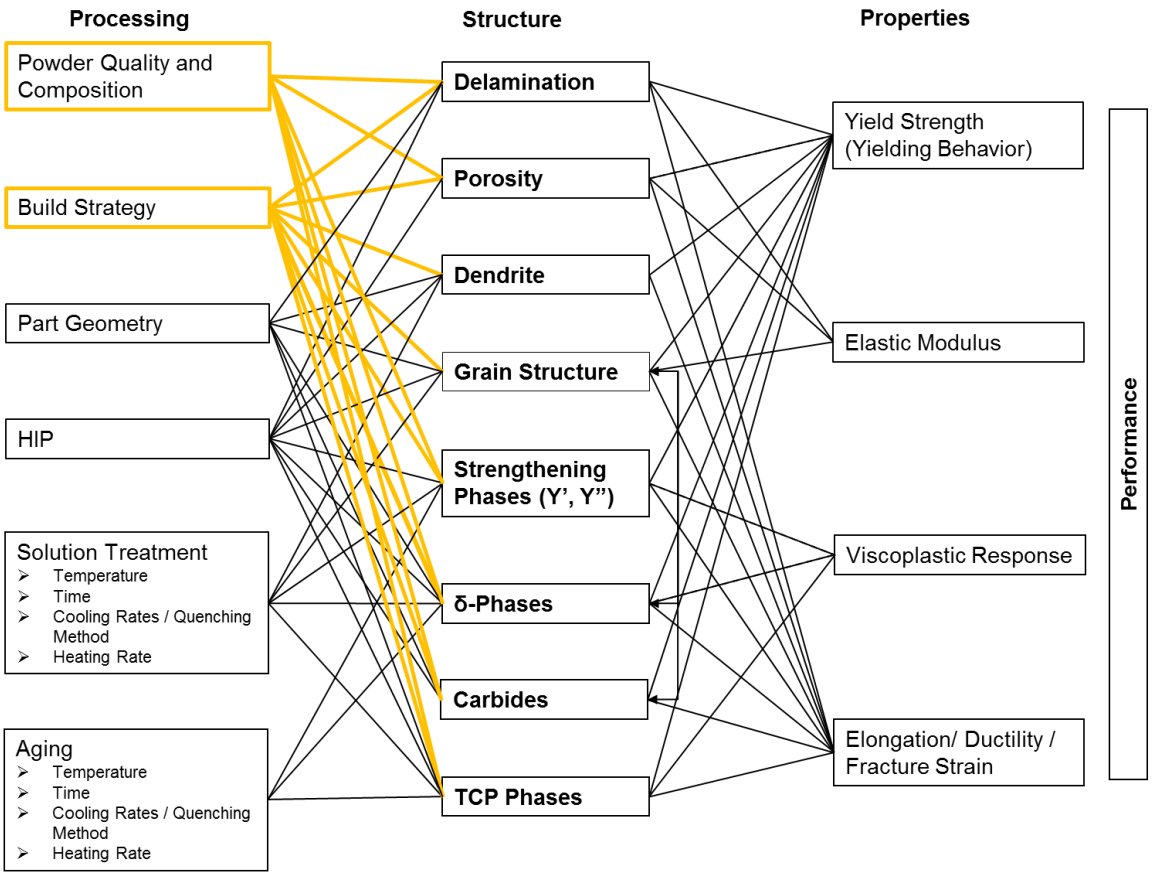

Figure 23: PSPP Chart of EBM Inconel 718 Illustrating State-of-the-Art in Processing the Alloy

Identification of Critical Research – Possible Parameter

As discussed above, the PSPP chart can be used to outline and discuss critical further tasks and therefore helps to identify where it is efficient to put resources in order to build knowledge.

Additionally the processing column contains possible influencing parameters for further studies. Furthermore the links to the structure column can help to derive critical structural analysis and mechanical tests related to the structure and properties which were linked to the processing steps attributed in the desired study. It therefore also illustrates what is not affected or not known to be affected by the considered processing steps.

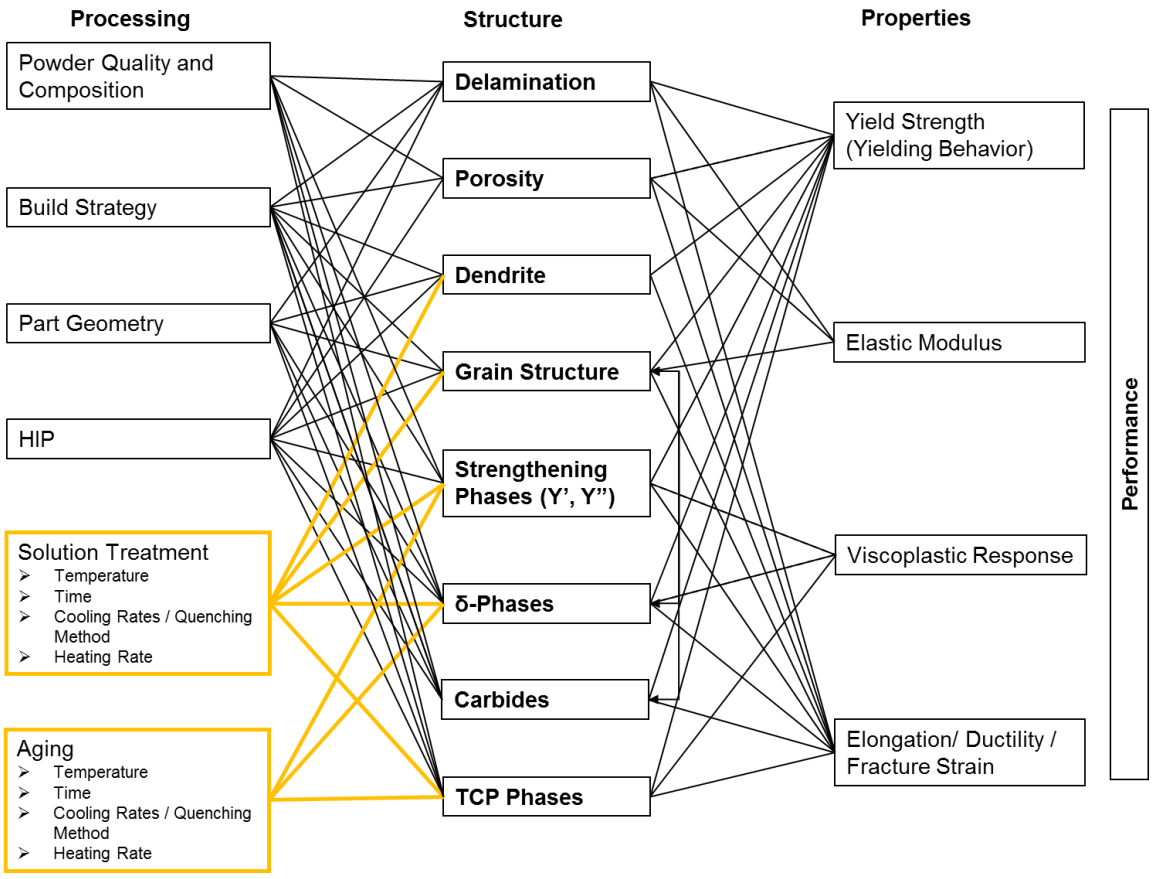

Figure 24: Further Tasks

Further tasks for EBM Inconel 718 PSPP research are illustrated in the PSPP chart (Figure 24). According to the state-of-the-art, melt themes are accessible which showed few porosity and promising grain structures. Nevertheless, microstructure gradients form in build direction due to variation in thermal history. Furthermore, it has been reported that varying the direct AM parameters of the build strategy (as anticipated in the original objective) is not feasible for conducting mechanical property studies as most of their combinations lead to extensive porosity. With this circumstance it is considered inefficient to build a test matrix for comparably large mechanical test specimen.

On the other hand experiments using standard heat treatment processes developed for forged parts achieved improvements in mechanical properties when applied on AM structures. The review on heat treatment effects for Inconel 718 also showed that the heat

treatment effect is dependent on the prior manufacturing process. Therefore heat treatment schedules developed for forged Inconel 718 cannot be expected to be optimal in terms of EBM. Other than for forged material EBM heat treatments additionally need to fulfill the requirement of homogenizing the microstructure gradients found in as-built condition.

The PSPP chart illustrates that heat treatment parameters are not suspected to influence the porosity of the samples. Therefore HIP is applied equally throughout the study. Porosity on the level observed in preliminary studies on non-HIPed as-built samples of the same processing history was found to result in good ductility [30]. Furthermore no fatigue or long-term creep experiments are planned for this study and instead mechanical experiments that provide an indication of these properties at much less time. For the sake of cost-efficiency and based on this argumentation it was agreed on simulating this HIP step. This means that the temperature cycle is applied on the samples to capture its influence on the microstructure. On the other hand, no pressure is applied on the samples which could close eventual porosity for this, as mentioned above, is estimated to be negligible [20].

Next to those objectives the following aspects need to be checked: The post-processing steps should not affect the grain structure for which the melt themes are found to be targeted. As this study aims at high-throughput methods, new and efficient build geometries are anticipated to be designed. This provides the benefit that the influence of build geometry changes can as well be studied. Knowing about the influence of build geometry on AM structure (see Figure 24) gives justification for this measure because the preliminary research on standard heat treatments has only be performed on very few build geometries. Including the standard heat treatment parameter combination in this study is therefore anticipated.

Figure 24 shows the main parameters that contribute to the solution treatment and aging performance. For the demonstration of the further process, three of these

parameters are selected. First of all, varying the solution treatment temperature is desired as the aging treatment effect depends on the phase dissolution prior to aging. Furthermore, the literature review revealed that grain growth is likely if the solution treatment dissolves the δ-phase pinning the grain boundaries. Additionally, the precipitation initiation temperature is anticipated to be varied as the TTT chart shows that the congruent precipitation of hardening phases and the δ-phase is temperature dependent. Finally, the total aging time is to be varied in order to depict the risk of over-aging at aging temperature which as well represents the maximum use temperature.

Identifying these parameters to be addressed in the anticipated study is a fundamental step for the later definition of the wide range in processing history which is achieved by adjusting these parameters systematically.

Library Design

In order to design an Additive Manufactured test library, requirements of test samples need to be identified. Both mechanical test and structural characterization are needed to identify the PSPP relations. The following paragraph discusses the requirements and methods selected.

In terms of requirements for the mechanical tests the most important aspect, as denoted in the objective, is “high-throughput”. By this means an efficient method for test specimen preparation as well as time-efficient analysis and conduction of the tests are vital. Figure 25 shows a chart which depicts different property tests evaluated in terms of test preparation and data analysis.

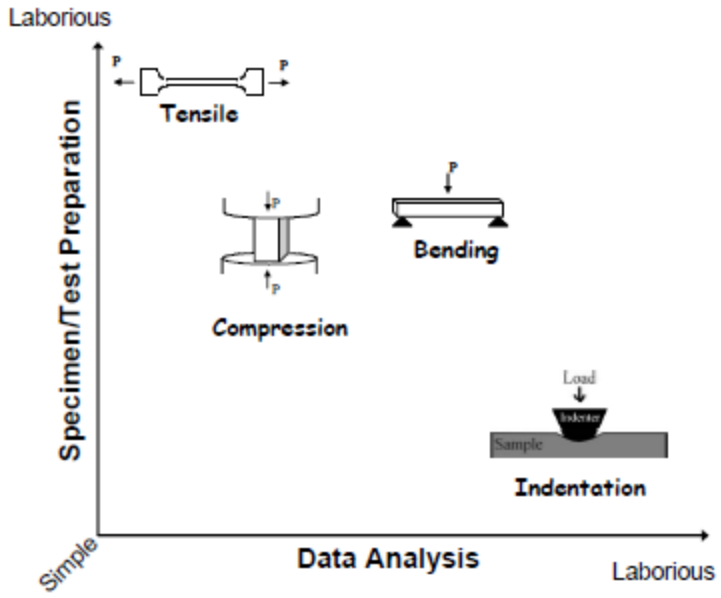

Figure 25: Test Opportunities [58]

It includes the opportunities considered for this study: tensile-, compression- and indentation tests. While tensile and compression tests are denoted to be more labors in specimen preparation, the indentation tests are by far more laborious in data analysis evaluating the indentation stress strain curves. Furthermore, tensile samples are generally larger than compression and indentation samples. This allows to build fewer samples in one build and therefore limits the opportunities regarding high-throughput.

Next to the aspect of high-throughput further considerations deriving from the AM process and the respective material have to be considered. As stated above, various extends of porosity have to be taken into account when dealing with AM. The mechanical tests are therefore required to depict major porosity's influence on the tensile result. Compression tests are less sensitive to major flaws and therefore compression stress strain curves do probably not well-represent the material's tensile behavior. Additionally it needs to be evaluated whether the material shows a tensile compression asymmetry. In this case the compression stress strain curves are also not conservatively representing the tensile behavior. Furthermore, the testing method needs to be stable with regards to minor porosity which needs to be encountered, even in good AM build qualities. Those pores

can negatively affect the stress strain curves derived from micro- or nanoindentation in case the indentation measures were taken in the regime of a pore. Knowing about these concerns with respect to the alternatives to tensile tests, further opportunities to enhance the test efficiency have to be considered. In contrary to indentation tests, tensile tests can be easily performed on elevated temperatures. Most materials show rate dependent flow-behavior at these temperatures. To determine this rate dependency, usually multiple tensile tests are needed to be conducted on various rates. One opportunity to enhance the test efficiency in suchlike situations is the use of strain rate jump tests. Applying this test method, the rate dependent behavior can be studied with one instead of multiple individual samples for each rate. Previous published studies [52] report the ability to test five rates on one sample instead of using five tensile samples.

Microstructural analysis needs to be encountered in the study. The first question regarding the required test sample is the area recommended for performing metallographic analysis. According to ASTM E112 [59] a minimum test plate of 12 mm x 12 mm is a general recommendation. Mostly, AM material is not a homogeneous as materials generated by traditional processing routes usually are. On one hand, a test library therefore needs to provide the option to assess microstructure on different sectioning planes. Anisotropy effects such as those recognized in build direction can be sufficiently evaluated by using two metallographic planes – one horizontally and one vertically oriented to the build orientation. Furthermore, the non-homogeneity in AM microstructure enforces different measures than those applied for traditional processing routes which provides higher homogeneity. Traditional methods assess microstructure throughout the whole considered part. Those are averaged and the results are statistically evaluated, assuming homogeneous microstructure throughout the entire build [59], [60]. This assumption doesn’t necessarily hold for AM. Therefore it is required to assess microstructure directly in the vicinity of the mechanical test specimen. Only this measure assures that the structure and property can be correlated without bias deriving from

averaging the microstructure over locations bigger than the one assessed with the mechanical test.

The library design is highly dependent on the geometry of the mechanical test sample. As both compression and indentation test samples indicate general restrictions in terms of applicability for AM the following chapter illustrates the design of a test library both applicable for tensile or strain-rate jump tests incorporating the general requirements stated in parameter selection and sample geometry discussion. Nevertheless, the requirements also hold for indentation and compression sample libraries.

Ordinary tensile sample geometries such as recommended by ASTM E8 are fairly large with respect to the AM build space of most systems. Therefore efficient library design for AM needs to put effort on reducing the size of the individual test specimen. Nevertheless, if high temperature experiments are anticipated, which is mostly the case for strain-rate jump tests, minimum size requirements are given. The sample dimensions need to match the high temperature extensometer's gage section. Furthermore, if induction heating is required to elevate the temperature, the sample needs to provide sufficient size in order to fit both the extensometer and the induction coil within the grips of the test frame. An additional way to reduce the library dimension is to use plate type tensile samples. In contrary to the common round samples, those plates are stackable closer to each other. Besides that, plate type samples provide flat surfaces which allow putting the metallography samples closer to the gage section. This fulfills the requirement that mechanical properties and structural features are supposed to be evaluated in the direct vicinity of each other.

For each test point, i.e. heat treatment condition, an individual set of samples is needed. This shall include three tensile samples and metallography samples for both the horizontal and the vertical orientation. The beneficial geometry of sheet type tensile samples allows to stack them very close to each other. The three samples will therefore be stacked according to Figure 26. The metallography samples will then be cut out of the

gage section before slicing the tensile samples from the parameter set (red in Figure 26). Additional samples in 90° orientation with respect to those metallography plates can be chopped of parallel to the tensile samples (orange in Figure 26). Cutting of material from the sides of the specimen is anyway required to assure a good surface finish of the samples while the surface finish produced by the AM process is not sufficient for that. The configuration in Figure 26 is anticipated to be used in horizontal orientation. This way two parameter sets can be stacked on top of each other in order to evaluate the microstructure gradient in build direction with respect to what has been reported in literature [30], [2]. Nevertheless the configuration can additionally be applied for vertically oriented samples. In that case it might be useful to additionally use horizontally cut off material as further metallography plates.

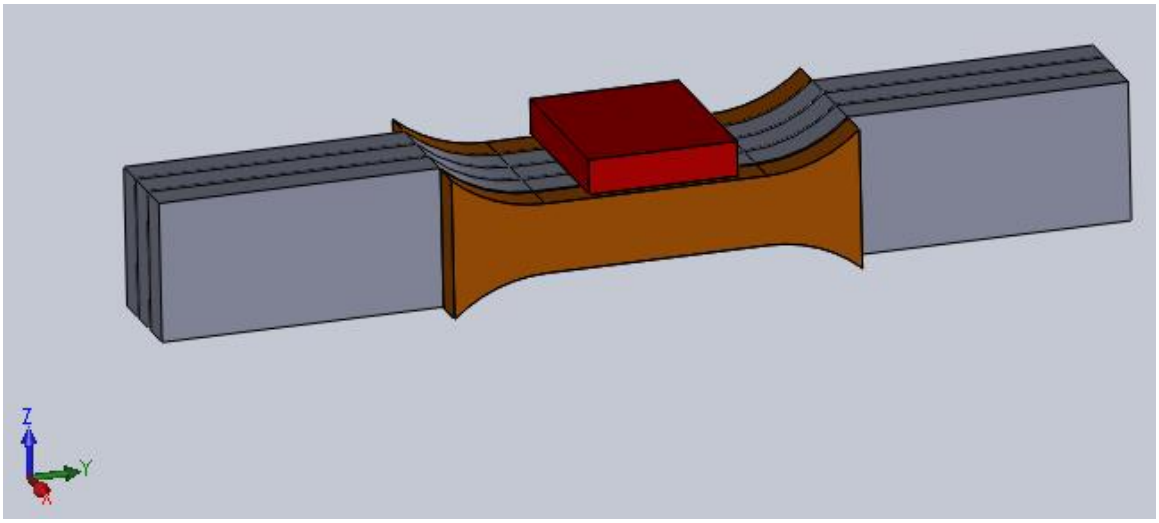

Figure 26: Parameter Set

A library design requires the efficient assembly of these parameter sets on the AM baseplate. This configuration is dependent on AM system specification. Figure 27 shows the configuration used in the presented study. The number of parameter sets is dependent on the number of tests anticipated for its evaluation. A smaller stack size results in a

flatter gradient library which reduces the risk as well as the costs associated with failing builds.

Figure 27: AM Build II on a 150 mm x 150 mm Baseplate

The following paragraph discusses the application of the general design guidelines stated above on Inconel 718. This alloy is designed for high temperature applications. Therefore the mechanical tests are required to be performed at elevated temperatures, e.g. the maximum use temperature of 650°C. At those temperatures tensile and compression tests are considerably easier to perform than indentation tests. Furthermore, Inconel 718 shows tensile compression asymmetry, as illustrated in Figure 28. These considerations, in combination with the general concerns of compression tests and indentation tests applicability for AM stated above, lead to the conclusion that tensile samples are studied in the following. As viscoplastic behavior is a relevant feature for

Inconel 718 at elevated temperatures, these tensile samples will be used in a strain-rate jump test.

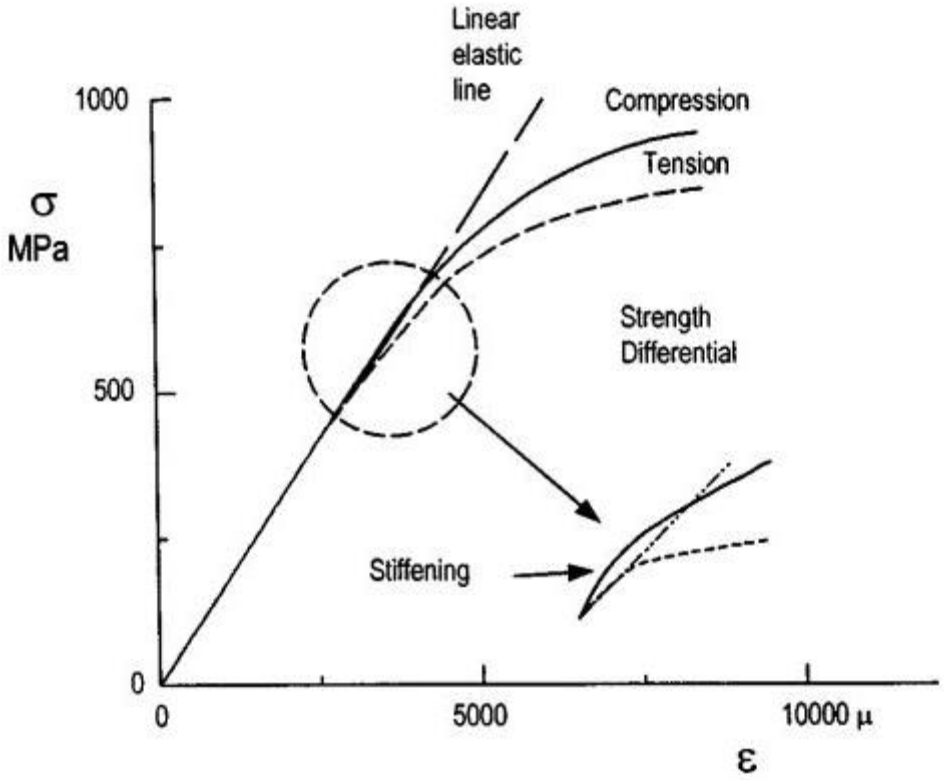

Figure 28: Tensile and Compressive Stress-Strain Responses of Inconel 718 [61]

Identification of Experimental Design

The PSPP chart in Figure 24 shows multiple parameter that were possible to be taken into consideration. A classical high-throughput approach would aim at testing all of these parameters on a sufficient amount of levels to gain insight into their effects and non-linear correlations with respect to the structure and the properties of the alloy. Doing so requires a highly efficient mechanical test method in terms of material consumption and testing time. Based on the considerations above, no valid high-throughput test method is in sight to the state-of-the-art that applies to AM. Especially the considered strain-rate jump test for higher temperature applications require a library that is too

material consuming for classical high-throughput purposes. Modified strategies were needed.

If higher efficiency is needed, it is desirable to identify the portion of the possible parameters which are effecting the structural feature and mechanical response most significantly. A high-throughput screening can help to get insight in that question and additionally provides information about the correlations of the influencing factors. This task is the purpose of Design of Experiments (DoE) test matrixes. The following paragraph therefore presents an approach using DoE to set up a basic experiment on the variation of post-processing parameter. Most DoE experiments evaluate the parameter range in two levels, a high and a low level which will then later be systematically combined with the respective levels of the other factors. This allows to identify whether the trend detected for the variation in the respective factor levels is correlating to the settings of the other considered factors.

These correlations have a significant relevance in material science. For example when a higher precipitation initiation temperature in a heat treatment precipitates a larger number of a secondary phase, the volume fraction of this phase is also dependent on the aging time for which the precipitates are allowed to grow. The aging time's effect on precipitate volume fraction is therefore correlating to the parameter "precipitation initiation temperature".

In addition to detecting significant factors and correlations, DoE approaches allow to apply a blocking factor. If there are parameters that are not of interest for the study but cannot be kept constant – for example if the samples used for the study belong to different batches – a blocking factor allows to determine whether the change in batch influences the results.

If significant effects are found from the DoE test, adding so-called center points (mean values of the factor levels) to the test matrix allows to perform a lack-of-fit-test. This helps to identify whether the effects found for the considered factors are linear or

whether non-linear correlations between processing parameters and quality features need to be expected [62]. In this case the DoE approach can be expanded to a Central Composite Design (CCD) which makes fitting a quadratic model to the data possible [63]. The option of this extension needs to be considered in advance because it is necessary to assure that the factor levels and combinations required for the extension are physically useful when setting up the basic test matrix. If higher non-linearity is expected for the factor's correlations and suitable high-throughput methods are available, further approaches have to be considered for expanding the test matrix. The DoE as well as the CCD matrix represent efficient and systematic approaches to evenly pattern and frame a multi-dimensional parameter space, independent of the number of parameters. Further increasing the density of test points can be done for example by using stochastic methods e.g. latin hypercubes [63].These extended test matrixes then are applicable for Artificial Neural Networks ANN modelling. Beginning the investigation with a framing DoE approach not only helps to investigate the significance of the considered parameters, but could also be useful to evaluate or calibrate the high-throughput test method to the reliable (high fidelity) tensile test data.

A critical step when it comes to applying DoE to material science tasks, e.g. heat treatment studies, is fitting reasonable data to the test matrix. DoE software [62] provides the general test matrixes containing factor levels and their combinations for a selected number of parameters and blocks.

For the easier handling of the level-combinations in later steps factor levels are often coded. A widely used code is to call the low level (–) and the high level (+). That can then be extended to (a); (-); (0); (+); and (A) if levels below, between and above the (-) and (+) levels should be evaluated in a CCD test matrix. The ratio between the DoE levels and the added CCD levels are predefined for statistical reasons [63].This is the reason why the CCD extension needs to be preliminary encountered in order to assure that the values which represent these extensions are reasonable, too.

The overall goal is to keep all values within a reasonable range and as well providing a variation large enough to expect significant change. Additionally, capturing the parameter's settings of preliminary studies (e.g. standard heat treatments) with the test matrix is necessary to enable the comparability (reality check) to those preliminary results. Defining the required values for each parameter individually is not sufficient, but rather it is needed to evaluate the risk of unreasonable or unfeasible combinations within the test matrix.

The following paragraph illustrates the set-up of the heat treatment experiment for the considered alloy EBM Inconel 718. Based on the number of samples provided for the presented research, the DoE approach on a three factor full factorial test matrix of two levels with the option to extend it to a CCD is selected. Figure 29 gives an illustration of this test matrix. Each of the three factors A, B, C is in this case tested on the high (+) and the low (-) level, visualized in an A, B, C coordinate system. This results in the eight necessary test points y1 to y8.

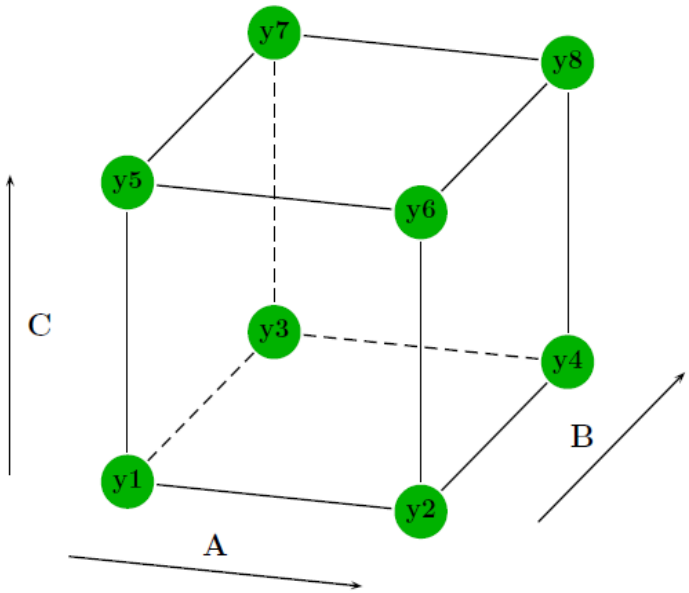

Figure 29: Design of Experiments Test Matrix [63]

With the extension to the CCD (orange points y10 to y15 in Figure 30), in total 17 test points were needed. This includes three center points (purple point y9 in Figure 30) for an eventual lack-of-fit-test. An additional test is desirable to test the non-heat-treated condition of the as-manufactured AM material, serving as a reference point.

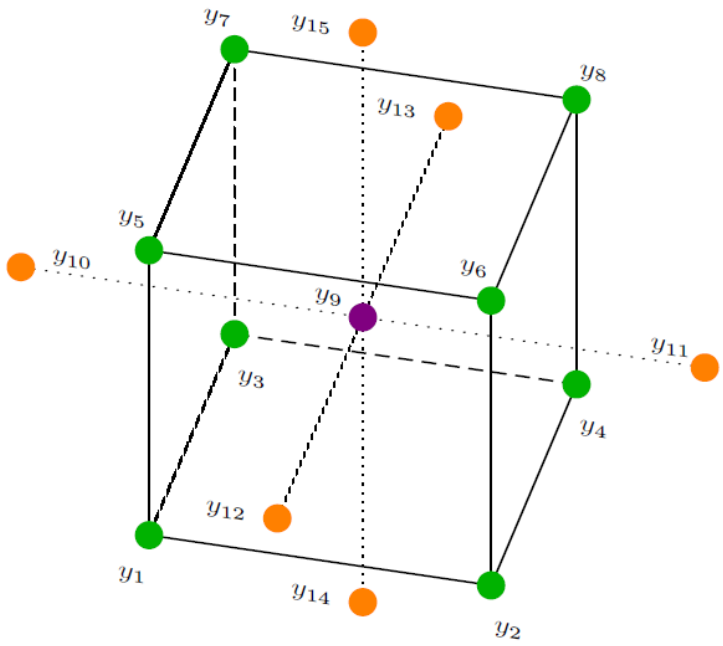

Figure 30: Central-Composite-Design Test Matrix [63]

As illustrated in Table 7 the DoE software provides factor level combinations for the CCD test matrix, e.g. Figure 30. The given ratios need to be linked to the parameter ranges of the heat treatment experiment.

Table 7: Normalized CCD of Three Parameters [62]

	Pattern	ST Temperature	A Temperature	A Time
1	a00	-1	0	0
2	−−−	-0,594603558	-0,594603558	-0,594603558
3	−−+	-0,594603558	-0,594603558	0,5946035575
4	−+−	-0,594603558	0,5946035575	-0,594603558
5	−++	-0,594603558	0,5946035575	0,5946035575
6	0a0	0	-1	0
7	00a	0	0	-1
8	000	0	0	0
9	000	0	0	0
10	00A	0	0	1
11	0A0	0	1	0
12	+−−	0,5946035575	-0,594603558	-0,594603558
13	+−+	0,5946035575	-0,594603558	0,5946035575
14	++−	0,5946035575	0,5946035575	-0,594603558
15	+++	0,5946035575	0,5946035575	0,5946035575
16	A00	1	0	0

Based on the information about precipitation temperatures and reported heat treatments stated in the chapter 2 of this thesis, the given CCD can be applied to the parameter window.

For solution treatment, the standard heat treatments recommend temperatures between 926°C and 1066°C (see Table 3). Previously reported results show, that the lower range of these temperatures were not sufficient to dissolve all δ-precipitates (see Figure 6). On the other hand, the higher range, above the δ-solvus temperature is reported to cause grain growth (see Figure 8 and Figure 9).

Precipitation treatment temperatures of the standard heat treatments were 720°C and 760°C (see Table 3). For this study they shall be limited by the aging temperature of 650°C (high temperature heat treatment in Table 3) which will not be varied and which also represents the testing temperature.

To get insight into the influence of time, the total aging time is considered in the study. It is specified in the standard heat treatments as 18 or 20 hours respectively (see Table 3).

The following testing scheme has been selected for the EBM Inconel 718 application: The temperatures of the lower standard heat treatment has been chosen to

represent the center point of the test. With 1010°C the upper end of the low level heat treatment's solution treatment range is selected (see Table 3). According to the TTT diagram (Figure 6) this is slightly above the precipitation temperature of the δ-phase. This data point will be tested three times to evaluate the lack of fit when applying a linear correlation model between the corner points and also to evaluate the standard deviation within similar heat treated samples. Doing this potentially allows insight into the spatially variance of the δ-dissolution temperature throughout the build. The high temperature standard heat treatment is selected to represent the "++–" values. This way, not only the actual heat treatment but also the effect of changing a single variable of this schedule can be explored. The set point "++– " is therefore selected to a solution treatment temperature of 1066°C, a precipitation initiation temperature of 760°C and an aging time of 20 hours (Table 3). This represents the heat treatment settings used by Kirka et al. [16] in a preliminary standard heat treatment of EBM Inconel 718 processed in the exact same processing condition.

The remainder of the values were then predefined by the DoE method and have to be checked whether they were reasonable. In solution treatment, the lowest value, which is included in only one parameter set is 920°C. This is slightly below the range proposed by the standard heat treatment (926°C, Table 3). The "-" value of solution treatment temperature is 955°C which is recommended within the lower standard heat treatment in Table 3. Additionally the highest level "A" is represented by 1100°C, which goes beyond the standard schedules as well but does not reach values where incipient melting should be encountered (Table 1).

The range of precipitation initiation temperature respects the limit which results from the aging temperature (650°C) on one side and is on the other side set with the limit of 787°C which is a temperature where a peak in γ" precipitation can be expected (Figure 6 c). Furthermore Figure 10 shows that a peak in yield stress is likely for temperatures in

this range which possibly is related to the concurrent precipitation of δ and strengthening phases.

The time values were selected independently from the standard treatments. Minimum Aging time is set to 10 hours which means doing no aging step at all and only applying the precipitation initiation step. This value is used for the (a) level in the extended test matrix. The (-) level is selected to 20 hours. This way, the standard heat treatment used by Kirka et al. [16] is included in the test matrix as the (++-) combination and serves as a reference point. On the other hand, aging time values above t_0 =20 h respectively illustrate the materials behavior after t-t_0 hours of life at 650°C (maximum use temperature). This way, the effect of over-aging can be studied and related to time at service. Table 8 sums up the selected levels of HIP temperature (HIP T), solution treatment temperature (ST T), precipitation initiation temperature (PI T) and aging temperature (A T).

Table 8: Selected Levels of Heat Treatment Schedule

	a	-	0	+	A	Delta	Unit
HIP T	1200	1200	1200	**1200**	1200	0	°C
ST T	920	955	1010	**1065**	1100	180	°C
PI T	653	680	720	**760**	787	134	°C
A t	10	**20**	34,7	49,3	59,3	49,3	h

As not only the single values of the heat treatments need to be reasonable, but also their combination in the test matrix, these have to be checked as well. Table 9 shows the core DoE test matrix. As two builds were needed to do these tests a blocking factor was added. The test matrix was set up using the software JMP Pro. This automatically gives out the test points in a randomized way, but sorted by blocks. The parameter-set ID therefore does not need to be randomized. Randomization is important as it prevents the factor effects from being overlaid by possible position dependencies within the build.

Table 9: Test Matrix for Heat Treatment Experiments of Inconel 718

Sample ID	Level Coding	Block	Solution Treatment Temperature [°C]	Precipitation Initiation Temperature [°C]	Total Aging Time [h]
III/YX/1	++−	1	1065	760	20
III/YX/2	−++	1	955	760	49,3
III/YX/3	0	1	1010	720	34,7
III/YX/4	−−−	1	955	680	20
III/YX/5	+−+	1	1065	680	49,3
III/YX/6	0	1	1010	720	34,7
II/YX/2	−−+	2	955	680	49,3
II/YX/3	+++	2	1065	760	49,3
II/YX/4	−+−	2	955	760	20
II/YX/5	0	2	1010	720	34,7
II/YX/6	+−−	2	1065	680	20

The test matrix' extension to the CCD can be achieved by using the following values:

Table 10: Test Matrix Extension for Centre Composite Design

Level Coding	Solution Treatment Temperature [°C]	Precipitation Initiation Temperature [°C]	Total Aging Time [h]
a00	917,5	720	34,7
A00	1102,5	720	34,7
0a0	1010	652,7	34,7
0A0	1010	787,3	34,7
00a	1010	720	10,0
00A	1010	720	59,3

At first, the as-built situation is examined. After that the center point and the two level DoE values (+ and – settings) were tested to gain insight into the significance of the changes and to evaluate correlations. Finally if the results of above tests are successful the A and a levels were added to establish the quadratic model.

Characterization of Structure and Properties

In terms of characterizing the structure and properties it needs to be assessed primary which sequence of tests is most efficient. Furthermore, efficient characterization methods need to be selected. The efficient mechanical test methods are already discussed

in relation to the library design. This paragraph additionally proposes efficient quantitative microstructure analysis.

Efficient Characterization Sequence:

The PSPP chart depicts the physical relations between processing parameters, structural features and mechanical properties. Processing parameters are influencing the structure of the material and the structure then in turn influences the mechanical properties. Therefore, the processing parameters only influence the mechanical properties indirectly. Facing this, the consequent sequence of characterization seems to be first testing the processing-structure-relation and then testing the structure-property-relation. However, it is not possible to directly adjust the structure in order to set up a systematical structure-property-test-matrix, but structure needs to be indirectly adjusted by varying processing parameters. Consequently, it is necessary to set up a processing-property-test-matrix (e.g. heat treatment – strain-rate jump test).

The main goal for this processing-property-test-matrix is to achieve a significant variance in mechanical properties which can be related to the microstructure. This can be anticipated by setting up the test matrix based on preliminary test results. However, it is not possible to guarantee the significance of the property's variation resulting from the test matrix. To ensure this, a complete understanding of the PSPP relations would be necessary which is actually the purpose and not the basis of this experiment. Conducting the processing-structure-analysis before ensuring that the process-property-variation is significant would be a risk, because a large number of structural features are necessary to be quantified to set up the PSPP relations. This is very laborious and therefore not time efficient. Also, this process causes considerable expenses.

In contrast the mechanical property tests are usually less time consuming once they are set up. It is therefore more efficient to first conduct the property test and evaluate the significance of the effects. This allows to start by analyzing the most likely structural

influence on these measured property values. Further, structural features then can be included into the test when the primary analysis does not explain the property variation sufficiently. This way a thorough understanding of the PSPP relations is accomplished in a target-oriented and therefore more efficient way than by following the physical sequence displayed in the PSPP chart. This paves the way for a top-down analysis.

Efficient Microstructure Characterization:

Next to efficient mechanical testing, which is already discussed in regards to the library design, efficient structural analysis needs to be performed on all structural features of interest. Porosity and delamination assessment can be done for example by automatically evaluating the volume fraction and number per unit area based on binarized optical microscopy images prior to etching. Furthermore the chain length for stringer porosity can be assessed in case such phenomena are observed e.g. as reported by Strondl et al. [21]. Grain size is for example evaluated by line counting on the etched metallographic samples in order to determine the average grain diameter or the average column diameter respectively. Precipitates can efficiently be analyzed by deriving their volume-fraction and number applying methods similar to the ones for porosity assessment on etched metallography samples. Nevertheless this eventually needs further shape detection algorithms as precipitates tend to overlap (Figure 4). As focusing on strain-rate jump tests and general strategy, the latter is beyond the scope of this thesis.

Drawing Conclusions

The mechanical test results can be evaluated with reference to the structural analysis on the one hand, and with respect to the other test points on the other hand. The latter analysis can be conducted either using the DoE related Analysis of Variance (ANOVA) and linear modelling or by setting up a quadratic model based on the CCD approach. Larger test matrixes can also be evaluated using Artificial Neural Networks.

CHAPTER IV

EXPERIMENTAL METHODS

The following chapter explains the experimental set-up for the anticipated experiments. First of all, the detailed geometry of the test library is explained, minding the requirements stated in the chapter Strategy. Finally the strain-rate jump test set up and the metallography methods used for this thesis are discussed. The chapter concludes with explaining the basic principles of data analysis using Design of Experiments.

Library Design

The following chapter discusses the sample geometry that is used for the presented study. Tensile and metallography samples are combined to a parameter-set in the configuration proposed in the chapter Strategy. Multiple of these sets will be produced in one AM build and will later be heat treated individually.

Tensile Sample

The strain-rate jump tests can be performed on standard tensile sample geometries such as proposed in ASTM E8. Nevertheless, the application in the given situation requires further considerations.

Specimen shapes and sizes are recommended generally by ASTM E8. These samples are comparably large and hence costly with respect to the limited build space in AM. Therefore a tensile specimen is designed that is smaller and yet meets necessary requirements proposed by ASTM E8. The specimen is selected to have a sheet type dog-bone shape. The sub-size specimen geometry proposed by ASTM E8 is comparably long with respect to the limited build space in EBM. Therefore a shorter alternative needs to be defined. Minimum requirements result on the one hand from the high temperature extensometer that has to fit on the gage section. ASTM E8 proposes a gage length of 25

mm. For the given situation, a half inch high temperature extensometer should be used what allows the reduction of the gage section to half inch or 12.7 mm. Additional limits on the minimum length of the sample result from the requirement that the experiment shall be conducted on elevated temperature. Thus, the sample needs to provide sufficient length for the application of the induction coil used for the heating. The length of the reduced section will therefore exceed the gage length. Instead of 32 mm as proposed by the ASTM E8, for the sub-size specimen 19 mm of reduced section length are selected. Figure 31 shows the final sample geometry used for the following study.

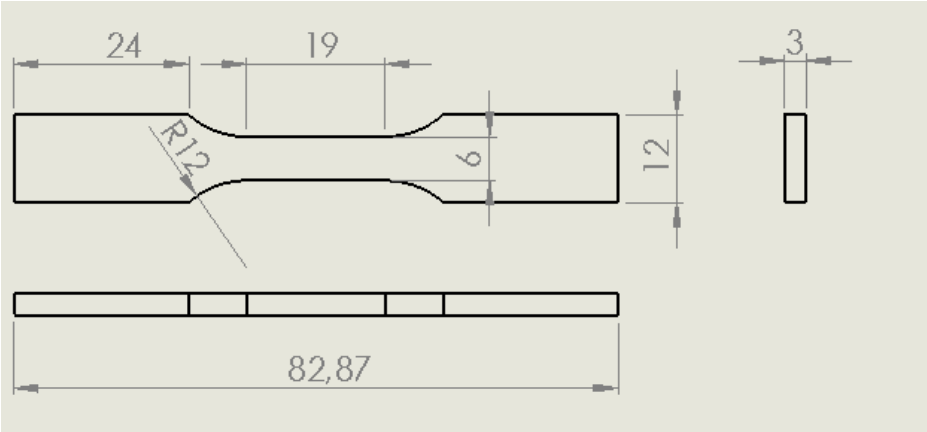

Figure 31: Adapted Tensile Sample Geometry

The width of the reduced section will remain at 6 mm proposed for the sub-size specimen [64] and the thickness is set to 3 mm in fulfillment of the ASTM E8 requirement of being below 6 mm [64]. By selecting 12 mm, larger radii at the shoulder of the samples are used than proposed in ASTM E8. To further decrease the specimen size, the grip length is reduced from 30 mm [64] to 24 mm. The grip width is therefore increased to 12 mm which assures a similar gripped area as for the ASTM sample.

Further requirements are that the specimen shall be symmetrical in width with the center line of the reduced section within 0.13 mm [64] and the radii of the filets shall be equal to each other with a tolerance of 1.25 mm [64]. Furthermore the centers of the fillet radii shall be on a line perpendicular to the specimen axis with a tolerance of 2.5 mm

[64]. The ends of the reduced section shall not differ in width by more than 0.02 mm [64]. Additionally ASTM E21-09 [65] requires that the axis of the reduced section needs to be straight within ± 0.5% of the diameter. The width of the sample shall not vary more than 0.5%.

Metallography Sample

Next to the more material efficient opportunities in stacking the samples, the main reason for using sheet type specimen is the flat surfaces provided by them. This way, metallography plates can be applied in the direct vicinity of the tensile samples. This assures that the observed mechanical properties are observed in correlation to the microstructure directly adjacent to where they have been tested. According to ASTM [66] sample sizes of 0.5 inch x 0.5 inch were sufficient for most metallography studies. As anisotropy effects were expected in AM material, metallography samples need to be included both in horizontal and vertical orientation.

AM Build

The configuration of the tensile and metallography samples which forms the parameter set is discussed previously in the chapter Strategy. As mentioned there, multiple of the parameter sets can be stacked above each other in order to test the material heterogeneity in height dependence. Figure 32 shows this configuration and the definition of the sample ID for each of the different types of samples. This ID will be combined with a parameter set ID. That way, each sample and test result can be located within the build. The parameter set ID begins with the number of the build: In the current study this varies from I to IV and will be expressed with roman numbers. ASTM [67] defines a standardized coordinate system for AM builds which will be used for the ID of the parameter sets. The build number is therefore followed by either XY for parameter sets in the XY plane of the coordinate system and oriented in X direction and YX for those oriented in Y direction. As multiple samples are build parallel to each other, a

further number is needed to count for the position of the individual parameter set in the build. This number starts with 1 at the origin of ordinates and counts in the direction of the second letter of the axis code. For example the parameter set ID II/YX/3 refers to the set that is taken from the second build of the study, is longitudinally oriented in Y direction and is the third parameter set in X direction. The sample ID is then combined to II/YX/3 T2;1 for the first tensile sample of the second layer taken from the parameter set of the example stated above.

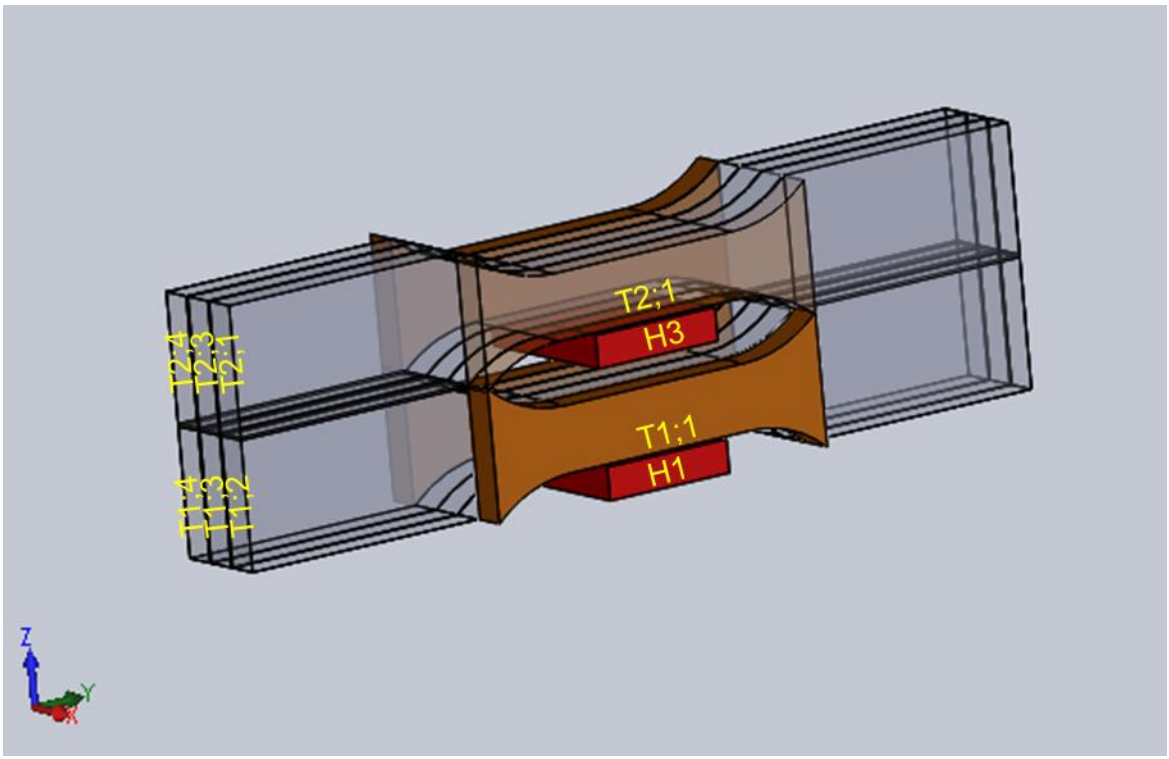

Figure 32: Nomenclature of a Double-Stack Parameter Set Section from each Block

The build space of the Arcam EBM system is 150 mm x 150 mm. Nevertheless, the system has been approved to provide better results when only the inner 120 mm x 120 mm are used. Blocks of 30 mm height by 83 mm length and 15 mm thickness were needed if two horizontal stacks (Figure 32) of the parameter set geometry shall be cut out of them. Using those blocks, 6 samples in YX direction and two samples in XY direction fit in one build (Figure 6). The parameter sets are cut form the base plate using a water cooled band saw. Afterwards, the samples, shown in above configuration (Figure 32) are

cut out of those blocks using wire Electrical Discharge Machining (EDM). In total 4 builds are made for the study. Higher stacks of parameter sets increase the risk of failing builds. Therefore only a double-stack is set up.

Furnace Set-up

Four furnaces are selected for efficiently performing the heat treatment study which is set up in chapter *Strategy*. The first necessary post-processing step is simulating the HIP treatment as discussed in *Strategy*. Thus, the samples are individually loaded to one zone tube furnace (MTI GLS 1600X), preheated to 1200°C. This furnace is sealed for vacuum and inertial gas applications and continuously flooded by Argon gas. Because the furnace sealing allows no application of load thermocouples, the time is measured after the built-in thermocouple reaches the temperature within the given tolerance according to industrial practice [68]. The HIP temperature cycle is applied for 4 hours in accordance with preliminary studies by Kirka et al. [16]. All samples are HIP-treated with the same conditions. The samples are loaded into the furnace on an Alumina boat as Graphite base plates were found to cause detrimental C diffusion in the samples which affects the chemistry [20]. After HIP treating, the samples are quenched in water to prohibit precipitation during cooling down. This measure is needed as the cool-down-rate cannot be controlled to resemble the real HIP process.

Afterwards the parameter sets are heated in a three zone tube furnace (Lindberg Type 59744-A) for the solution treatment study. Temperatures are applied individually according to the test matrix set up in the chapter *Strategy* minding the sample ID. For solution treatment temperatures above 1010°C, Argon flooding on the same rate as during the HIP step is used but without the availability of tube sealing. The temperature is held for 1 hour and 20 minutes after the load thermocouple, attached to the center top surface of the parameter set, reaches the set point within tolerance. For the given sample

geometry, heating to this level takes about 20 to 30 minutes. Afterwards the samples are quenched in water to conserve the phase dissolution. After HIP and solution treatment, the oxidation layer on the parameter sets is evaluated for the black and green color, referenced by Special Metals [12] to be the desired condition.

Afterwards the lot of 4 samples which undergo the same precipitation initiation treatment according to the DoE test matrix set-up, mentioned in chapter *Strategy*, are heated in atmospheric environment of a box furnace (Carbolite ELF 11006-230 SN) to the respective temperature. Again, load thermocouples are applied to measure the time at which each individual sample reaches the tolerance. From this point on, 10 hours of precipitation initiation treatment are conducted. Subsequently they are furnace-cooled to the aging temperature of 650°C and then directly transferred to a second box furnace (Thermolyne Type 10500) on 650°C. This allows increasing the efficiency of the heat treatment as the precipitation initiation treatment for another lot can be initiated in the higher temperature box furnace, while the first lot is aging. Samples were taken out of the furnace individually after the prescribed total aging time, defined in the test matrix. They were afterwards cooled in air.

Tolerances for the heat treatment are set to the same values as used for the heat treatment studies published by Kirka et. al. [16]: Temperature variance within 1% is considered good, within 2-3% is acceptable. Time variance within 10-15% is acceptable.

The schedule is visible in Table 11.

Table 11: Heat Treatment Set-Up

Step	Time	Temperature [°C]	Device
Heating	Load in hot furnace	20-1200	MTI GLS 1600X Argon atmosphere
HIP	4 h	1200	MTI GLS 1600X, Argon atmosphere
Cooling	Quench in water	1200-20	Metallic bucket
Heating	Load in hot furnace	20- (920-1100)	Lindberg Type 59744-A), Argon atmosphere above 1010°C
ST	1.2 h	(920-1100)	Lindberg Type 59744-A, Argon atmosphere above 1010°C
Cooling	Quench in water	(920-1100)-20	Metallic bucket
Heating	Load in hot furnace	20-(653-787)	Carbolite ELF 11006-230 SN
PI	10 h	(653-787)	Carbolite ELF 11006-230 SN
Cooling	Furnace cooling	(653-787)-650	Carbolite ELF 11006-230 SN
Aging	10 – 60 h	650	Thermolyne Type 10500
Cooling	Air cooling	650-20	Alumina plate

Mechanical Testing

As explained in the chapter *Strategy*, strain-rate jump tests shall be performed on the different heat treatment conditions set-up above. The following paragraph details the conduction of these tests.

Strain-Rate Jump Test

Before inserting the test specimen into the grip, the width and thickness of the samples is measured at the ends and at the center of the gage section. Furthermore the specimen are washed with acetone to remove pollutants remaining from the sectioning process.

As the viscoplastic behavior is temperature activated and Inconel 718 is a high temperature alloy, the tests need to be performed at elevated temperatures. The temperature is therefore set to 650°C, which represents the limit of Inconel 718 applicability and is a commonly used temperature for this alloy. A K-type thermocouple is spot-welded on the surface of the sample to maintain and control the temperature.

For operating the mechanical tests, 20000 lbf test frame, equipped with a 100 kN (22 k lbs) load cell, is used. Once the sample is aligned and mounted in the water-cooled hydraulic wedge grips with serrated inserts, a half inch high temperature extensometer with flat-tip ceramic rods is then applied on the sample. The temperature is increased to the final test temperature of 650°C using induction heating. Afterwards the strain measurement of the extensometer needs to be reset to zero.

Once the test is set up the loading initiates with an elastic loading section in strain control at a rate of 0.005 1/min which is recommmended by ASTM E21 [65] and also was applied by the preliminary studies of Kirka et al. [16]. Using the data on yield strength (YS = 814 MPa) published in [13] and the modulus of Inconel 718 referenced in Special Metals [12] and applying a plastic offset of 0.2% the yield point can be roughly predicted to 0.7% strain. Therefore the elastic loading rate is applied for 1% strain.

After reaching plastic material behavior the strain-rate jumps are performed in strain control by a series of ramps with a constant rate each. Five different strain-rates are anticipated for that test. Published results [16], [13] show that 5% strain at 650°C is a reasonable value to construct the test schedule. Therefore, after straining the material by 1% in the elastic step already, 0.8% strain at each rate will add up to the final 5% at the end of the strain rate jump schedule. The first jump goes from the elastic rate (0.005 1/min to 10-5 1/s at which the sample is strained for 0.8%. After that the rate is reduced by the order of magnitude and the sample is elongated by another 0.8% strain at a strain rate of 10^{-6} 1/s (10^{-4} %/s). This procedure is repeated with the rates of 10^{-4}, 10^{-3} up to a strain rate of 10^{-2} 1/s.

If the sample does not break within the jumps, the test is continued with a straining set-up similar to YS determination until extensometer limit is reached at 9.0% strain. Then the test program continues in displacement control with a rate of crosshead motion of 0.05 times the length of the reduced section (19 mm) as recommended by ASTM [65]. A program hold at 9.5% strain allows to take the extensometer of. Afterwards the loading continues until fracture. Other than in the test schedule described above, previously reported tests [52] do not determine the yield strength at the rate recommended by ASTM [65] for comparable yield strength determination.

The test time from initial loading to the end of the strain-rate jumps is 2.5 hours and therefore considerably longer than for tensile test. This is due to the very slow rate of 10^{-6} 1/s. For each jump 200 data points are acquired for Time, Running Time, Force, Strain, Strain Command, Strain Absolute Error, Displacement, Displacement Command, Displacement Absolute Error, respectively.

The tensile tests were set up using Inconel 718 samples of the same geometry as proposed for the AM study. The material for this purpose is taken from a forged turbine disc. The same disc has been studied in Radzicki [25]. It meets the industrial standards and could therefore serve as a valid reference point to compare with the AM results. After successfully setting up the experimental method with the forged material, the anticipated AM material can be tested. Therefore the sample with the ID *T2;2* of each point in the test matrix was tested first. Additionally the samples *T2;2* and *T1;2* of the non-heat treated as-built conditioned sample are planned to provide insight in the build-height dependence of the results. Further samples of the respective parameter set are supposed to serve as back-up in case a test fails and can be used for room temperature tests or confirmation runs if necessary.

Induction Coil

Designing an induction coil is an iterative and experience-based process. Nevertheless there are some rules that are mainly derived from transformers and basic physics [69].

One main issue forming an induction coil is the coupling distance of the coil to the sample. The larger it is, the more uniform the heating pattern becomes. On the other hand, the smaller it is, the better is the energy transfer from coil to part [69].

The flux is dependent on the distance between the sample and the coil. It is higher in regions closer to the induction coil and weaker at its geometric center [69]. Due to this gradient it is anticipated to increase the distance between coil and sample in the direction of the width of the sample. By means of that step a more uniform induction is expected.

The magnetic field is weaker where the leads and the coil join [69]. Therefore this section is anticipated to be in the thickness area of the sample. Additionally, the magnetic flux tends to increase towards the center of the length of the coil. This effect might be increased by the cooled wedge grips applied in high temperature testing. In order to compensate those differences, there are multiple methods to "characterize" the coil. This way it is possible to achieve a uniform heating of the gage section of the samples. Varying the distance between the specimen and the coil or adapting the distance within the turns of the coil are the main methods of achieving uniformity [69]. The coil, which was used in the final application, has three turns close to each other above and below the gage section respectively. In contrast to that, the gage section itself is covered by a single turn only.

To decrease "barber poling" (non-uniform spiral heating) a step and flattened tubing can be applied to the coil [69]. These steps are applied for the gage section in the thickness region of the sample.

The leads to the coil should be kept close enough for not dissipating too much energy [69]. The minimum distance is dictated by the need of sufficiently isolating the

leads with respect to each other in order to avoid arcing. Also, the risk of heating nearby metal components through the leads should be avoided [69].

Wooden cores that are bigger than the sample itself can be used to form the coil [69]. The core for the final coil has a width of 25 mm and a thickness of 13 mm with corner radii of about 5 mm. The used tubing has an outside diameter of 1/8 inch. To maximize the uniformity, the turns of the coil were winded onto the core as close as possible. The spacing for the extensometer movement is applied afterwards. As copper work hardens with increasing deformation one needs to be aware of the risk that the tubing might fracture when deformed too often. To heat the tube until it reaches bright red color followed by water quenching helps avoiding this effect if necessary [69].
In order to evaluate the temperature distribution throughout the heated material, well-grounded thermocouple readers are necessary. Handheld thermocouple readers are found to be inappropriate as the noise induced from the induction coil to the thermocouple is considerably affecting the temperature reading. For reduced sections of the tensile specimen of less than 2 inch, ASTM [65] proposes to use two thermocouples to calibrate the induction coil – one near each end of the reduced section. For these readings, ASTM [65] proposes a temperature uniformity of ±3°C for test temperatures below 1000°C [65]. For the coil used in this study, those tolerances are reached and approved by three thermocouple readings at the edges and the center of the gage section of a non-deformed sample. The induction coil and operation can be seen in Figure 33.

The coil must be water-cooled during the operation. The induction heater is controlled by a thermo-controller reading a TC at the center of the reduced section.

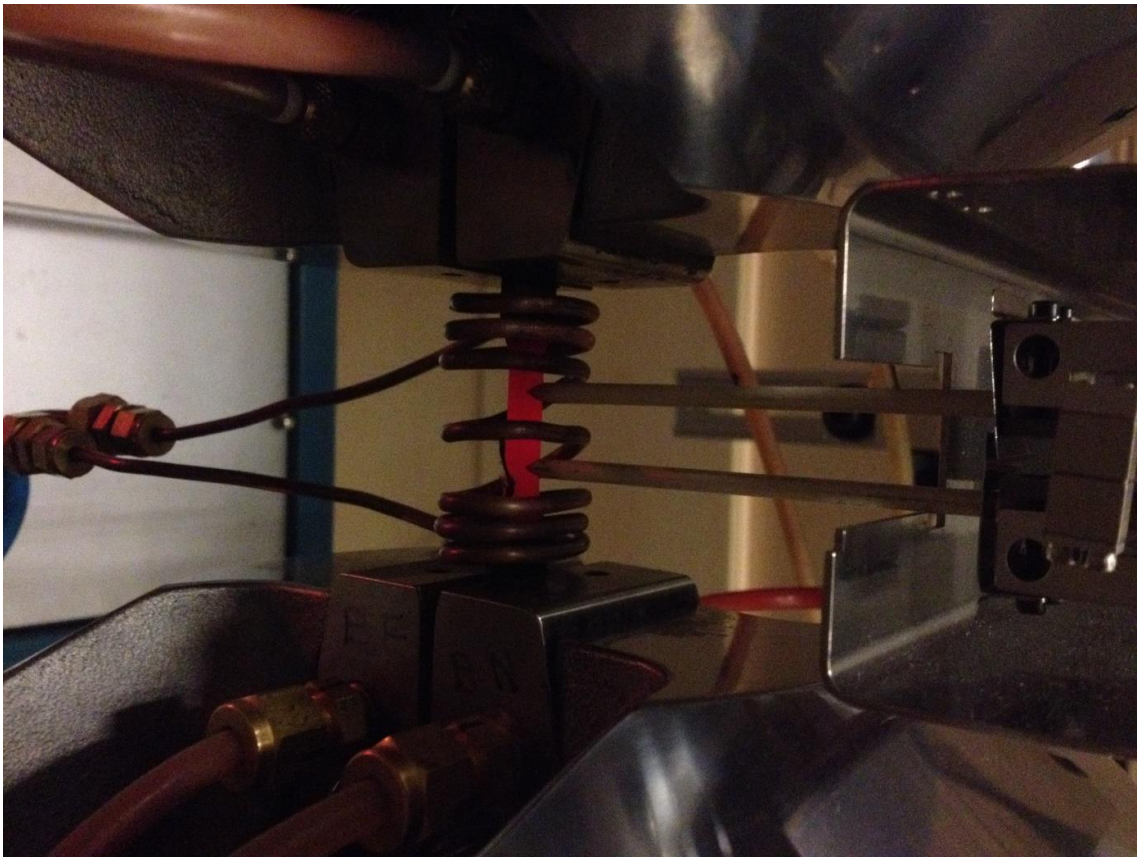

Figure 33: Strain-Rate Jump Test Set-Up

Metallography

The final goal of this thesis is to set up an efficient method which allows establishing the PSPP relationships. Next to strain-rate jump tests which link the processing parameters to the mechanical response, the structural features have to be included as well. As described above, metallography plates are therefore included into the parameter sets. The following steps are taken to prepare structural analysis.

Mounting

The metallography samples are mounted in transparent epoxy using 1.25 inch diameter mounts. After hardening of the epoxy in a pressure and humidity reduced atmosphere, the sample ID is engraved into the epoxy. Next to that an arrow indicating orientation of the vertical samples to the build orientation is engraved.

Polishing and Etching

As the EDM cut surface is already very smooth, grinding the samples starts with a comparable fine grit size. SiC Paper is used on a water-cooled polishing machine (Struers RotoPol-15). The abrasive size is continuously reduced form P500 over P800 to P1200. The SiC papers are applied for 5 minutes each with a load of 15N and a disc speed of 150 RPM. Afterwards water based diamond suspension of 9µm, 3µm and 1µm for 3 minutes each on the same disc speed and load are found to give good results. Final polishing is performed using the 0.02 µm Acidic Alumina Suspension (Struers OP-AA). The polishing schedule is summarized in Table 12.

Table 12: Polishing Schedule

Polishing Agent	Abrasive Size	Time	Load	Disc Speed
SiC Paper	P500	5 minutes	15N	150 RPM
SiC Paper	P800	5 minutes	15N	150 RPM
SiC Paper	P1200	5 minutes	15N	150 RPM
Diamond suspension	9µm	3 minutes	15N	150 RPM
Diamond suspension	3µm	3 minutes	15N	150 RPM
Diamond suspension	1µm	3 minutes	15N	150 RPM
Acidic Alumina Suspension	0.02 µm	3 minutes	15N	150 RPM

Waterless Kallings II Etchant with a composition of 40 ml ethanol, 2 g copper chloride and 40 ml hydrochloric acid was found to provide good etchant results on the forged Inconel 718 disc material. Etching of the AM material has turned out to be problematic. Etchant concentrated in the pores of the material is found to locally over-etch the samples. This way no useable etching result can be achieved using the given set of samples. Investigating the alternatives revealed that the best results on the extensive porous samples are gained by vibratory-polishing them between 1.5 and 4 hours in 50%

0.02 µm acidic alumina suspension (Struers OP-A) and 50% water which reveals the columnar grain structure of the vertical oriented samples. The method did not work on the 0 0 1 textured horizontal samples, because it etches the matrix and therefore grain contrasts depend on the differences in crystallographic orientation. Furthermore, pitting had a detrimental influence on the horizontal surfaces which could probably be attributed to horizontally aligned fine porosity along the layers.

Data Analysis

The following paragraph sums up the tasks of data analysis.

Mechanical Tests

A Matlab code is used to analyze the data files from the tensile tests. This code automatically loads the data files of multiple tests, performs the calculations and saves the mechanical properties to an excel sheet as well as it plots and saves the stress strain curves. Therefore the stress values are calculated from the force measurements.

Afterwards the code calculates the elastic modulus by fitting the slope of the first 50 data points. Yield strength is calculated using intersection of the 0.2% strain offset to that curve with the stress strain curve. Finally the flow stress needed for the viscoplasticity evaluation is determined by the average value of the last 50 data points captured on the respective strain-rate. Using a coordinate transformation of the flow stress over strain-rate plot to the double logarithmic coordinate system allows then to fit the Norton creep equation.

Grain size

The etched microstructure can be captured with an optical microscope. Afterwards these images are stitched using Adobe Photoshop. Grain sizes are counted on eight lines of 3 mm length. A Matlab code is set up to be used to calculate the mean column diameter of the columnar grains.

Porosity

Porosity can be evaluated using two different methods. On the one hand, images on 50x magnification are taken with a bright field illumination on an optical microscope. A total number of 20 images each sample (280 images in total) are captured. The vertical metallography samples are therefore imaged on two horizontal rows and ten images each row. A Matlab code, set up for the evaluation of volume fraction and number of the pores, then automatically loads these images. Afterwards they were transformed to a binary image. A threshold value of 0.7 on the gray scale was found to give the best representation of the captured porosity images. Furthermore the code is set up to determine the number of black pixels on the image which refers to the volume fraction of the pores. Additionally, the number of pores per image is determined by automatically counting the number of individual black areas on the image.

Furthermore the length, number and spatial distribution of stringer porosity can be documented. A very basic approach can be selected if the total number of porosity chains is low. For this purpose, a grid of 250 µm is applied on optical images of the whole sample are taken on low magnification using an optical microscope. Based on these images the spanning and location of the porosity chains can be estimated if the individual porosity chains are found to be well-represented by line interpolation. Then the length of the interpolation line can be estimated based on the grids.

Design of Experiments

Figure 34 shows an exemplary DoE test matrix for three factors in a 3-dimensional coordinate system. In case of a three factorial test, this spatial illustration is feasible. However, DoE test matrixes can still be constructed for higher factorial experiments. The evaluation of a DoE experiment will be explained for this example of three factors and therefore eight parameter.

If all of these eight experimental results were gathered, the effects of each parameter can be calculated as the difference between the average of the high factor level (+) and the low factor level (-) [63], [70]. For example the effect of factor A in Figure 34 is calculated by the equation in Figure 34 where y2, y4, y6 and y8 represent the high level of factor A.

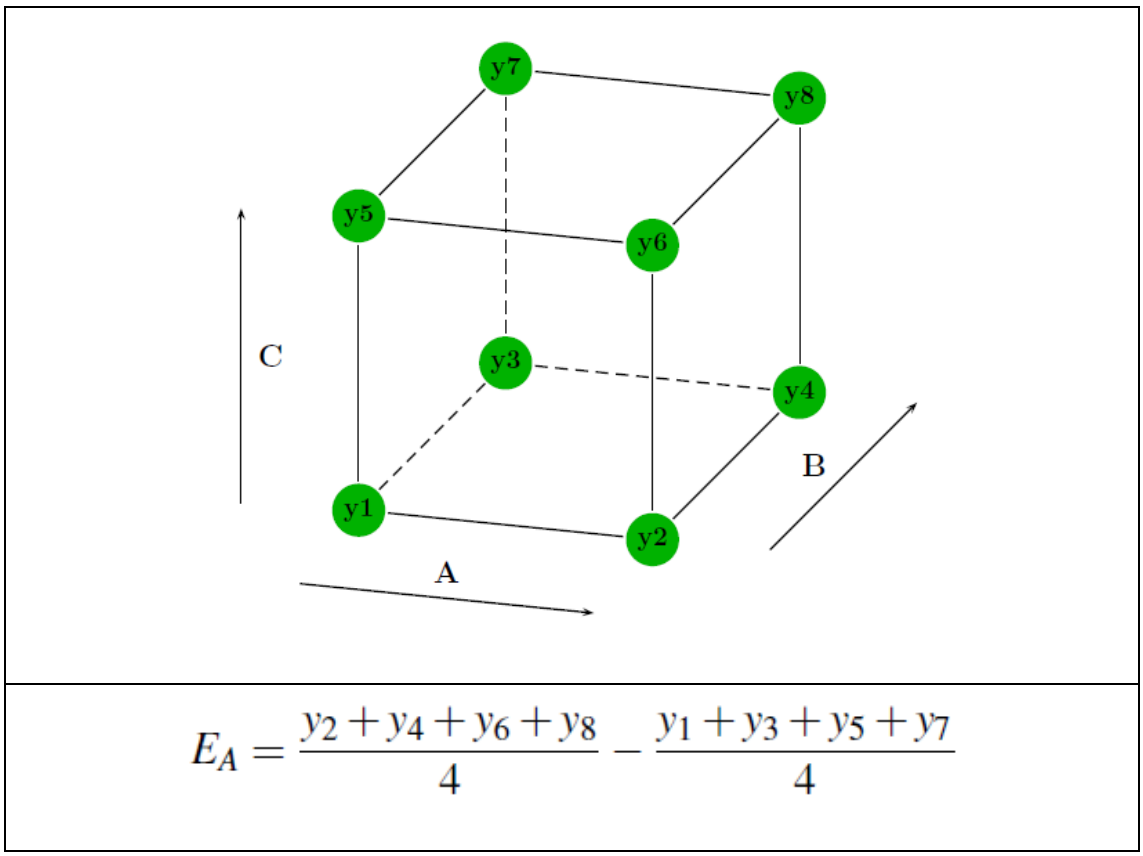

$$E_A = \frac{y_2 + y_4 + y_6 + y_8}{4} - \frac{y_1 + y_3 + y_5 + y_7}{4}$$

Figure 34: Effect Calculation for a Three Factorial DoE Test Matrix [63]

Calculating this average increases the stability of the effect with respect on scatter and allows on the other hand to check for the existence of the effect on multiple configurations (combinations of the other factors).

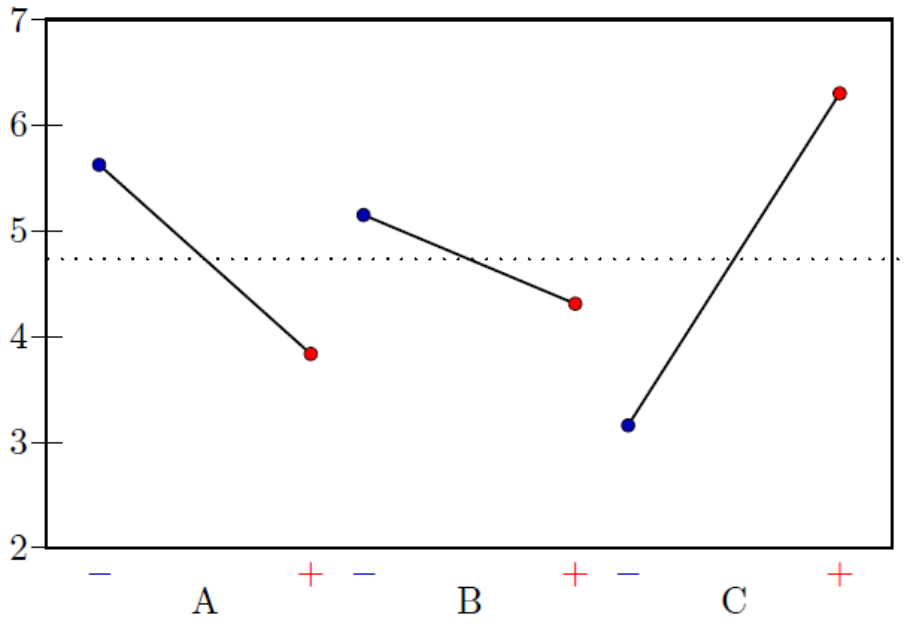

Figure 35: Effect Diagram for DoE Calculation [63]

A widely used illustration for the effects is shown in Figure 35. For each factor (A, B, C) this diagram shows the mean value of the low (-) level and the high (+) level. The slope of the line which links the two data points illustrates the effect of the respective factor.

The calculation of the correlations, e.g. of the factors A and B work in the same way as discussed above for the main effects. The difference is that the level $(+)_{AB}$ is defined as the situation where the two considered factors A and B were on the same level ($(+)_A$,$(+)_B$ and $(-)_A$,$(-)_B$) whereas the level $(-)_{AB}$ is defined as ($(+)_A$,$(-)_B$ and $(-)_A$,$(+)_B$). The larger this correlation is, the more effective is the correlation between the respective factors.

Significant Results / Analysis of Variance

In order to find out which of the effects and correlations are significant, hence are larger than what could be explained by natural scatter, two terms are defined in Analysis of Variance (ANOVA) – the F-value and the p-value. Using these, the big picture of ANOVA can be displayed as follows:

The analysis starts with regarding the observed effect of a factor (e.g. the effect of solution treatment temperature) on a quality feature (e.g. grain size). The calculation of the effect is demonstrated above (Figure 35). Now, the "null-hypothesis" can be checked for this effect. It represents the assumption, that the factor (solution treatment temperature) has no effect on the quality feature (grain size). This hypothesis can then be verified. Therefore, a so-called F-ratio is defined which represents the ratio between the factor's effect (on grain size) and the natural scatter (of grain size) observed in the experiment. This allows to calculate the probability of finding an F-value with the given experiment that is at least as big as the F-value which is actually observed in the experiment. This represents the probability that the observed effect is likely to be caused by natural scatter instead of being caused by the factor. This probability value is called the p-value. If the p-value is small, the "null-hypothesis" is being rejected because the effect is larger than what can be expected by natural scatter. The effect is then considered as "significant". Typical values to decide for significance were 10%, 5% or 1% [63]. For example, accepting p-values smaller than 5% means that an effect is called "significant", if the probability that the effect is caused by the factor is higher than 95% and therefore the probability that the effect is caused by scatter is less than 5%.

When it comes to establish a linear model that relates the targeted quality feature (i.e. structural feature or mechanical property) to the varied factors (i.e. the targeted processing parameter) only effective (significant) factors and correlations shall be considered. Therefore non-significant factors have to be eliminated from the model. For this task a ratio R^2 can be defined. R^2 measures how much of the variability is described by a model and therefore how well the model represents the experiment.

The way it is defined, R^2 increases with the number of factors included in the experiment, and hence it cannot be used to judge whether a step in the reduction of non-significant factors is suitable or not. Therefore the $R^2_{adjusted}$-value is defined, which minds the number of model parameter needed to get the model, relative to the number of data

points of the experiment. Other than R^2, the value of $R^2_{adjusted}$ shows a peak at the step in reduction of non-significant factors at which the model is most efficient. The decision on which factor is to be removed is based on its p-value.

In case blocks were used in the set-up of the experiment the factor "block" can be used in the model as well. If the factor block is significant, it is possible to identify its significance and not to blur the results. If block is not significant, it will be removed from the model equation and is checked for non-significance. The factor "block", if existing, should be checked for significance at first.

After that the model parameter are reduced stepwise by non-significant ones, beginning with the highest order interactions which normally have the lowest effect. Non-significant effects have to remain in the model, in case their interactions were significant. If scientific insight contradicts the result that claims a factor not to be significant, the factor certainly may remain included in the model.

More details and exact calculation of the F, p, R^2, and $R^2_{adjusted}$ values can be found in basic literature e.g. [63] and are as well programmed in DoE software e.g. [62] and is therefore not part of this review.

CHAPTER V

MICROSTRUCTURE AND MECHANICAL PROPERTY CHARACTERIZATION

Experimental results of the study are based on the methods and strategies as set out above. They will be presented in this following chapter.

Tensile Test Results

As a baseline, the deformation responds of a forged Inconel 718 sample, sectioned from an as-processed turbine disk used in jet propulsion is shown in Figure 36. Testing this reference material shows a high elongation of 18.9% at 650°C. Clear strain-rate dependent behavior is visible as the strain-rates decrease form the elastic strain-rate to 10^{-5} 1/s and from there to 10^{-6} 1/s. After that the strain-rate stepwise increases again to 10^{-4} 1/s, 10^{-3} 1/s and 10^{-2} 1/s. Accordingly also the stress needed to strain the material is increasing.

These flow stresses illustrated in Figure 36 are then averaged over the last portion of the measured data, shown by the red line and summarized in Table 13. The graph has been truncated after completing the jumps for providing better insight in these.

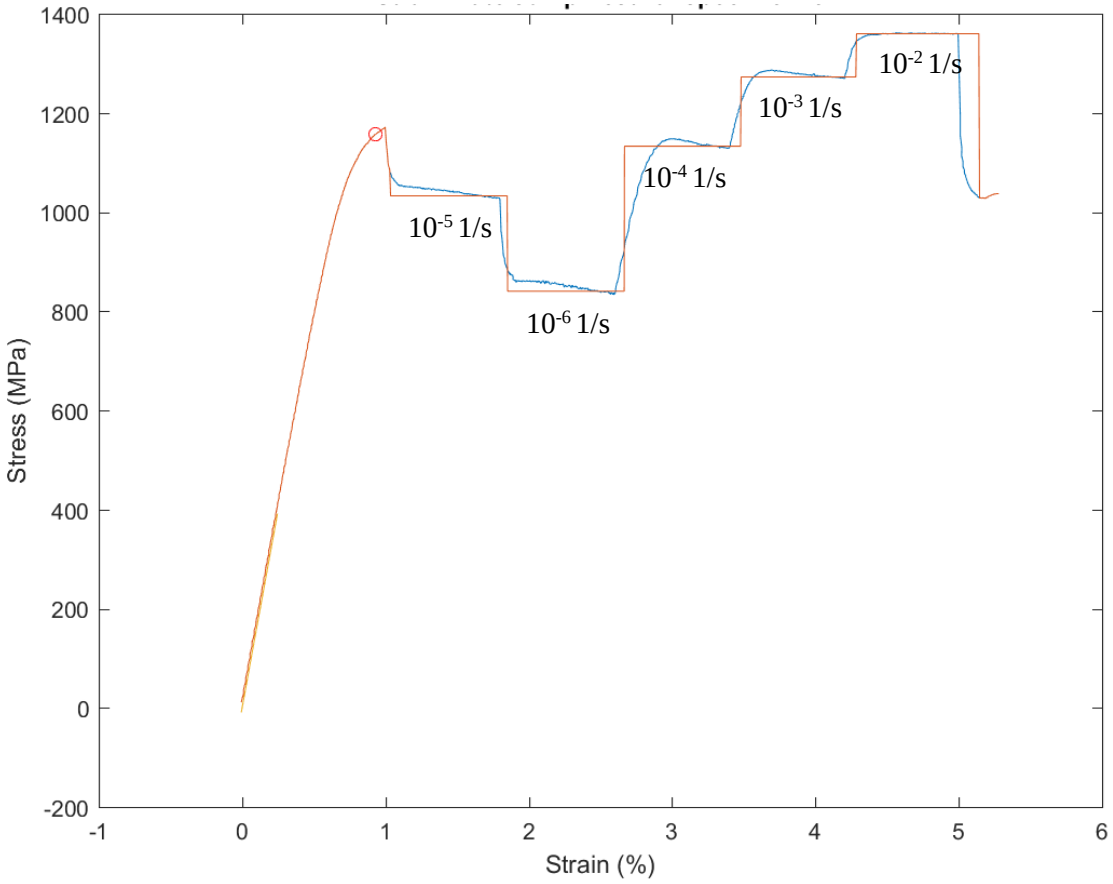

Figure 36: Strain-Rate Jump Test of Forged Inconel 718 Turbine Disc Material

Table 13: Rate-Dependent Flow Stresses of Forged Inconel 718

Strain Rate	10^{-6} 1/s	10^{-5} 1/s	10^{-4} 1/s	10^{-3} 1/s	10^{-2} 1/s
Flow Stress	804,60	988,58	1084,46	1218,13	1301,84

The rate dependence is found by linear regression analysis, shown in Figure 37. A strain-rate exponent of n = 18.8 has been found, which is comparable to the values published in literature. The power law creep equation fits well to the experimental data (Figure 37). While experiments at higher temperatures were reported to show a lower exponent n of 5 to 10 [56], another study at 650°C has reported a higher n-value of 36.5 [57]. Sugahara et al. [57] tested the creep viscoplastic properties at lower ranges from $6.7*10^{-9}$ 1/s to $1.7*10^{-6}$ 1/s Both the reported and the value shown in the study indicate good creep resistance of the alloy at use-temperatures. Sugahara et al. [57] reports a flow

stress of 814 MPa for a strain rate of $1.7*10^{-6}$ 1/s which is roughly in the same range as the flow stress value of this study.

The strain-rate jump test represents a high-throughput method to accelerate investigation of viscoplasticity and reduces the material cost considerably. Instead of five samples, only one tensile sample is needed to gain the desired data. This is only possible at the cost of accuracy as the used flow stresses were not exactly the long term values they approximate. Using equal jumps (on the logarithmic scale) and equal strain each jump reduces the error induced by that. Therefore it is anticipated as a consequence of the result in Figure 36 to increase the strain at the 10^{-4} 1/s rate because for this the jump is larger. Further discussion about the strain-rate jump test can be found in the study of Neu et al. [52].

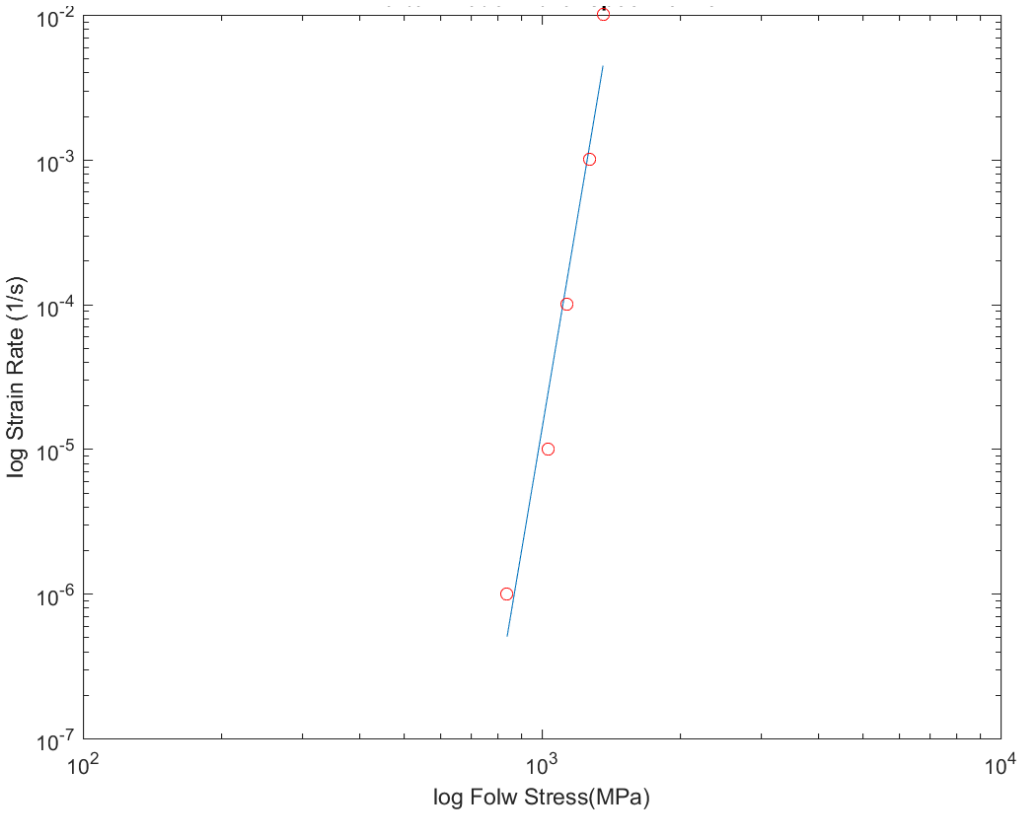

Figure 37: Norton Model Fit for Forged Inconel 718 Turbine Disc Material

Other than the forged material discussed above, the AM samples showed a highly brittle behavior. All tests performed are listed in Table 14.

Table 14: Mechanical Test Results

Sample ID	Heat Treatment pattern	Elastic Modulus (GPa)	Yield Strength (MPa)	Ultimate Strength (MPa)	Ductility (%)
Heat Treated:					
II/YX/2T22	−−+	102.30	597.66	601.14	6.58
II/YX/3T23	+++	112.39	none	255.86	0.22
II/YX/4T22	−+−	119.21	none	271.83	0.22
II/YX/4T23	−+−	115.05	none	359.60	0.31
II/YX/5T22	0	117.25	509.30	590.04	0.86
II/YX/6T22	+−−	141.66	561.76	578.16	2.84
III/YX/1T22	++−	107.55	833.10	836.43	1.03
III/YX/2T22	−++	112.80	770.41	781.68	1.09
III/YX/3T22	0	105.87	none	648.98	0.66
III/YX/4T22	−−−	112.69	489.43	505.94	1.58
III/YX/5T22	+−+	141.28	none	377.21	0.29
III/YX/6T22	0	149.82	797.82	815.25	5.58
As-built:					
IV/YX/2T23	none	137.64	none	248.76	0.21
IV/YX/2T12	none	133.58	506.62	523.10	0.73
Forged Disc:					
Forged Disc	unknown	152.01	1107.48	n.a. *	18.88
* UTS not determined in Strain-Rate Jump Test					

Five out of eight samples fractured before reaching the 0.2% yield strength (Table 14). Over all the average ductility is at about 0.91%[1]. It is noticeable that all strength values are way below the yield strength of the forged Inconel 718 sample. Furthermore, they are far below the strength values reported by preliminary studies on the same processing conditions.

[1] Excluding sample II/YX/2 T2;2 and III/YX/6 T2;2 which don't allow ductility calculation due to slow cracking during slow rates of the strain-rate jumps.

The brittle behavior appears on samples throughout the whole range of the test matrix as well as on the non-heat treated sample *IV/YX/2T2;3* and *IV/YX/2T1;2*. Next to this observation one can see a significant variance in elastic modulus. Performing the tests, metallic clicking sounds have been noticeable. These were going along with an upward jump in strain and a downward jump in force indicated in the scope view. Repeating the tests of samples which fractured before yielding has been done for two samples using the adjacent T2;2 samples. All tests failed in about the same range as those in the first place. Only the repetition of the as-built sample by a *T1;2* that has been further away from the defective location brought some improvement. However, it did not show a much better result than the rest of the samples. Stress strain curves of all samples in Table 14 are listed in Figure 54 to Figure 56 in Appendix.

Discussion of Mechanical Tests

The reduced results on modulus, strength and ductility suggest that porosity or delamination induced during the build process might be causing a non-uniform or pre-cracked cross section in the material based on which the tensile samples strain locally through failure/crack growth at some kind of a stress concentrating notch and therefore show that reduced modulus, strength and ductility. The observation of the noise emission supports this theory. It could be interpreted as sudden coalescence of failure sites such as voids. The observation that the adjacent samples show similar fracture behavior, points towards larger scale flaws spanning multiple samples in the parameter set.

The result of the mechanical tests described above is highly unexpected. When planning the experiment, emphasis was placed on cooperating and checking back with the experience developed by the material supplier [20]. The assumption that the material in as-built condition provides a ductility of more than the 5%, which were needed for successfully performing tensile tests, is based on the test results on studies using equally heat treatment [16] as well as on as-built [30] tensile test results published by the material

supplier [20]. Those studies have been performed on samples using the same standard-Arcam-scan-strategy and heat treatments that were also included in the test matrix presented in this work. If the theory of flaws causing the early fracture (as discussed above) holds, there must be flaws that exceed what was prognosticated by ORNL [20], other published AM data (summed up by Kirka et al. [16]) as well as the material standards [27] on AM Inconel 718 property requirements. The HIP cycle was only "simulated" temperature-wise as recommended by Kirka [20] who found good control over porosity and high as-built ductility in his studies [30].

The results contradict the assumptions of "good control over porosity" and repeatable results in the as-built condition. While checking the repeatability of the build quality by repeating the test is beyond the scope, the differences to studies performed by the material supplier [20] as outlined above indicate few repeatability. Comparing the tensile results to the result of strain-rate jump test of forged disc material, shows that there is no issue with the set-up of the mechanical test that maliciously affected the results.

Structural Reasons for Poor Tensile Performance and Structure Performance Link

As no reliable viscoplasticity and yielding data is provided by the above stated results, the preliminary goal is – according to the previously described methodology – to relate the observed tensile performance to its cause. According to the methodology this investigation should start with the structural feature which is most likely causing the observed behavior. For the indications stated above, analyzing the porosity and delamination should hence be the priority of the investigation. The PSPP chart indicates that porosity and delamination both link to the unexpected mechanical properties.

The test sample configuration is designed targeting at investigating the mechanical properties and structural features in direct vicinity. It remains to be checked

whether the sample geometry allows tracing the reasons for the flaws and the extent of the flaws.

Fractography

The mechanical response of the AM samples indicates that flaws reduce the ductility of the samples. The main observations that lead to this assumptions are outlined above and are summarized as follows: These flaws seem to coalescence while loading the sample, indicated by a sound and in the stress-strain-profile. Furthermore these flaws seem to be spatially varying and spanning multiple neighboring samples. The following paragraph shows further investigations for tracing and documenting the reasons for the insufficient material behavior.

The fracture surface of the sample shows an intergranular fracture, unveiling the columnar grain structure. The fracture surface of ORNL showed similar fracture surfaces when doing their studies [30], [16] & [20] on the same build conditions. Other than the samples used for the purposes of this presented study, they did not find the blue discoloration that some of the current samples show, e.g. Figure 38 [20]. These blue zones indicate crack surfaces that have already been exposed to the environment for longer time.

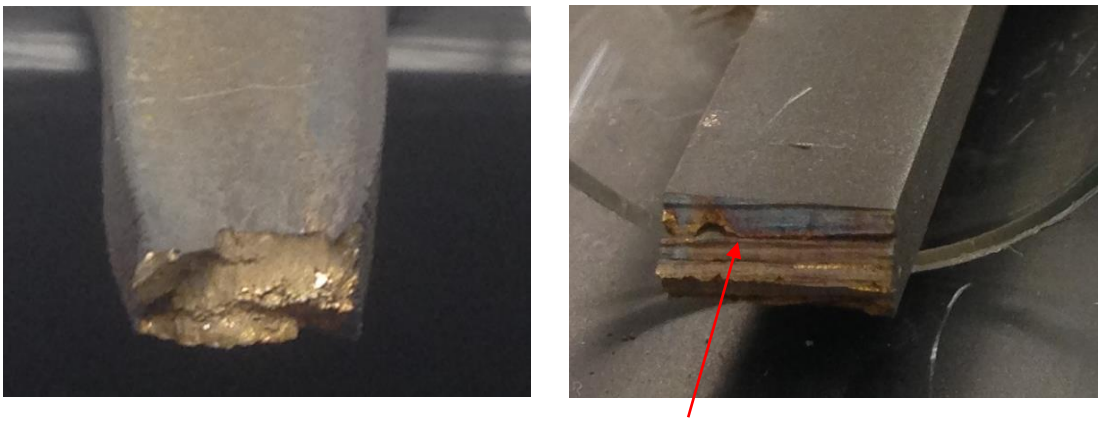

A: Fracture Surface of Forged Inconel 718 Sample

B: Blue discoloration in AM built Inconel 718 Sample II/YX/3

Figure 38: Fracture Surface of forged sample (A) and AM sample (B)

The sampling geometry designed for this study emphasizes the importance of metallographic samples, located as close as possible to the tested material, i.e. the gage section of the tensile sample. The width of the sample lays attached to one of these metallography planes and is just spaced to it by the sub-millimeter EDM wire diameter used for making the cut. Therefore a flaw, as indicated on the fracture surface, must also be visible on the metallographic plane. Figure 39 shows one of the vertical *T2;1* metallography samples. Using the optical microscope reveals extensive chain porosity spanning the complete width of the sample in build direction. The green line in Figure 39 illustrates that these chains have the same angle and location as the two major cracks in the adjacent tensile sample *T2;2*.

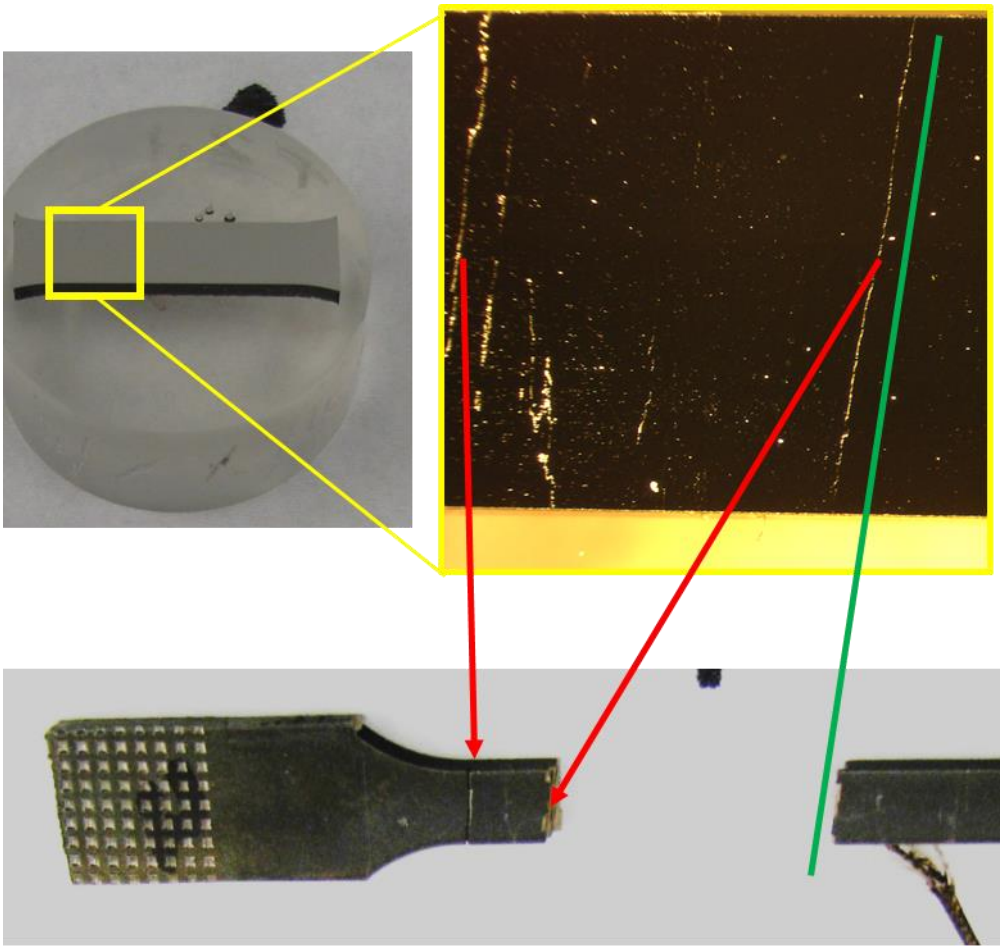

Figure 39: Correlation of Porosity and Material Failure in Sample II/YX/4

Porosity

The observations discussed above, give reason to research and document the porosity features that deteriorate the mechanical properties to this extend. The preliminary studies of the material supplier [20] have not shown as much chain porosity as detected in the current study [16]. While stringer porosity has been reported to deteriorate the AM mechanical properties of EBM Inconel 718 in preliminary studies, the depicted porosity has been by far less extensive. Figure 40 shows a comparison of those chain porosities reported by Strondl et al. [21] to the aligned pores found in this study.

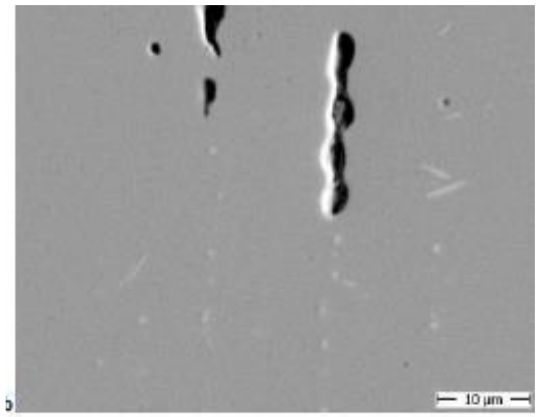

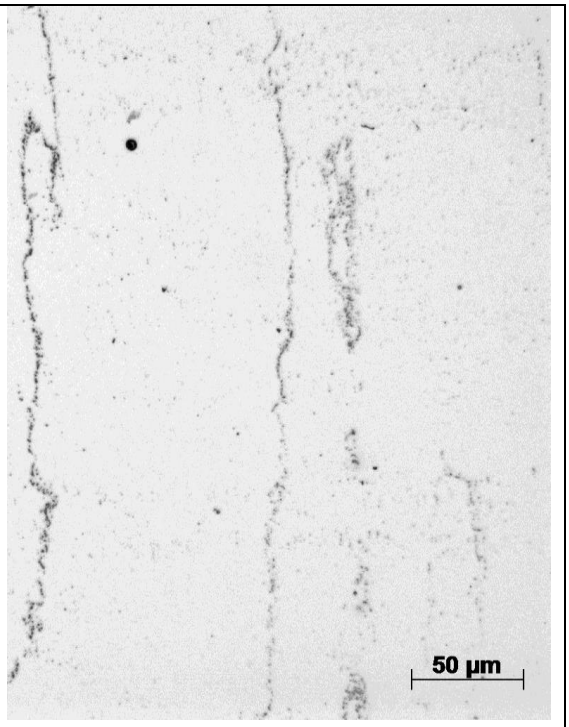

A: Stringer Porosity reported by Strondl et al. [21]	**B: Stringer Porosity observed in this Study**

Figure 40: Comparison of Stringer Porosity Earlier Reported to Porosity Discovered

Additionally Figure 41 shows the different morphologies of pores detected in this study. The whole build is suffused by various numbers of evenly distributed small to medium size round pores (Figure 41 A) and some larger round pores (Figure 41 B). Stringer porosity as reported by Strondl et al. [21] is also present in the material of this

study (Figure 41 C). Moreover the builds indicate very coarse irregularly shaped pores (e.g. visible in Figure 41 D) which are sometimes found in vicinity of the pore chains (Figure 41 E). The pore chains span large linear distances in build orientation as they form at the boundaries of the columnar grains (Figure 41 E). Horizontal images show their rather two dimensional shape (Figure 41 F).which makes the term *pore plane* more useful. Also, some samples show small size pore chains oriented in build direction (Figure 41 G). Few images furthermore show some horizontal porosity (Figure 41 H) most likely attributable to delamination effects within the layers.

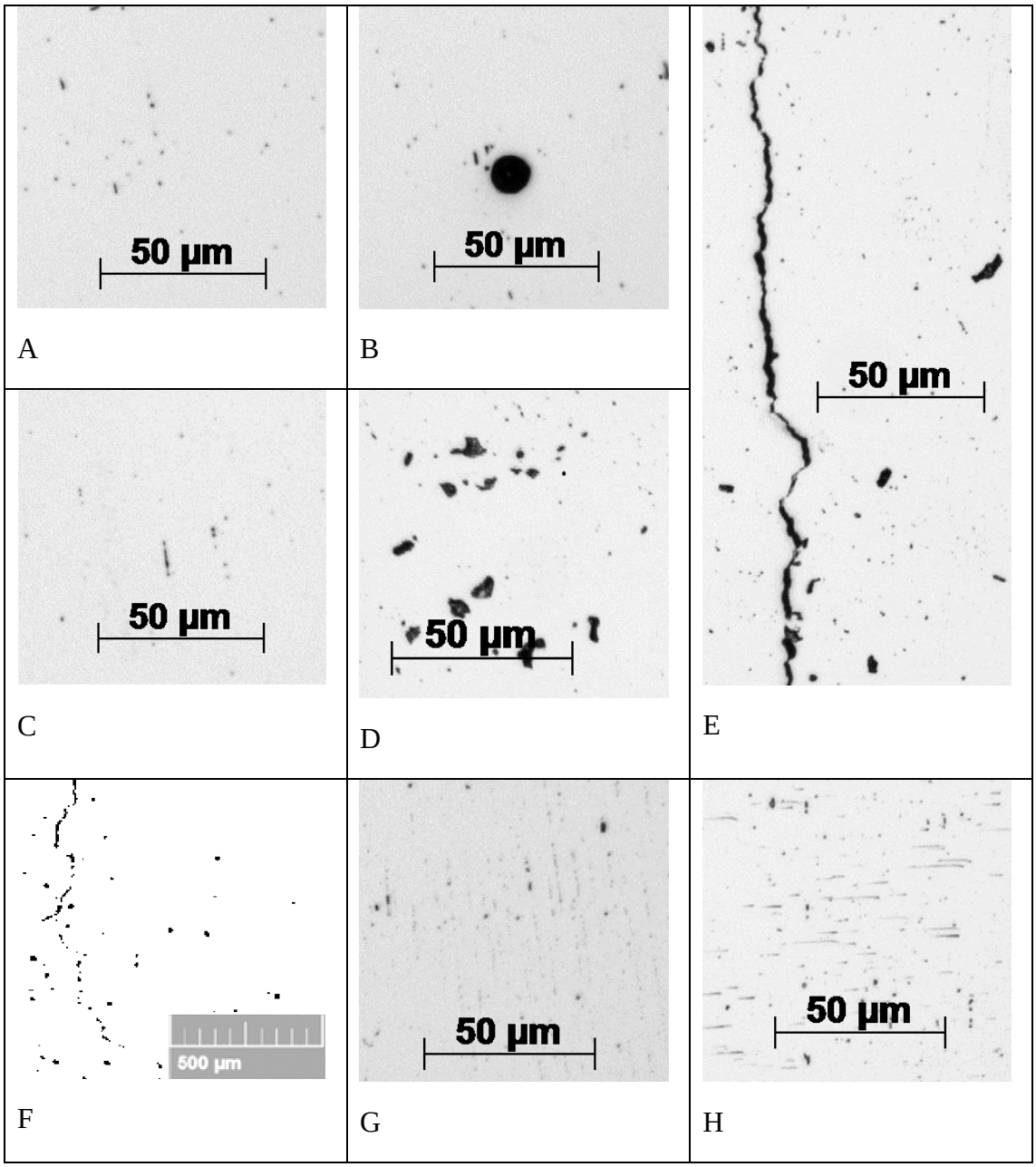

Figure 41: Morphology of AM Porosity

As Figure 39 indicates, the early fracture of the samples is most likely to be attributed to the one largest flaw in the volume covered by the sample. This feature cannot be detected by a two dimensional quantitative metallography method and therefore relations between volume fraction or number per unit area and the tensile results were relatively unlikely. It is rather an objective for quality assurance methods to

trace these features before the use of AM parts. One opportunity to find such a major flaw is neutron beam radiography e.g. described in Dehoff et al. [19] for the use on AM Inconel 718. Nonetheless, a good documentation on the quantitative aspects of porosity is vital to quantify future improvements in build quality and to gain statistical data for the estimation of initial flaws for future fracture mechanics studies. Therefore the next sections provide quantitative insight in the volume fraction and number per unit area of pores as well as the number and chain length of stringer porosity.

Volume Fraction and Number per Unit Area

Quantifying the total amount of porosity in the samples as well as their volume fraction can be done based on quantitative methods presented in the previous chapter. The binarization, which is the basis for the analysis of the volume fraction and the number of pores, is conducted with a threshold value that turns the darker 70% of the pixels to black (see Figure 42).

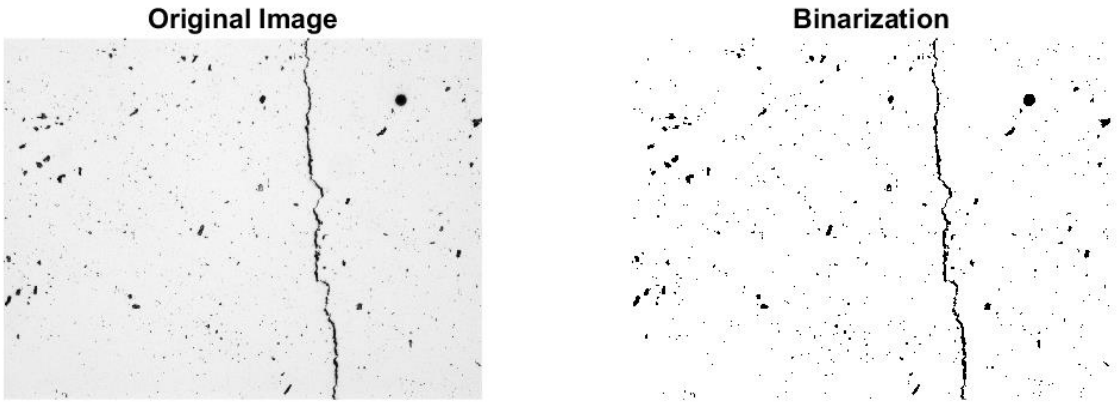

Figure 42: Binarization of Porosity Images

By doing this analysis on 20 images each metallography sample the average values are shown in Table 15.

Table 15: Volume Fraction and Number of Pores per Unit

Sample ID	Position in Build	Volume Fraction	Number of Pores [1/mm²]
IIYX2T21	2	0.56%	3996
IIYX3T21	3	1.05%	6202
IIYX4T21	3	0.51%	1957
IIYX5T21	2	0.35%	4659
IIYX6T21	1	0.42%	2529
IIIYX1T21	1	0.56%	3886
IIIYX2T21	2	0.16%	1434
IIIYX3T21	3	0.44%	3484
IIIYX3T11	3	0.84%	8045
IIIYX4T21	3	0.75%	4353
IIIYX5T21	2	0.40%	2892
IIIYX6T21	1	0.64%	2483
IVYX2T21	3	0.63%	4654
IVYX2T11	3	0.15%	1041
Mean (Build II & III)		0,56%	3827
Standard Deviation (Build II & III)		0,24%	1862

The analysis of the given numbers with respect to the position of the sample in build space is shown in Figure 43. The level 3 in this context relates to the center of the build space, whereas level 1 relates to the outskirts.

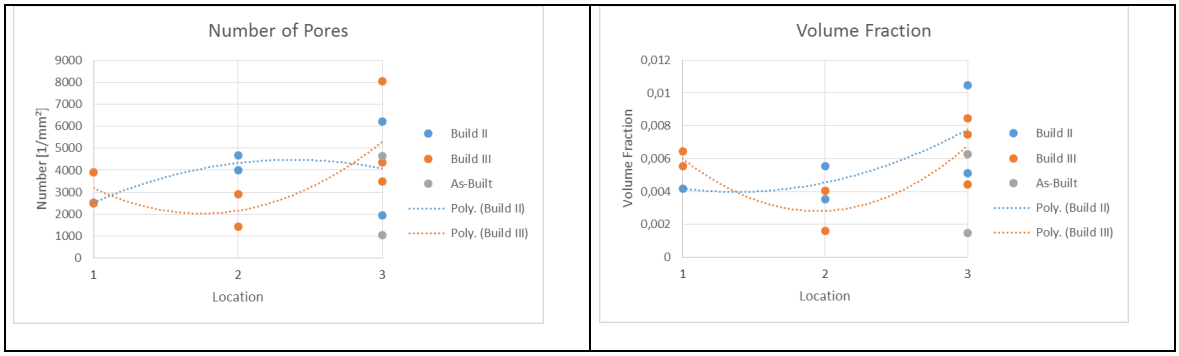

Figure 43: Number of Pores and Volume Fraction over Build Space Position

Furthermore, the number of pores and the porous volume fraction can be checked for correlation to the mechanical properties observed in the strain-rate jump test. No clear dependence of mechanical properties on porosity can be concluded from these measures (as shown in Figure 44 A to F).

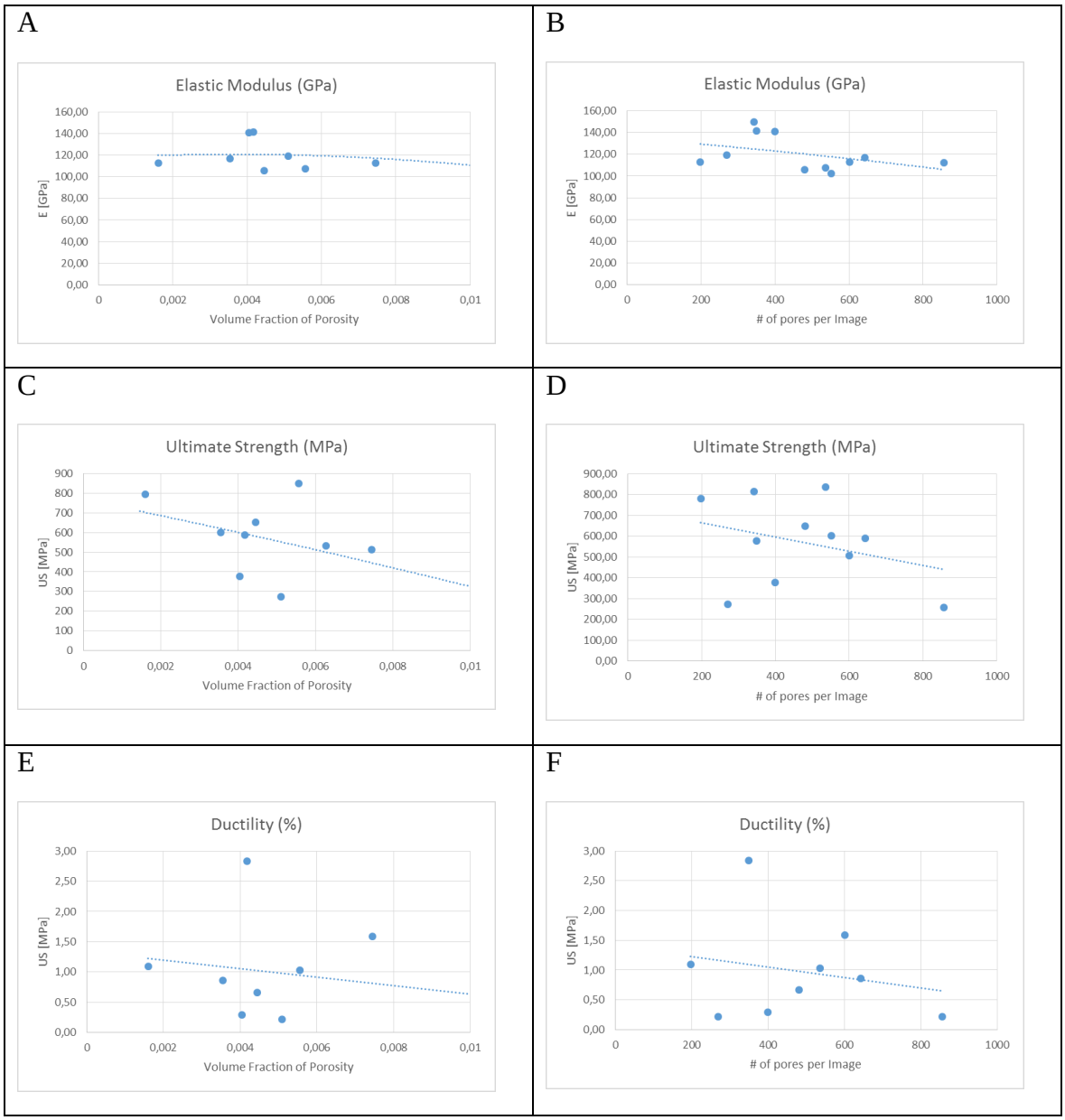

Figure 44: Mechanical Properties with Respect to Volume Fraction and Pores per Image

Using the results of the data on volume fraction and number of pores allows to check whether the porosity has been affected by the post-built heat treatment. It is for example possible that fast quenching after the high temperatures of the HIP treatment led to coalescence of minor pores and weakened the material this way. Table 14 shows the data needed for this comparison. It is indicated that the top of the as-built sample has a porosity volume fraction that is above the average of the heat treated samples, which is

calculated based on images captured on the same build height. It is therefore unlikely that the heat treatment affected porosity. Investigating the underlying images confirmed the presence of coarse chain porosity in the non-heat treated sample *IV/YX/2 T2;1* (e.g. Figure 45).

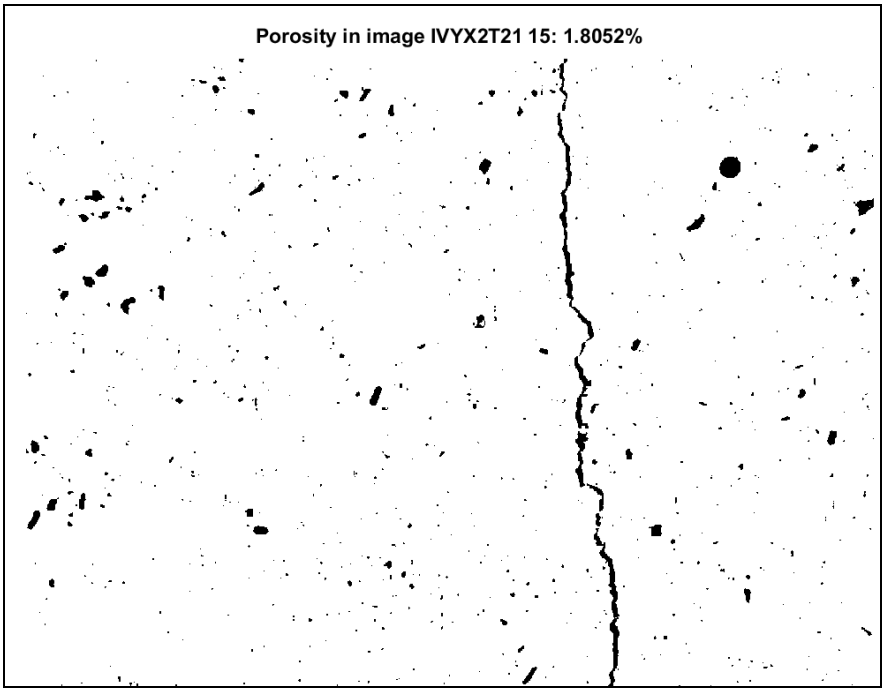

Figure 45: Exemplary Chain Porosity in As-Built Sample IV/YX/2 T2;1

The results indicate that no obvious spatial distribution of porosity over the build space has been detected on the experimental results. No significant link between the number and volume fraction to the tensile test results can be detected from Figure 44. This result supports the theory that the fracture of the samples is related to a single peak flaw, rather than to a collectivity of minor flaws.

Chain Porosity

The methods above can serve as a good documentation of the volume fraction and the number of pores per image. Furthermore, they support the theory that individual large flaws caused the early fracture of the tensile samples. As Figure 39 illustrates, the larger

pore chains have the worst effect on the sample. Therefore an individual method to document and investigate the very coarse pore chains has to be applied.

The total plot of length of pores over the gage section shows no general accumulation within the sample (see Figure 46). Individual plots of chain porosity in individual samples show spatial accumulation of those features illustrated in Figure 47.

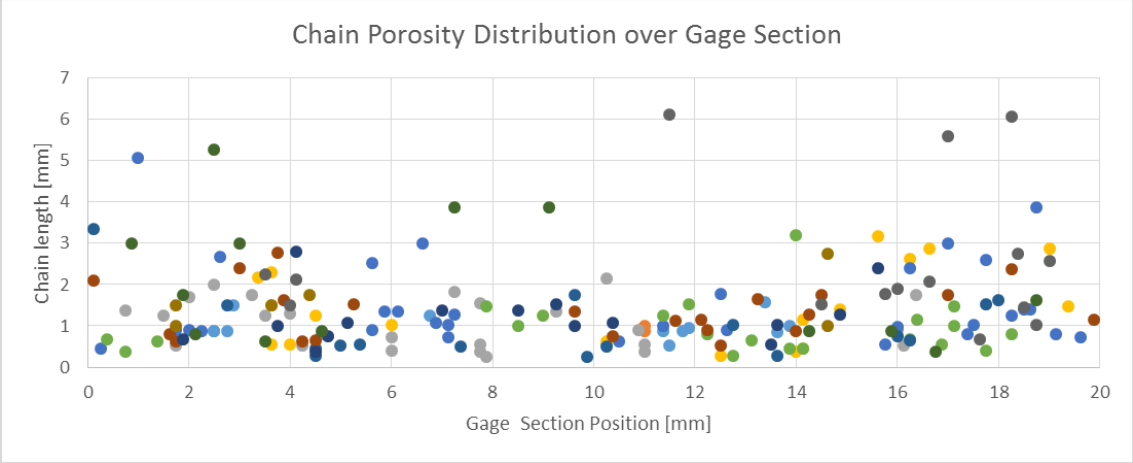

Figure 46: Chain Porosity Length and Distribution over Gage Section

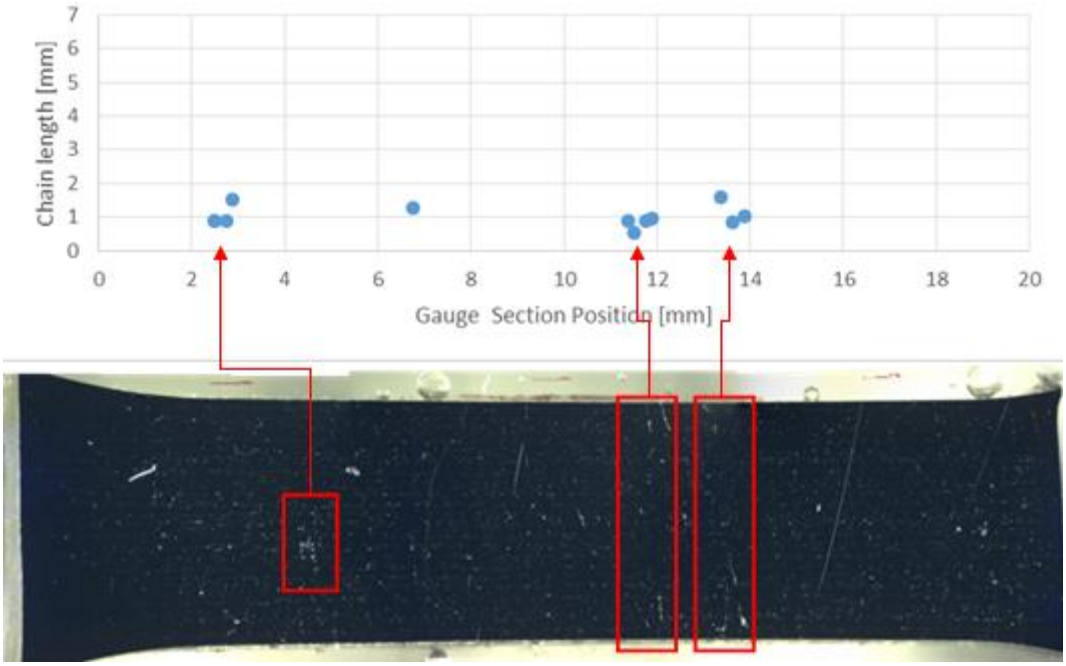

Figure 47: Spatial Accumulation of Chain Porosity Sample III/2

Further charts and tables documenting the chain porosity can be found in Figure 48 and Figure 49. Again no dependence of porosity on sample location in the build is

recognizable. The downward trend of the ultimate tensile strength and ductility which are expected to occur with an increasing amount of porosity is not disproved by these results. However, the trend is small compared to scatter. Once more the individual flaw configuration seems to be more relevant. This is in line with the findings described above, that the variance in mechanical tests is spatially dependent. The local agglomeration of pore chains, which is expected to enhance their deteriorative influence on mechanical properties supports the theory of peak flaws causing material failure.

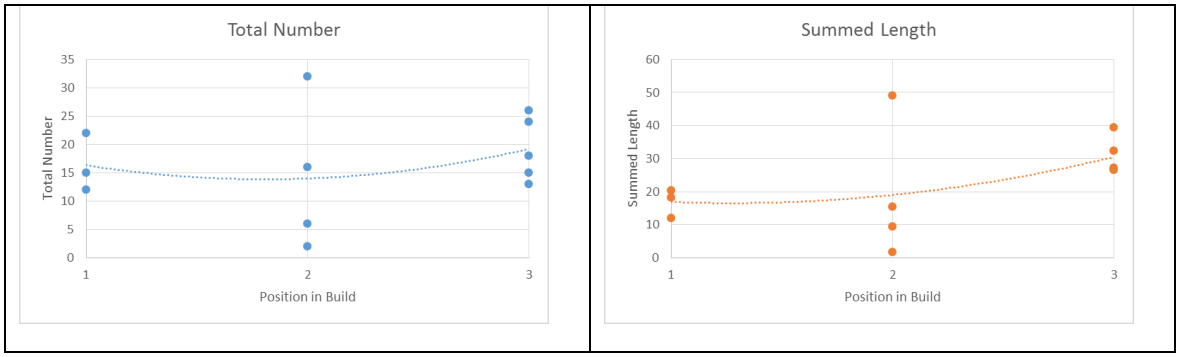

Figure 48: Total Number of Pore Chains and Summed Length of Pore Chains over the Build Space

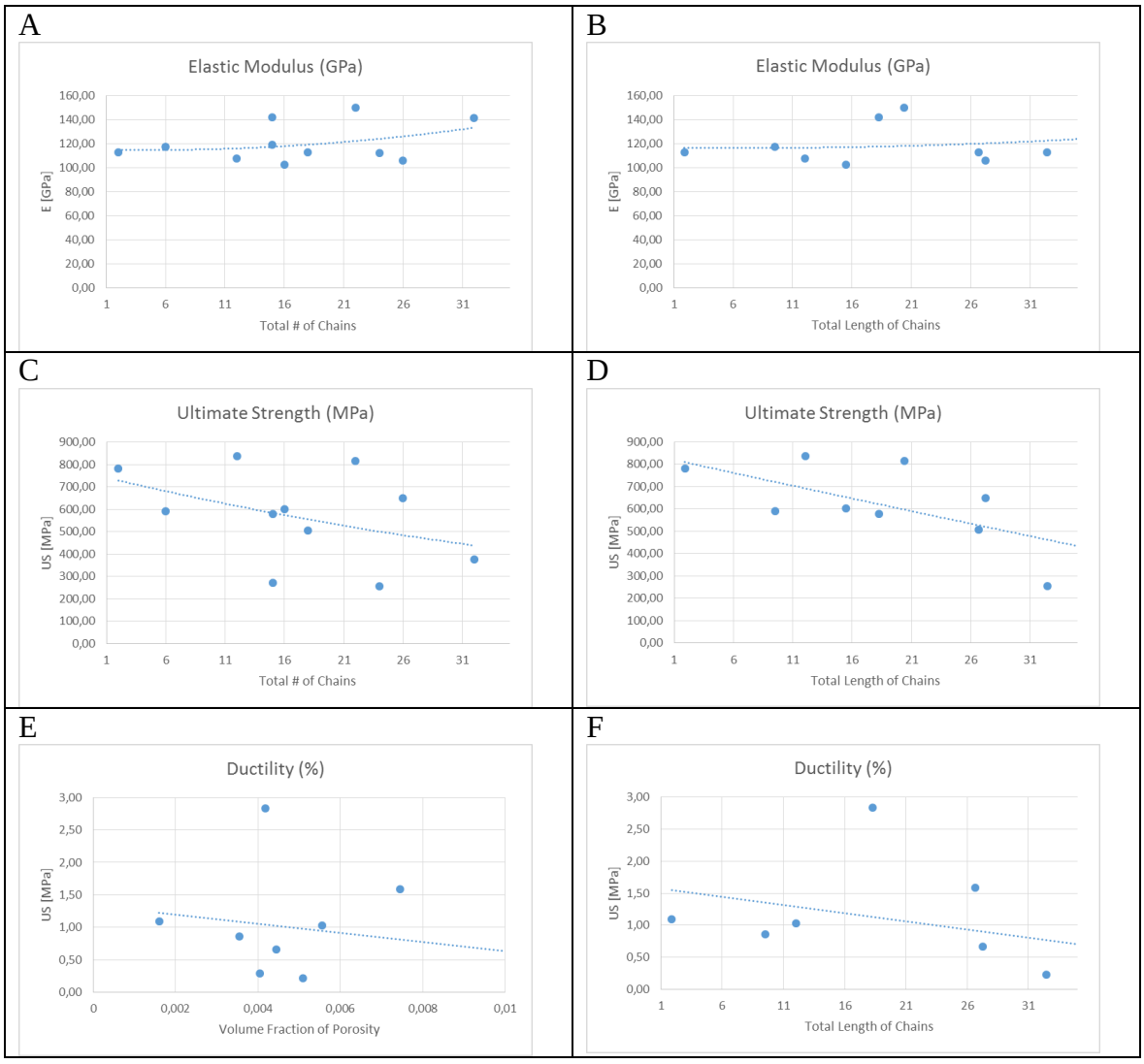

Figure 49: Influence of Total Number of Pore Chains and Summed Length of Pore Chains on Mechanical Properties

Theory on Chain Porosity Formation

Prabhakar et al. [71] hypothesizes that the warping of the baseplate usually takes place during the first few layers of the build. This phenomenon is known in EBM [71] but compared to the build geometries [20] fabricated in comparable studies [16], [30], the builds for this study warped extensively.

Figure 50: Extensive Warping of the Baseplate in Presented Study (Build II)

During the build when the baseplate is lowered and more layers were added in between the heat source (beam) and the baseplate, Prabhakar et al. [71] states that "the bulge in the base plate reduces with increasing number of layers of the build". This change in baseplate geometry might lead to tensile residual stress on the samples during the time at which the build is fabricated. During this baseplate deformation the samples attached to it are on build temperature between 1000°C and 1500°C [71]. That is far beyond Inconel 718 use-temperature. The reported high rate sensitivity (n≈5 [56]) at that temperature range combined with the long time exposure of about a day, could lead to critical tensile residual stresses and the material forming creep-like damage (chain porosity along the grain boundaries) by creep relaxation. Further insight in computational modeling of the residual stress formation for the given build would be needed to verify this theory.

Grain Size

Grain size analysis is performed in the direct vicinity of the metallography samples. Therefore the vertical samples *T2;1* are etched and the mean columnar grain diameter is evaluated (see Figure 51 for an example of the etched surface).

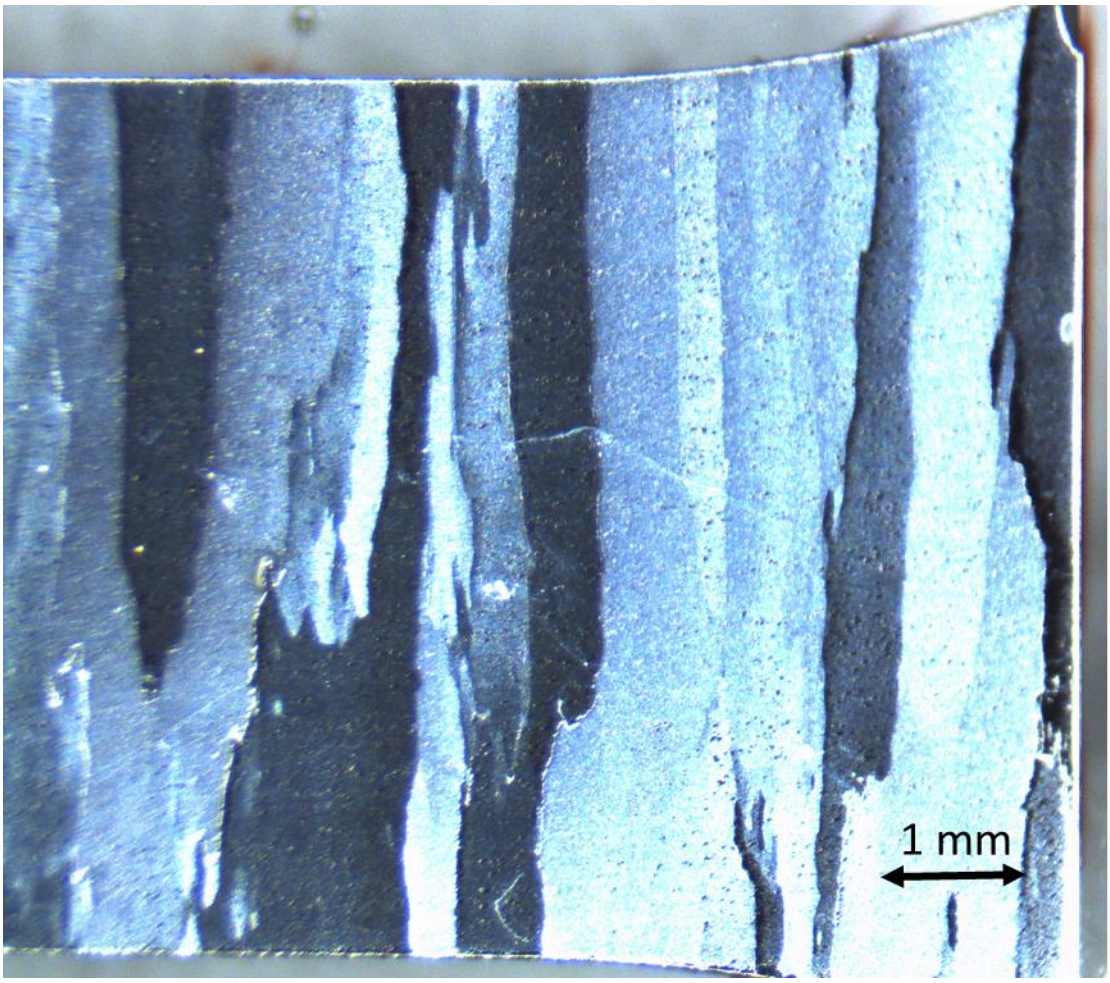

Figure 51: Etched Sample of the Columnar Grain Structure in Sample II/YX/3 T2;1

Table 16: Grain Sizes

Sample ID	Average Grain Diameter [mm]
IIYX2	0.29
IIYX3	0.48
IIYX4	0.58
IIYX5	0.44
IIYX6	0.15
IIIYX1	0.36
IIIYX2	0.43
IIIYX3	0.20
IIIYX4	0.42
IIIYX5	0.58
IIIYX6	0.12
IVYX2	0.25

It stands out that some builds show smaller grains than as-built samples and that as-built samples show gradient in grain size (Table 16). Plus, there is no point of grain shrinkage during heat treatment.

The relationship between mechanical properties and grain size is depicted in Figure 52. The correlation found for ductility can be explained when keeping in mind that the chain porosity forms at grain boundaries, hence larger grains could relate to larger porosity chains. Nevertheless, a larger data set would be necessary to underline this theory. Same circumstances are found for ultimate tensile strength.

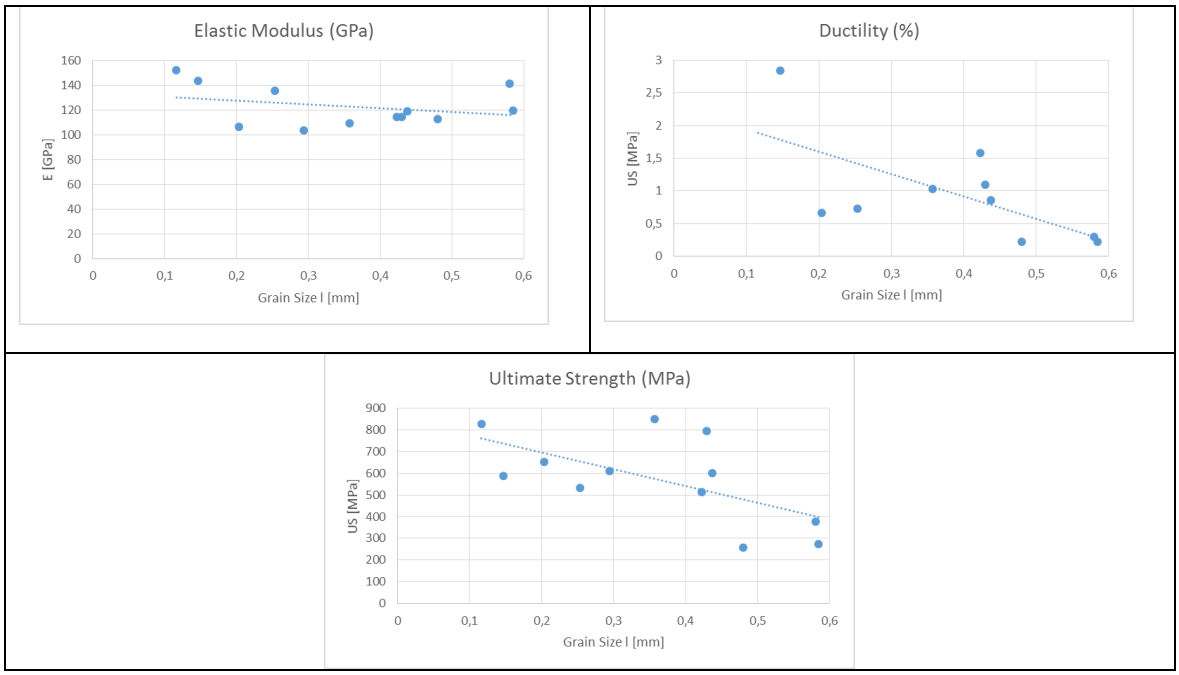

Figure 52: Relation between Mechanical Properties and Grain Size

ANOVA Analysis

Using the gathered data for the ANOVA analysis shows that neither the effect of the varied heat treatment parameter nor their correlations is indicated as significant (p-value < 0.05). The maximum predicted likelyness of solution treatment temperature having a significant influence on grain size is 25%. The probability of the batch (build II or build III) having an significant influence on grain size is according to the ANOVA

analysis 32%. Furthermore the analysis shows that modelling the grain size distribution with the heat treatment parameter does not result in a meaningful model. The $R^2_{adjacent}$ value is at peak 12%, whereas well-fitting models are indicated by values close to 100% [63]. That the grain size sees a significant variation throughout the tests is therefore to be attributed to scatter, i.e. influences not included in the test parameter. The following paragraph depicts possible reasons.

The initial guess is that the material shows an inhomogeneous grain structure already in the as-built condition. The following would substantiate this guess. The other metallographic features like porosity vary significantly from sample to sample indicating differences in the influence of the processing parameter.

Furthermore the builds have different locations in the build chamber. Finally, the most significant observations that support this guess is that the as-built sample shows larger grains than some of the heat treated samples.

Another factor that could amplify the differences in post-heat treated grain size is a possible gradient in the contents of grain boundary pinning precipitates (δ and carbides) in the as-built condition.

An analysis of the spatial variance of the sample throughout the build space leads to the following chart (Figure 53). Build II shows a pronounced peak of grain size at the center (position 3 and 4) of the build. This could be rationalized by the higher temperatures in the center of a build, which can be related to more heat transfer through radiation from the outside sample to the colder walls of the build. Samples located at the center of the build space were on the other hand surrounded by equally hot samples. The extensive warpage of the baseplate observed in this study is explained with the same argumentation and could be an evidence for an over-average gradient in build temperature in the builds with respect to other studies [16], [30]. This temperature gradient could be sufficient for influencing the grain boundary pinning δ phase

precipitation, as this phase dissolves at temperatures in the same range of the build temperature.

Build III on the other hand shows a dent in that curve and therefore a minimum of grain size at the center of the build. The respective sample (III/YX/3) shows the low solution treatment temperature and so spent less time at temperatures known for grain growth. Nevertheless the above observations suggest that the solution treatment has no significant influence on grain growth when compared to the influence of HIP and build conditions (scatter). Therefore the orange curve in Figure 53 argues against a clear conclusion.

Finally the as-built sample (grey single point) speaks for a combination of both theories. While there are HIP and heat treated samples that show smaller grains than the as-built one and there is no point for assuming grain shrinkage, an initial variation is more than likely. Furthermore, the fact that two of the build center samples contradict the theory of grain size peak at the center. Therefore either a random variation in grain size or the effect of different pre-existing δ could have affected the irregular shape of the curve. Further experiments were needed to finally determine the underlying reasons.

Nevertheless it needs to be stated that all samples showed the columnar grain structure. The statement by Kirka [20] that this structure is retained throughout HIP, solution treatment and aging holds with respect of the current study.

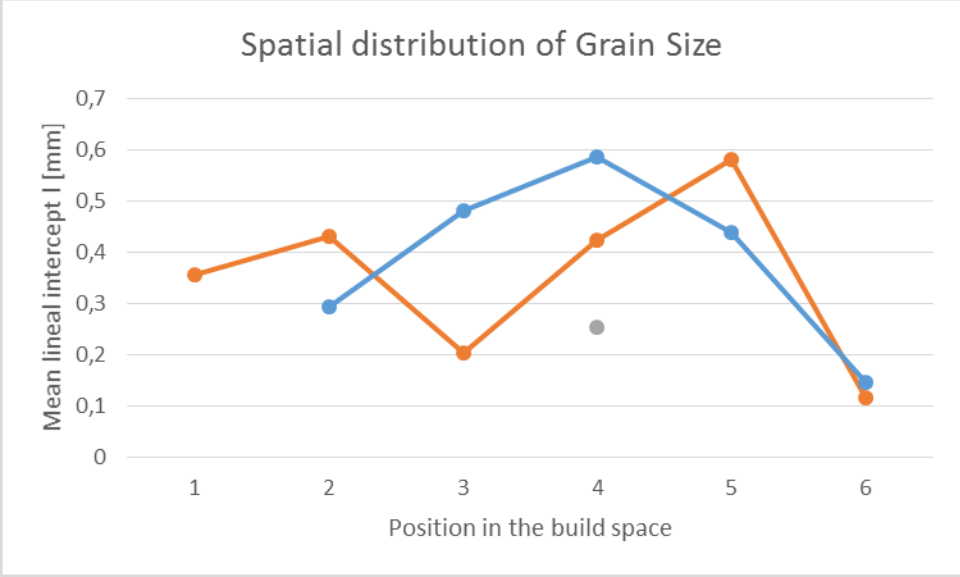

Figure 53: Spatial Distribution of Grain Size throughout the Builds

CHAPTER VI

CONCLUSION

The study seeks to create an experimental methodology for efficiently establishing Process-Structure-Property relationships for Additive Manufactured age-hardened alloys and has showcased the implementation of this methodology for the post-built heat treatment of the nickel-base superalloy Inconel 718, processed by Electron Beam Melting. Applying a sound experimental strategy is crucial with regards to AM which combines the demands of highly efficient process development with complex and novel processing routes.

In order to accomplish this primary purpose, the first step of the intended methodology is generating a PSPP chart based on literature review. The chart illustrates the knowledge on the material system's behavior with respect to the selected processing route. It reveals lack of knowledge on critical PSP linkages and therefore helps the researcher to identify critical subsequent investigations. Furthermore it supports determining and selecting the processing parameter of consideration for the anticipated study.

The next step of the strategy is selecting an appropriate test method in order to determine a material and time efficient library, consisting of samples for testing relevant metallography and mechanical properties. Strain-rate jump tests are found to be an appropriate method for the purpose of high temperature investigations as they allow to efficiently characterize viscoplastic behavior next to the basic tensile properties.

Knowing about the library configuration allows a definition of the feasible test extend and the experimental design. The Design of Experiment test matrix fulfills the requirements of a promising method for sampling the parameter space of interest,

targeting on the investigation of significant effects and correlations by utilizing a minimum amount of test samples.

The above-mentioned measures provide a profound basis for Additive Manufacturing the test library and post-processing its parameter sets individually in accordance with the test matrix. The influence of the parameter variation is found to be most efficiently investigated if started with the analysis of the mechanical properties, as they define the performance and hence are the quality features. Thereafter structural investigations can focus on the features suspected to be most likely explaining the targeted properties. Afterwards, further detailing studies are applicable in case these features do not sufficiently allow drawing conclusions on the cause of the observed material behavior.

The proposed methodology is showcased on EBM Inconel 718. Based on the PSPP chart for this system, solution treatment temperature, precipitation initiation temperature, and aging time are detected as promising variables for investigating and optimizing the age-hardening behavior of EBM Inconel 718.

Strain-rate jump tests are successfully applied on a forged Inconel 718 reference test while AM material showed unexpected low ductility. This made an investigation of the desired mechanical properties impossible. The change in EBM Inconel 718 ductility is found to be most likely attributed to the change in build geometry with respect to preliminary reference studies on identically processing conditions. The idea of performing the metallography investigations on the material in direct vicinity to the mechanically test samples, proved to be a vital feature of the library for the PSPP investigation in AM. This allows linking of structure and properties and therefore enables the conclusions drawn from the study. The applied DoE method fits heat treatment test matrixes and is reusable for future tests on newly developed AM Inconel 718 microstructure due to its structure-independent character.

Starting with the mechanical tests instead of the structural analysis contributed to the immediate targeting of the critical structural feature accountable for the observed lack in ductility.

Phenomenologically unexpected chain porosity is found to be crucial for explaining the observed reduced ductility. It occurred that the extent and morphology of the porosity was not reported in the previous studies on EBM Inconel 718. The beneficial library geometry allowed a direct link to this structural feature of unexpected brittle intergranular tensile behavior. Quantitative analysis on porosity volume fraction, number of pores, and the average chain porosity features proved that the brittleness correlates to one peak flaw, rather than to the average values throughout the sample. Other than drawn as a conclusion in preliminary studies, the assumption of a negligible influence of HIPing is proved to be invalid due to the lack in repeatability. Hence it remains to be assessed whether HIPing could sufficiently reduce the extensive porosity observed. As characterizing the influence of peak flaws is not feasible with tensile testing, further investigations on fracture mechanics studies for EBM Inconel 718 are recommendable.

Solemnly changing the build geometry caused both the observed extensive warping of the baseplate as well as the chain porosity. Therefore these phenomena are suspected to link. A theory for the link of chain porosity to tensile residual stresses during the build is proposed. Nevertheless, the influence of baseplate warping causing these tensile stresses remains to be assessed in future computational analysis on the build geometry. Furthermore efficient methods to predict and avoid this phenomenon are needed to be incorporated in the EBM strategies.

Next to the lack of repeatability in EBM build quality a lack of structural uniformity is found throughout the build space. Analysis showed no relation between the post-built parameter and the measured grain size to be significant with relation to the variation in non-controlled influences, most likely on as-built grain size. Detailed studies

and further investigations are needed for final clarification of these links as they are yet unknown and not targeted with this study.

Homogeneous and repeatable basic material properties are vital for the analysis of parameter effects and conclusions in any kind of study and have been not yet been attributed in-depth by the EBM Inconel 718 research community. Facing this, further investigations are needed. Despite the reported drawbacks relating to insufficient feedstock material properties, main aspects of the methodology (in particular the PSPP chart and the library design) proved their value with regard to revealing Processing-Structure-Property relations. The study reveals an unexpected structural feature: the large scale chain porosity, and illustrates its influence on mechanical properties. It provides a theory for the suspected relation to processing parameter. The experimental set up and design established in this thesis is available for a time efficient repetition of the post-processing study on less porous AM samples. The developed strategy serves as a guideline for future studies on the AM processing of EBM Inconel 718.

CHAPTER VII

RECOMMENDATIONS

Next to the recommendations on further studies as stated in the conclusions, the designed test matrix should be repeated on better material conditions than those observed on the feedstock material used for the study discussed in this thesis. The following recommendations serve as a guideline for following researches to incorporate the outcome of this study.

The presented results highly suggest the application of a HIP cycle to close the encountered porosity. Further preliminary studies on leftover material can help to investigate the parameter which is able to close larger scale pores.

By incorporating less samples per build and by using proven build configurations for cutting out the material library samples, can potentially reduce the amount of warping and chain porosity.

Furthermore equiaxed grain scan strategies or samples vertically oriented in the textured orientation of the columnar grain structure could improve the ductility values and assure that the necessary deformation for the viscoplasticity evaluation is achieved.

In order to achieve a minimum possible influence of build position, future studies on vertical builds could consider a radial distribution of the samples around the center of the baseplate. These measures have not been possible for the current builds due to limited build space combined with minimum size requirements for high temperature experiments and the limited number of individual builds affordable.

To investigate the as-built grain-structure variation and to relate the post-processing effects to the starting conditions, as-built metallography samples should be added to each individual parameter-set of the study.

APPENDIX

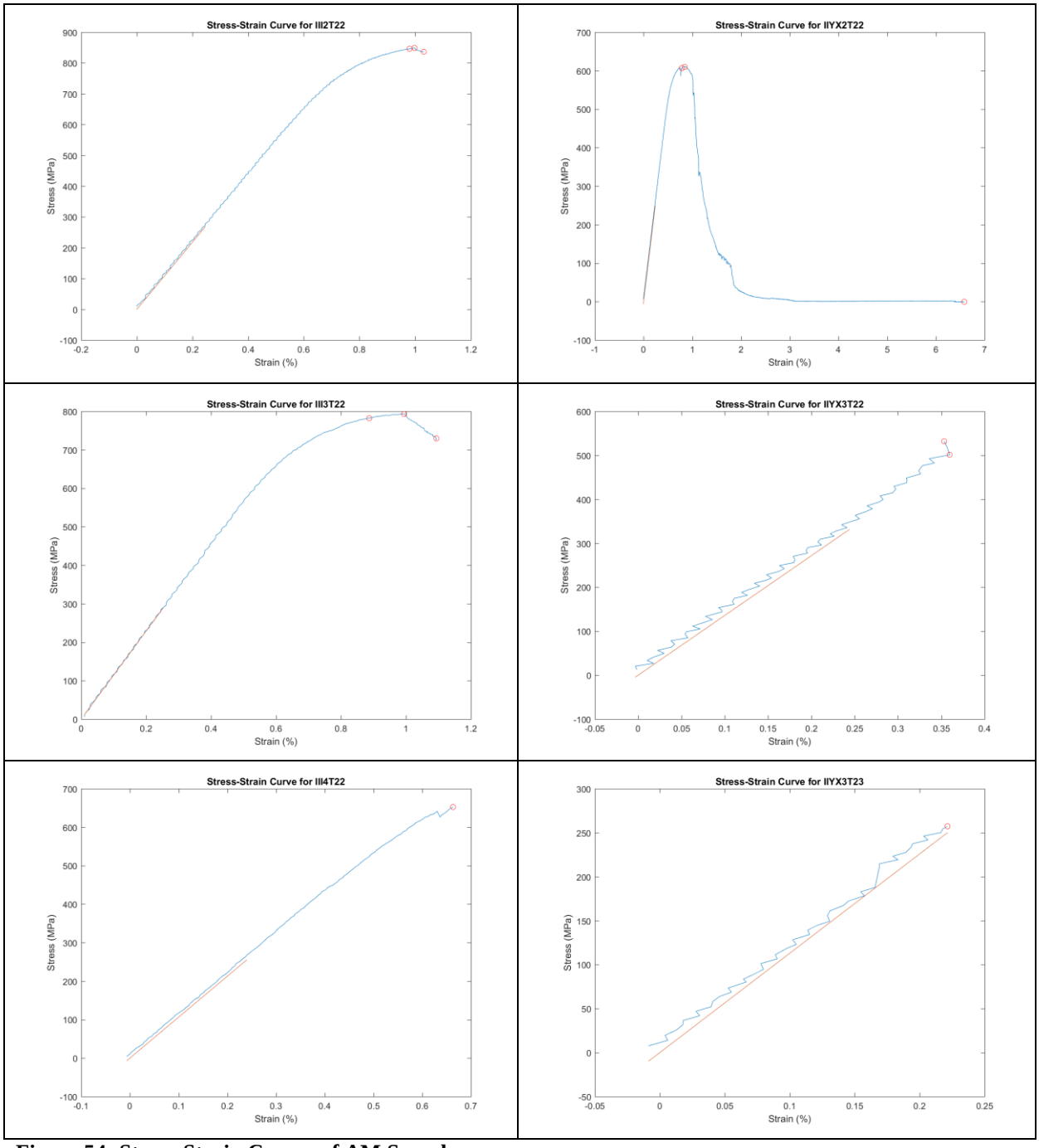

Figure 54: Stress-Strain Curves of AM Samples

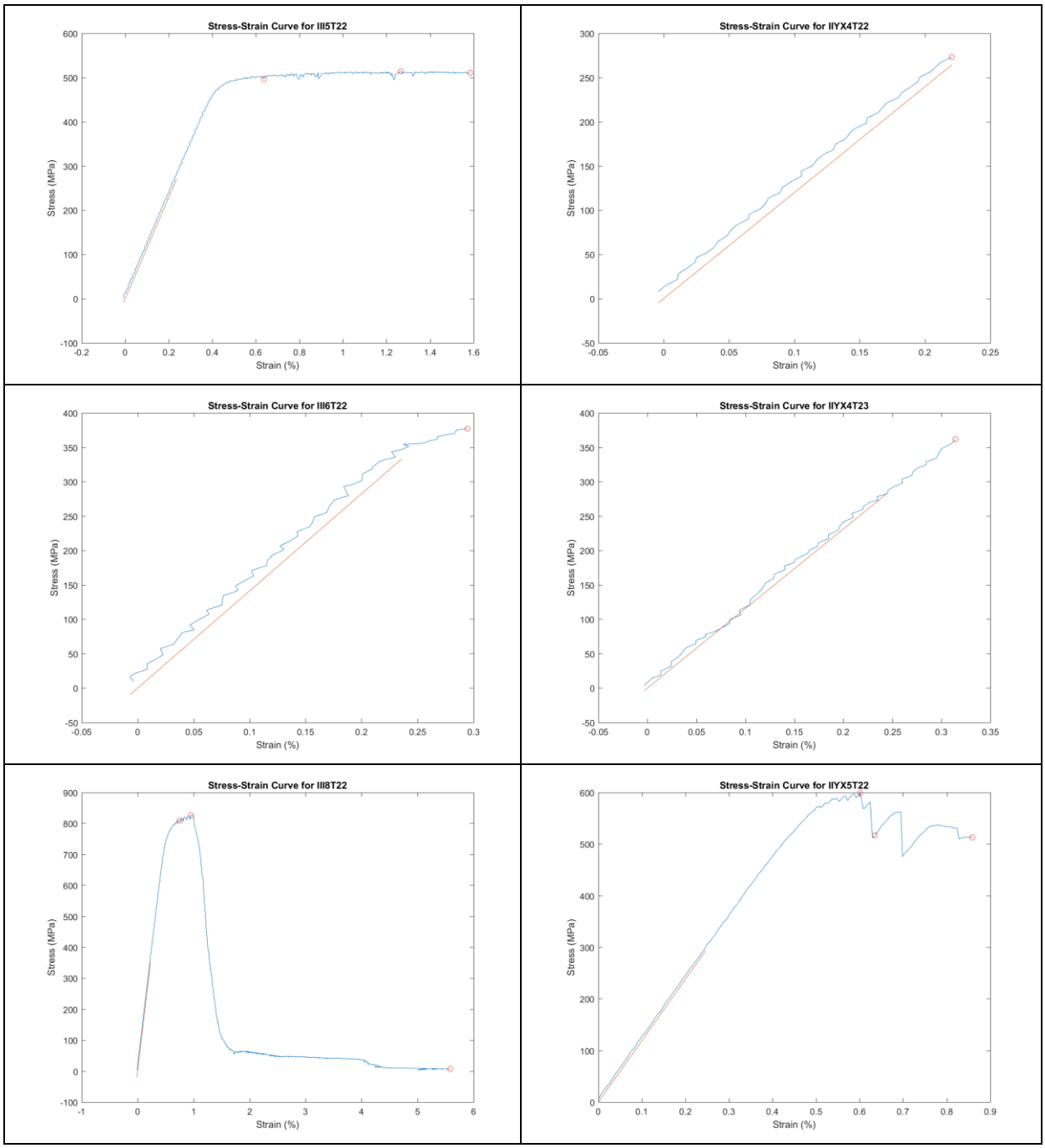

Figure 55: Stress-Strain Curves of AM Samples

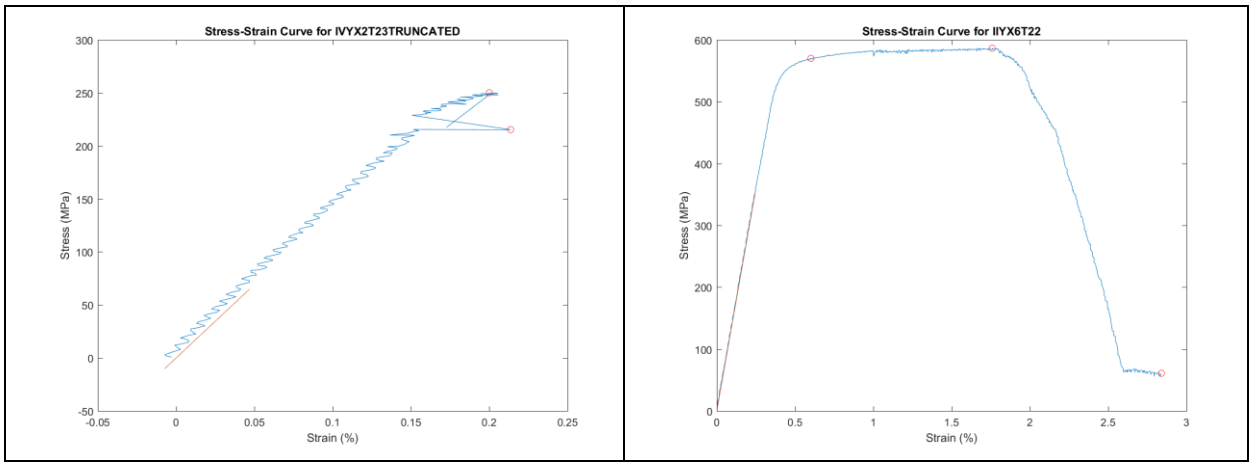

Figure 56: Stress-Strain Curves of AM Samples

REFERENCES

[1] ANON., “About the Materials Genome Initiative”, www.whitehouse.gov/mgi (Accessed August 1, 2016).

[2] SAMES, W. J., UNOCIC, K. A., DEHOFF, R. R., LOLLA, T. and BABU, S. S., "Thermal effects on microstructural heterogeneity of Inconel 718 materials fabricated by electron beam melting," Texas A&M University, College Station, TX, 2014.

[3] SPIERINGS, A., "Additive Manufacturing mit Metall. Ein Überblick über die Forschung," PRODEX/Swiss Tech Conference Basel, Switzerland, November 2014.

[4] BURBLIES, A., "Design und Herstellung gradierter zellularer Endprothesen und Leichtbaustrukturen," Fraunhofer Institut für Fertigungstechnik und Angewandte Materialforschung, Bremen, Germany, August 2013.

[5] MEDINA, F., KIRKA, M. M., ACKELID, U., and DEHOFF, R. R., "Developing Processing Parameters for Nickel-base Superalloys for the Electron Beam Melting Additive Manufacturing Process," Edison Welding Institute, Buffalo, NY.

[6] FANNING, P. , "Aero engines benefit from additive manufacturing processes. Eureka - The Site For Engineer Design," 2013. [Online]. Available: http://www.eurekamagazine.co.uk/design-engineering-features/technology/aero-engines-benefit-from-additive-manufacturing/4789. [Accessed August 2, 2016].

[7] WOHLERS, T., "Wohlers Report 2015.", 2015. [Online]. Available: https://lirias.kuleuven.be/handle/123456789/372635. [Accessed August 25, 2016].

[8] OLSON, G. B., "Pathways of Discovery - Designing a New Material World," *Science Magazine, Vol. 288*, pp. 993-998, May 12, 2000.

[9] GOULDING, A. N., NEU, R. W., and SANDERS, Jr., T. H., "The Development of a Process-Structure-Properties-Performance (PSPP) Map for Aluminum-Zinc-Magnesium-Copper Alloys Used In Aircraft Applications," George W. Woodruff School of Mechanical Engineering, Georgia Institute of Technology, Atlanta, GA, 2016.

[10] BOWMAN, R., "Superalloys: A Primer and History," The Minerals, Metals and Materials Society (TMS), [Online]. Available: http://www.tms.org/meetings/specialty/superalloys2000/superalloyshistory.html. [Accessed August 2, 2016].

[11] BHADESHIA, H. K. D. H., "Nickel Based Superalloys, " University of Cambridge, [Online]. Available: http://www.msm.cam.ac.uk/phase-trans/2003/Superalloys/superalloys.html. [Accessed August 2, 2016].

[12] SPECIAL METALS CORPORATION, "Inconel-Alloy-600," September 2008. [Online]. Available: http://specialmetals.com/assets/documents/alloys/inconel/inconel-alloy-600.pdf. [Accessed August 2, 2016].

[13] UNOCIC, K. A., KOLBUS, L., DEHOFF, R. R. and PINT, B. A., "High-Temperature Performance of UNS N07718 Processed by Additive Manufacturing," NACE International Paper 2013, Presented at the Corrosion Conference, San Antonio, TX, 2014.

[14] ARCAM AB, "Material Safety Data Sheet, Product: Arcam Inco 718 Powder," Mölndal, Sweden, 2015.

[15] STRONDL, A., FISCHER, R., FROMMEYER G., and SCHNEIDER, A., "Investigations of MX and γ'/γ" precipitates in the nickel-based superalloy 718 produced by electron beam melting," *Materials Science & Engineering,* pp. 138-147, July 2, 2007.

[16] KIRKA, M. M., MEDINA, F., DEHOFF R. R., and OKELLO, A., "Mechanical Behavior of Post-processed Inconel 718 Manufactured Through the Electron Beam Melting Process," Manufacturing Demonstration Facility, Oak Ridge National Laboratory, Knoxville, TN.

[17] KÖRNER, C., HELMER, H., BAUEREISS, A., and SINGER, R. F., "Tailoring the grain structure of IN718 during selective electron beam," University of Erlangen-Nuremberg, Erlangen, Germany, 2014.

[18] DEHOFF, R. R., KIRKA, M. M., LIST III, F. A., UNOCIC, K. A., and SAMES, W. J., "Crystallographic texture engineering through novel melt strategies via electron beam melting: Inconel 718," *Materials Science and Technology, Vol. 31, No. 8,* pp. 939-943, 2015.

[19] DEHOFF, R. R., KIRKA, M. M., SAMES, W. J., BILHEUX, H., TREMSIN, A. S., LOWE, L. E., and BABU, S. S., "Site specific control of crystallographic grain orientation through electron beam additive manufacturing," *Materials Science and Technology,* 2015.

[20] KIRKA, M. M. (Oak Ridge National Laboratory, Manufacturing Demonstration Facility), personal communication, 2016.

[21] STRONDL, A., PALM, M., GNAUK, J. and FROMMEYER, G., "Microstructure and mechanical properties of nickel based superalloy IN718 produced by rapid prototyping with electron beam melting (EBM)," *Materials Science and Technology, Vol. 27, No. 5,* pp. 876-883, November 12, 2013.

[22] KITAGUCHI, H., "Microstructure-Property Relationship in Advanced Ni-Based Superalloys," Department of Materials, University of Oxford, OX1 3PH, Oxford, UK, 2012.

[23] JANAKI RAM, G. D., VENUGOPAL REDDY, A., PRASAD RAO, K., REDDY, G. M., and SARIN SUNDAR, J. K., "Microstructure and tensile properties of Inconel 718 pulsed Nd-YAG laser welds," *Journal of Materials Processing Technology, Vol. 167,* pp. 73-82, 2005.

[24] ROOS, E., and MAILE, K., Werkstoffkunde für Ingenieure. Grundlagen, Anwendung, Prüfung, Berlin, Germany: Springer-Verlag, 2002 and 2005.

[25] RADZICKI, A. T., "Characterization and Modeling of the Thermomechanical Fatigue Crack Growth Behavior of Inconel 718 Superalloy," George W. Woodruff School of Mechanical Engineering, Georgia Institute of Technology, Atlanta, GA, 2016.

[26] MCCLUNG, R. C., LEE, Y. D., TSCHOPP, J. A., SRIVATSA, S. K., LEVERANT, G. R., WALDHART, C. J., JAMEEL, M. A., ENRIGHT, M. P., MILLWATER, H. R., LEHMANN, D. J., HUYSE, L., FITCH, S. H. K., and DUBKE, J. P., “Turbine rotor material design - phase II," tech. rep., DOT/FAA/AR-07/13, 2008.

[27] ASTM F3055-14a, "Standard Specification for Additive Manufacturing Nickel Alloy (UNS N07718) with Powder Bed Fusion," ASTM International, West Conshohocken, PA, 2016.

[28] LOOKMAN, T., ALEXANDER F., and RAJAN, K., Information Science for Materials Discovery and Design (Springer Series in Materials Science, Vol. 225), Cham, Switzerland: Springer International Publishing, 2016.

[29] HELMER, H. E., KÖRNER, C., and SINGER, R. F., "Additive manufacturing of nickel-based superalloy Inconel 718 by selective electron beam melting: Processing window and microstructure," *Magazine of the Materials Research Society, Vol. 29, No. 17,* pp. 1987-1996, September 14, 2014.

[30] KIRKA, M. M., UNOCIC, K. A., RAGHAVAN, N., MEDINA, F., DEHOFF, R. R., and BABU, S. S., "Microstructure Development in Electron Beam Melted Inconel 718 and Associated Tensile Properties," Manufacturing Demonstration Facility, Oak Ridge National Laboratory, Knoxville, TN.

[31] UNOCIC, K. A., KOLBUS, L. M., DEHOFF, R. R., DRYEPONDT, S. N. and PINT, B. A., "Unpublished Research," Oak Ridge National Laboratory, Oak Ridge, TN, 2014.

[32] ZHAO, X., CHEN, J., LIN, X., and HUANG, W., "Study on microstructure and mechanical properties of laser rapid forming Inconel 718," *Materials Science and Engineering,* pp. 119-124, 2008.

[33] CAO, X., RIVAUX, B., JAHAZI, M., and CUDDY, J., "Effect of pre- and post-weld heat treatment on metallurgical and tensile properties of Inconel 718 alloy butt joints welded using 4 kW Nd:YAG laser," National Research Council Canada, Montreal (QC), Canada, 2009.

[34] RENHOF, L., "Mikrostruktur und mechanische Eigenschaften der Nickellegierung IN 718", Technische Universität München, München, 2007.

[35] SRINIVASAN, R. PRASAD, Y.V.R.K., "Microstructural control in hot working of IN-718 superalloy using processing map.". In *Metallurgical and Materials Transactions,* Vol. 25A, pp. 2275–2284, 1994.

[36] AZADIAN, S., WEI, L.-Y., and WARREN, R., "Delta phase precipitation in Inconel 718," *Materials Characterization,* pp. 7-16, 2004.

[37] OBLAK, J. M., PAULONIS, D. F., and DUVALL, D. S., 1974. "Coherency Strengthening in Ni Base Alloys, 36 Hardened by $D0_{22}$ γ" Precipitates". In *Metallurgical and Materials Transactions*, Vol. 5, pp. 143-154.

[38] RAO, G. A., KUMAR, M., SRINIVAS, M., and SARMA, D. S., "Effect of standard heat treatment on the microstructure and mechanical properties of hot isostatically pressed superalloy inconel 718," *Materials Science and Engineering,* pp. 114-125, 2003.

[39] AZADIAN, S., WEI, L.-Y., NIKLASSON, F., and WARREN, R., "Precipitation in spray-formed IN 718," in *Superalloys 718, 625 and various derivatives*, Warrendale, PA, Minerals, Metals and Materials Society, 2001, pp. 617-26.

[40] HONG, J. K., PARK, J. H., PARK, N. H., EOM, I. S., KIM, M. B., and KANG, C. Y., "Microstructures and mechanical properties of Inconel 718 welds by CO2 laser welding," *Journal of Materials Processing Technology,* pp. 515-520, 2007.

[41] DESVALLEES, Y., BOUZIDI, M., BOIS, F., BEAUDE, N., "Delta phase in Inconel 718: mechanical properties and forging process requirements", in *Loria EA, editor. Superalloy 718—metallurgy and applications,* Warrendale, PA, Minerals, Metals & Materials Society, 1994. pp. 281– 91.

[42] MULLER, JF, DONACHIE, MJ. "Superalloys a technical guide.", Materials Park, OH, ASM International, 1975, pp. 211 –86.

[43] SJÖBERG, G., INGESTEN, NG., "Grain boundary y-phase morphology, carbides and notch rupture sensitivities of cast alloy 718.", in *Loria EA, editor. Superalloy 718—metallurgy and applications,* Warrendale, PA, Minerals, Metals & Materials Society, 1991, pp. 603– 21.

[44] JANAKI RAM, G. D., VENUGOPAL REDDY, A., PRASAD RAO, K., REDDY G. M., and SARIN SUNDAR, J. K., "Microstructure and tensile properties of Inconel 718 pulsed Nd-YAG laser welds," *Journal of Materials Processing Technology,* pp. 73-82, 2005.

[45] ASM INTERNATIONAL ®, Nickel, Cobalt, and Their Alloys, Materials Park, OH, 2000.

[46] SWINDEMAN, R. W., SWINDEMAN, M. J., "A comparison of creep models for nickel base alloys for advanced energy systems," *International Journal of Pressure Vessels and Piping,* pp. 72-79, 2008.

[47] CHANDLER, H., Heat Treater's Guide - Practices and Procedures for Nonferrous Alloys, ASM International, 1996. Available: http://app.knovel.com/hotlink/toc/id:kpHTGPPNA2/heat-treaters-guide-practices-2/heat-treaters-guide-practices-2 [Accessed August 2, 2016].

[48] OAK RIDGE NATIONAL LABORATORY MANUFACTURING DEMONSTRATION FACILITY, "Unpublished Resources," Knoxville, TN, 2016.

[49] AZADIAN, S., WEI, L.-Y., and WARREN, R., "Delta phase precipitation in Inconel 718," *Materials Characterization,* pp. 7-16, 2004.

[50] NANDWANA, P., PETER, W. H., DEHOFF, R. R., LOWE, L. E., KIRKA, M. M., MEDINA, F., and BABU, S. S., "Recyclability Study on Inconel 718 and Ti-6Al-4V Powders for Use in Electron Beam Melting," *The Minerals, Metals and Materials Society and ASM International,* 2015.

[51] REED, R. C., "The Superalloys - Fundamentals and Applications," Cambridge University Press, New York, NY, 2006.

[52] NEU, R. W., SCOTT, D. T., and WOODMANSEE, W. M., "Thermomechanical Behavior of 96Sn-4Ag and Castin Alloy," *Journal of Electronic Packaging by ASME, Vol. 123,* pp. 238-246, September 2001.

[53] NORTON, F., The creep of steel at high temperatures, London: McGraw-Hill Ltd., 1929.

[54] GIBBONS, T.B., HOPKINS, B.E., "Creep behaviour and microstructure of Ni-Cr base alloys", in *Metal Science*, Vol. 18, 1984, pp. 273–280.

[55] PIERAGGI, B., and UGINET, J. F., "Fatigue and creep properties in relation with alloy 718 microstructure," in *Superalloys 718, 625, 706 and various derivatives*, The Minerals, Metals and Materials Society, 1994, pp. 535-544.

[56] THOMAS, A., EL-WAHABI, M., CABRERA, J. M., and PRADO, J. M., "High temperature deformation of Inconel 718," *Journal of Materials Processing Technology*, pp. 469-472, 2006.

[57] SUGAHARA, T., MARTINOLLI, K., REIS, D. A. P., MOURA NETO, C., COUTO, A. A., PIORINO NETO, F., and BARBOZA, M. J. R., "Creep Behavior of the Inconel 718 Superalloy," *Defect and Diffusion Forum*, pp. 509-514, 2012.

[58] PATHAK, S., and KALIDINDI, S. R., "Spherical Nanoindentation Stress-Strain Curves," Center for Integrated Nanotechnologies, Los Alamos National Laboratory, Los Alamos, NM.

[59] ASTM E112-13, "Standard Test Methods for Determining Average Grain Size," ASTM International, West Conshohocken, PA, 2016.

[60] ASTM E1245-03, "Standard Practice for Determining the Inclusion or Second-Phase Constituent Content of Metals by Automatic Image Analysis," ASTM International, West Conshohocken, PA, 2016.

[61] IYER, S. K., and LISSENDEN, C. J., "Inelastic Anisotropy of Inconel 718: Experiments and Mathematical Representation," *Journal of Engineering Materials and Technology by ASME, Vol. 122*, pp. 321-326, July 2000.

[62] SAS Institute Inc., JMP® 12 Design of Experiments Guide, Cary, NC, 2015.

[63] SIEBERTZ, K., VAN BEBBER, D., and HOCHKIRCHEN, T., Statistische Versuchsplanung. Design of Experiments (DoE), Berlin, Germany: Springer-Verlag, 2010.

[64] ASTM E8 / E8M-15a, "Standard Test Methods for Tension Testing of Metallic Materials," ASTM International, West Conshohocken, PA, 2015.

[65] ASTM E21-09, "Standard Test Methods for Elevated Temperature Tension Tests of Metallic Materials," ASTM International, West Conshohocken, PA, 2016.

[66] ASTM E3-11, "Standard Guide for Preparation of Metallographic Specimens," ASTM International, West Conshohocken, PA, 2011.

[67] ASTM F2971-13, "Standard Practice for Reporting Data for Test Specimens Prepared by Additive Manufacturing," ASTM International, West Conshohocken, PA, 2015.

[68] SATIN, M. (Braddock Metallurgical), personal communication, 2016.

[69] ZINN, S., and SEMIATIN, S. L., "Coil design and fabrication: basic design and modifications," *Heat Treating,* pp. 32-41, June 1968

[70] GROVE, D., DAVIS, T. "Engineering, Quality and Experimental Design", *Longman Scientific and Technical*, Harlow, pp. 12, 1992.

[71] PRABHAKAR, P., SAMES, W. J., DEHOFF, R. R., and BABU, S. S., "Computational modeling of residual stress formation during the electron beam melting process for Inconel 718," *Additive Manufacturing,* pp. 83-91, 2015.